INFORMATION TO USERS

This manuscript has been reproduced from the microfilm master. UMI films the text directly from the original or copy submitted. Thus, some thesis and dissertation copies are in typewriter face, while others may be from any type of computer printer.

The quality of this reproduction is dependent upon the quality of the copy submitted. Broken or indistinct print, colored or poor quality illustrations and photographs, print bleedthrough, substandard margins, and improper alignment can adversely affect reproduction.

In the unlikely event that the author did not send UMI a complete manuscript and there are missing pages, these will be noted. Also, if unauthorized copyright material had to be removed, a note will indicate the deletion.

Oversize materials (e.g., maps, drawings, charts) are reproduced by sectioning the original, beginning at the upper left-hand corner and continuing from left to right in equal sections with small overlaps.

ProQuest Information and Learning
300 North Zeeb Road, Ann Arbor, MI 48106-1346 USA
800-521-0600

Studies on the Structure and Morphology of Perylene Containing Polymers

by
Dianjun Yao

A thesis submitted to the

Faculty of Graduate Studies and Research

in partial fulfillment of the requirements

for the degree of

Doctor of Philosophy

Carleton University

Department of Chemistry

1125 Colonel By Drive

Ottawa, Ontario, Canada

August, 2005

ABSTRACT

Incorporating functional small molecules as part of a polymer, either in the main chain or side group, is a strategy to improve the mechanical properties, processing options etc. for device applications. The structure and morphology of such polymers play a vital role in the performance and life-time of the device. This thesis describes the structure and morphological studies on polymers containing perylene. We discuss the crystalline conformations of perylene polyimides (PPIs), with alkyl spacers varying in length from C_3 to C_{12} in Chapter 3. Several changes in the spectra are seen with an increase in annealing time, at a given temperature. With an increase in annealing time, X-ray diffraction patterns indicate a crystal to mesogenic transition.

The polymers described above are notoriously insoluble in most organic solvents. Co-polymerization to disrupt the crystal packing is a common strategy to impart solubility. Chapter 4 describes the work on a series of perylene-containing block copolyimides with different ratios of perylenetetracarboxylic dianhydride and 4, 4'-(hexafluoroisopropylidene)diphthalic anhydride (6FDA). The copolymers are semi-crystalline up to a concentration of 60% (mol) 6FDA and are "*conformational* isomorphism" with homopolymer of PPI-12.

We have also designed a new approach to novel perylene-based self-assembled structure. Self-assembly of the perylene segment leads to vesicle formation of perylene end-capped poly(dimethyl siloxane) (perylene end-cap-PDMS) in non-aqueous media. TEM images of the vesicles show either a bilayer or a trilayer structure depending on the solubility parameter of the solvent. This initial attempt to prepare such vesicles in non-aqueous media may be applicable to similar systems.

ACKNOWLEDGEMENTS

I am very grateful to have an opportunity to do my Ph.D. under the supervision of Professor P. R. Sundararajan. In the last four and half years, I was blessed with his affection and impressed by his wisdom and teaching philosophy. I appreciate him for the guidance and continuous support. I thank Dr. Z.Y. Wang for his guidance. I thank technical support from Mr. P. Gerroir and Dr T. Bender of Xerox. I also thank Dr. D. Fogg for the use of Cerius^2 modeling software.

This work was supported by the Natural Sciences and Engineering Research Council of Canada (NSERC) and Xerox Research Centre of Canada (XRCC). I thank Ontario Graduate Scholarship for Science and Technology (OGSST) for four year financial support.

I would like to thank my colleagues Dr. F. Khan, Dr. M. Monirazzaman, B. Tuteja, S. Singh, H. Xu, Dr. V. Sriram, S. Bhalla and S. Khanna for their help and friendly discussions. I thank all students and postdoctors, especially Dr. N. Song, in Dr. Z.Y. Wang's lab for showing me the different instruments and discussion.

Last but not the least I would like to thank my wife Xiaoyun (Sharon) Guan and my son Allan Yao for their support and understanding.

TABLE OF CONTENTS

Abstract i

Acknowledgements ii

Table of Contents iii

List of Tables viii

List of Figures and Schemes.....ix

Chapter 1: Introduction

1.1 Perylenetetracarboxylic Acid Bisimides.....2

1.1.1 Synthesis of Perylene Tetracarboxylic Acid Bisimides.....3

1.1.2 Crystal Structure and Packing Behavior.....5

1.1.3 Solution and Film Spectroscopic Behaviors.....7

1.1.4 Liquid Crystalline Perylene Bisimides.....10

1.2 Polyimides.....11

1.2.1 Synthesis of Polyimides.....12

1.2.2 Structure-Property Relationships of Polyimides.....13

1.2.3 Structure Modification of Polyimides 14

1.2.4 Chain-Chain Interaction of Polyimides.....17

1.3 Perylene Polyimides 18

1.3.1 Synthesis of Perylene Polyimides.....18

1.3.2 Spectroscopic Properties of Perylene Polyimides.....20

1.3.2a UV-visible absorption.....20

1.3.2b Fluorescent spectra.....21

1.3.2c Infrared spectra 22

1.3.3 Thermal Properties.....23

1.3.4 Solubilities of Perylene Polyimides.....24

1.4 Thesis Outline and Objective.....24

References 28

Chapter 2: Characterization Methods

2.1 Introduction.....34

2.2 Instruments and Methods.....34

2.2.1 Infrared (IR) Spectroscopy.....34

2.2.2 Nuclear Magnetic Resonance Spectroscopy (NMR).....36

2.2.3 Differential Scanning Calorimetry (DSC).....37

2.2.4 Thermogravimetric analysis (TGA).....39

2.2.5 Transmission Electron Microscopy (TEM).....40

2.2.6 X-ray Diffraction 42

2.2.7 UV-visible Spectroscopy.....47

2.2.8 Fluorescent Spectroscopy.....48

2.3 Molecular Modeling.....49

2.3.1 Introduction.....49

2.3.2 Molecular Simulation.....51

2.3.3 Cerius^2 Software 51

2.3.4 HyperChem Software.....53

Reference 54

Chapter 3: Time Dependent Crystal-Smectic Transformation in Perylene-Containing Polyimides

3.1. Introduction 57

3.2. Synthesis 59

3.2.1. Raw Materials 59

3.2.2. Synthesis Procedure 60

3.3. Results and Discussions 61

3.3.1. Synthesis and Solubility.....61

3.3.2. Thermal Characteristics.....62

3.3.3. Effect of Annealing on the UV-visible Absorption Behavior.....65

3.3.4. Chain Conformation 69

3.3.5. Mesomorphic Transition 76

3.3.6. Chain Folding 86

3.4. Conclusions 87

References 89

Chapter 4: Effect of 4,4'-(Hexafluoroisopropylidene)diphthalic Anhydride (6FDA) on the Structural Features of Perylene Containing Co-Polyimides

4.1 Introduction 92

4.2 Experimental 94

4.2.1 Materials 94

4.2.2 Characterization 95

4.2.3 Synthesis of Diamine 4 95

4.2.4 Synthesis of Alternating Copolyimides.....96

4.2.5 Synthesis of Block Perylene-containing Copolyimide with 6FDA (Cop80) 97

4.3 Results and Discussions.....98

4.3.1 Synthesis.....98

4.3.2 Viscosity and Solubility.....101

4.3.3 Thermal Analysis 103

4.3.4 UV-visible & Fluorescence Spectra 106

4.3.5 X-ray Diffraction.....110

4.4 Conclusion.....116

References 117

Chapter 5: Self-Assembled Vesicular Nanostructures of Perylene end-capped Poly (dimethylsiloxane)

5.1 Introduction 119

I. Poly(dimethyl siloxane)-endcapped-perylene (PDMS-end-perylene)

5.2 Experimental 120

5.2.1 Materials.....120

5.2.2 Synthesis of N-(2,5-di-tert-butylphenyl) Perylene-3,4-dicarboximide...122

5.2.3 Synthesis of perylene-3,4-dicarboxylic anhydride 123

5.2.4 Synthesis of PDMS-end-perylene M900 (6) (Scheme 5.2).....124

5.3 Results and Discussion 126

5.3.1 Synthesis.....126

5.3.2 Crystallization and Melting Behavoir 128

5.3.3 X-ray Diffraction.....131

5.3.4 UV-visible and Fluorescence Spectra 132

5.3.5 TEM Analysis 135

5.3.6 Conclusions.....143

II. Poly(dimethyl siloxane) Perylene Bisimides (PDMS Perylene Bisimide)

5.4 Synthesis of PDMS Perylene Bisimides D900 (9) (Scheme 5.3) 144

5.5 Results and Discussion 145

5.5.1 Synthesis.....145

5.5.2 Thermal Properties 147

5.5.3 X-ray Diffraction ..... .148

5.5.4 UV-visible Spectra..... .149

5.5.5 TEM Analysis 149

5.5.6 Conclusion 150

References 151

Chapter 6 Conclusions and Recommendations for Future Work

Conclusions 155

Recommendations for Future Work 157

LIST OF TABLES

Table 3.1 Results of thermogravimetric analysis (TGA) 65

Table 3.2 Comparison of the d-spacings and the relative intensities observed in the X-ray diffraction patterns for the various perylene polyimides.....75

Table 3.3 Observed IR wave numbers (cm^{-1}) and their assignments for PPI-12.....85

Table 4.1 Intrinsic Viscosities and Solubilities..... ...102

Table 4.2 Comparison of the X-ray *d*-spacings of the copolymers with the homopolymer PPI-12 113

LIST OF FIGURES AND SCHEMES

Figure 1.1 Structures of perylene bisimdes.....2

Scheme 1.1 Reaction of Perylene Dianhydride and Amines 3

Figure 1.2 Packing and d-spacing of perylene bisimides.....5

Figure 1.3 π-π stacking of perylene bisimides in the solid state involving longitudinal and transverse offsets.....6

Figure 1.4 Frontier orbitals for the N,N' model compound of perylene bisimide.....8

Figure 1.5 Molecular and simplified crystal structures for N,N'-dialkyl perylene bisimide pigments.....10

Scheme 1.2 The Mechanism of polyimide formation.....13

Figure 1.6 Chain-chain interactions between polyimides 18

Figure 1.7 UV-visible spectra of monomer and polymer PTDI 21

Figure 1.8 Fluorescence emission spectra of monomer and polymer PTDI 22

Figure 2.1 Schematic representation of DSC cell 38

Figure 2.2 Bragg construction illustrating the principle of diffraction where *d* is the spacing between two atomic planes 43

Figure 2.3 Schematic of the Bragg diffraction with the powder X-ray diffractometer used for the present study. Here, S_1, S_2 and S_3 are the divergence slit, receiving slit and scatter slit respectively; α = 1-4°.....44

Figure 2.4 Fitted profile of a diffractogram with overlap of peaks 45

Figure 2.5 Schematic of a Statton-type Warhus flat film camera (top) and the Bragg diffraction (bottom).....46

Figure 3.1 Schematic of the perylene-containing polyimide polymers studied.....59

Scheme 3.1 One-step condensation polymerization of perylene tetracarboxylic dianhydride and aliphatic diamines.....61

Figure 3.2 Thermogravimetric analysis curves of perylene polyimides with odd number spacers and even number spacers.....63

Figure 3.3 DSC thermograms of perylene polyimides with odd-spacer and even-spacer 64

Figure 3.4 The effect of annealing for different times, on the UV-visible absorption spectra of PPI-7 and PPI-12 at 320°C 66

Figure 3.5 The orientation of transition dipole moments (or molecular long axes) for linear H and J aggregates.....68

Figure 3.6 (a) Extended zig-zag conformation of PPI-12 with 3 monomer units (b) helical conformation of PPI-9 with 10 monomer units.....70

Figure 3.6 (c) extended conformation of PPI-9 when the aliphatic C-C bond is at about 90° with respect to the perylene plane; (d) and (e): schematics of the aliphatic C-C bond at 90° and 0° respectively, with respect to the perylene plane.....71

Figure 3.7 Variation of the longest d-spacing with the number of CH_2 groups in the spacer; and the lengths of the monomers, with the spacers in the extended conformation (calculated using HyperChem) 73

Figure 3.8 The variation of crystallinity of perylene polyimides, with the number of CH_2 groups in the spacer.....76

Figure 3.9 X-ray diffraction patterns of PPI-12 annealed for different times at 320°C.....77

Figure 3.10 X-ray diffraction patterns of PPI-10 with annealed at different temperatures and for various time.....78

Figure 3.11 X-ray diffraction patterns of PPI-7 annealed for different times at 320°C.....78

Figure 3.12 X-ray diffraction recorded on films: (a) diffraction of PPI-12, (b) diffraction of PPI-12 annealed for 4h at 320 °C; (c) diffraction of PPI-10, (d) diffraction of PPI-10 annealed for 4h at 320°C. 80

Figure 3.13 Isothermal thermogravimetric analysis curves of PPI-10 held for 9h at 320°C.....81

Figure 3.14 X-ray diffraction of PPI-12: (a) PPI-12 annealed 4 h at 320°C, then dissolved in m-cresol, and dried; (b) original PPI-12; (c) PPI-12 annealed 4h at 320°C.....83

Figure 3.15 X-ray diffraction patterns of PPI-12 annealed at 320°C in nitrogen and air atmosphere.....84

Figure 3.16 IR spectra of PPI-12: (a) original sample, (b) annealing for 6 h at 320°C.....84

Figure 3.17 Chain conformation of PPI-12 after dynamics 500ps by Cerius^2 86

Scheme 4.1 Synthesis of alternating perylene-containing copolyimide.....96

Scheme 4.2 Synthetic route of perylene-containing polyimides co-6FDA.....98

Figure 4.1 Thermogravimetric analysis (TGA) thermograms of copolymer Cop20, Cop40, Cop60, Cop80 and homopolymer PPI-12. 103

Figure 4.2a Differential scanning calorimeter (DSC) thermograms of copolymer Cop20, Cop40, Cop50, Cop60, Cop80 and homopolymer PPI-12 104

Figure 4.2b The relationship between Tg and the ratio of 6FDA in copolymers.....104

Figure 4.3 Differential scanning calorimeter (DSC) thermograms of alternating polymer — PPI-6FDA. 105

Figure 4.4a UV-visible absorption of copolymers in $CHCl_3$.....108

Figure 4.4b UV-visible absorption of Cop80 and Cop60 as films.....108

Figure 4.5a Fluorescent emission (λ_{exc} = 450nm) spectrum of Cop80 in chloroform.....109

Figure 4.5b Fluorescent emission (λ_{exc} = 450nm) spectrum of alternating copolyimide – PPI-6FDA in chloroform.....110

Figure 4.6a Powder-wide-angle X-ray diffractograms of copolymers.....111

Figure 4.6b Comparision of crystallinity of different ratio of copolymers with homopolymer PPI12.....111

Figure 4.7a Conformational map of 6FDA 114

Figure 4.7b Conformational map of bisphenol-A.....114

Figure 4.7 (c) Structure of 6FDA after using Ramachandran map and the energy minimized conformation; (d) conformation of two units of the copolymer by using Ramachandran map and the energy minimization; (e) conformation of 3 units of the homopolymer PPI-12.....115

Figure 5.1 Atomic position of N-(2,5-di-*tert*-butylphenyl) perylene-3,4-dicarboximide.....123

Scheme 5.1 Synthesis of perylene 3,4-dicarboxylic anhydride 124

Scheme 5.2 Synthesis of PDMS-end-perylene.....126

Figure 5.2 ^{1}H NMR of M900 using 400MHz NMR instrument 128

Figure 5.3 DSC thermograms of M900, (a) first heating, (b) cooling, and (c) second heating; (d) DSC thermogram of M3000 at the second run.....130

Figure 5.4 X-ray diffractogram of M1500.....131

Figure 5.5 Comparison of UV-visible spectra for M900 in mixtures of dichloromethane and hexane, mixture of chloroform and hexane, mixture of dichlorobenzene and carbon tetrachloride; M3000 in mixtures of dichloromethane and hexane.....133-4

Figure 5.6 Comparison of fluorescent spectra in mixtures of dichloromethane and hexane for M900 and M1500.....136

Figure 5.7 TEM images of (a) M900 in $CHCl_3$; (b), (c) cryo-TEM image of M900 in $CHCl_3$; (d) M900 in CH_2Cl_2/ Hexane (50:50); (e) M900 in hexane; (f) an enlarged view of a vesicle of M900 in hexane. The scale bars in b and c correspond to 100 nm.....139-141

Figure 5.8 Trilayer packing model of perylene end-cap PDMS (from molecular mechanics modeling using Hyperchem). 142

Scheme 5.3 Synthesis of PDMS perylene bisimides.....145

Figure 5.9 ^1H NMR of D900 146

Figure 5.10 DSC thermograms of D900, D1500, D3000 at the second run.....147

Figure 5.11 TGA thermograms of D900, D1500, D3000 148

Figure 5.12 X-ray diffraction of D900, D1500, and D 3000.....149

Figure 5.13 UV-visible absorption spectrum of D900 in different solvents.....150

Chapter 1

Introduction

1.1 Perylene Tetracarboxylic Acid Bisimides

Perylene tetracarboxylic acid bisimides, abbreviated as perylene bisimides (Figure 1.1), have received considerable attention in academic as well as industrial dye and pigment research for a long time. Perylene dyes were first discovered by Kardos[1] in 1913 as very lightfast dyes. After 1950, high grade perylene bisimides were found for industrial

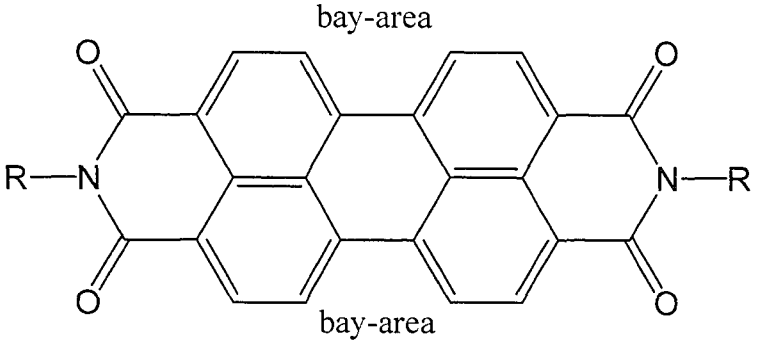

R = alkyl, aromatic or mixture substituents

Figure 1.1 Structure of perylene bisimides

applications as pigments (especially in automotive finishes) due to the favorable combination of insolubility and superior stability, light- and weather-fastness, thermal stability and chemical inertness as well as high tinctorial strength with colors ranging from red to violet, and even black shades.[2] After the high fluorescent potential[3] was discovered in 1959, novel applications arose from the strong fluorescence of the dyes in combination with other unique properties. Their high fluorescence quantum yield and photostability can be used in the field of laser dyes and fluorescent light collectors.[4-7] Recently, the applications of perylene bisimides focus on the field of electronic materials. In these applications, some researchers found that perylene bisimides are the best n-type

semi-conductors available today.[8,9] The n-type semiconductors are electron-acceptors, in which the majority charge carriers are electrons in the conduction band. In contrast, most organic materials are described as p-type of conductors (electron donors), in which holes in the valence band are the majority charge carriers. Furthermore, based on their unique combination of optical, redox, and thermal stabilities, perylene bisimides have been investigated for more than ten years in xerographic photoreceptors[10] and photovoltaics.[11]

1.1.1 Synthesis of Perylene Tetracarboxylic Acid Bisimides

Synthesis of perylene bisimides from dianhydrides and diamines is straightforward. It involves the condensation of perylene-3,4,9,10-tetracarboxylic dianhydride (PTDA) with the appropriate amines in a solvent.[12] The synthesis is extremely efficient and isolated yields are normally more than 90 %. A general reaction scheme is given in Scheme 1.1.

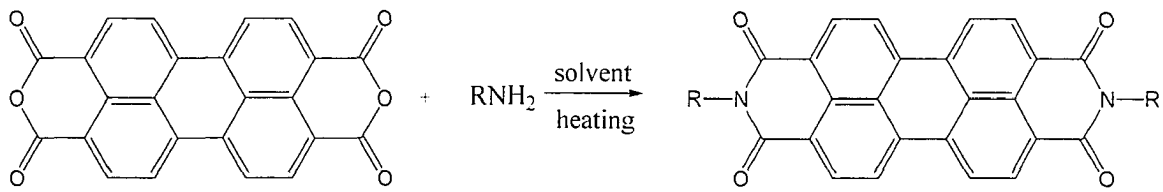

Scheme 1.1 Reaction of perylene dianhydride and amines.

The condensation reaction is stepwise.[13] The starting dianhydride reaction intermediate and the perylene products are not soluble in the reaction solvents. Thus, the synthesis typically involves the transformation of one red solid to another. Contamination of the perylene product by the starting dianhydride and/or the intermediate is common. While the concentration of impurities in perylene bisimides usually does not affect their

performance as colorants, impurities are certainly undesirable for photoconductive devices. Techniques to purify perylene bisimides, by washing perylene bisimides with alkaline solutions, in which the starting dianhydride and the intermediate become hydrolyzed and soluble, by acid pasting, or by vacuum sublimation are known in the dye industry.

Since perylene dianhydride is weakly reactive, the use of a catalyst is necessary. Typical catalysts are isoquinoline, imidazole, or even zinc salts such as zinc acetate or zinc chloride. The role of the zinc salts may be as a dehydrating agent, but is not clear. One interpretation is that the zinc salts might act as solubilizers since they may complex with the anhydride. As noted above, the dianhydride and the bisimide are insoluble in any organic solvent used for synthesis. However, their solubility is strongly increased by the addition of zinc salts.[14] The use of high boiling point protonic solvents, such as *m*-cresol, or chlorophenol etc., is also necessary. Most perylene bisimides are still insoluble in common solvents, and hence the current research activities are focused on designing soluble materials.

To improve the solubility of perylene bisimides, there are two different strategies which proved to be successful. The first one was to introduce solubilizing substituents at the imide nitrogen.[14] The solubilizing substituents included long-chain aliphatic groups, *tert*-butyl groups attached to aromatic groups, or long-chain secondary alkyl groups etc. The second strategy was to introduce substituents at the carbocyclic scaffold in the so-called bay-area (Figure 1.1). Seybold et al[6] at BASF were the first to introduce this approach. In

the bay area, chloride, bromide, cyano, and phenoxy are the most used functional groups. Due to the ease of synthesis, only the first method was used in this thesis.

1.1.2 Crystal Structure and Packing Behavior in the Crystal

According to X-ray diffraction studies of single crystals,[15,16] perylene bisimides are coplanar flat π –systems, which means all atoms of perylene bisimides are in the same plane. In the solid state, these platelet-like molecules then pack with each other, as shown in Figure 1.2.

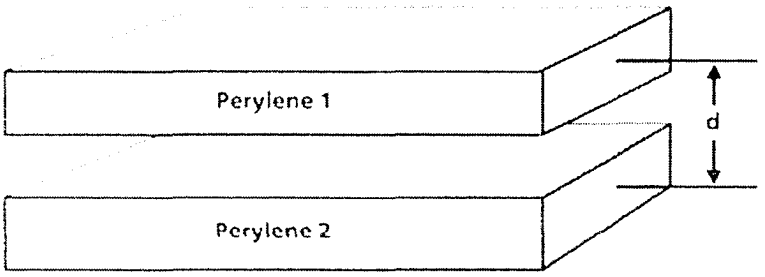

Figure 1.2 Packing and d-spacing of perylene bisimides (reproduced from ref. 17).

The packing of perylene bisimides has been fully studied by Graser, Hädicke and Klebe.[15] In their papers, the crystal structures of 18 perylene bisimides were discovered. The only difference between these 18 bisimides is the imide substituent. Six more derivatives have been reported recently by Zugenmaier *et al.*[16] All these imides exhibit similar crystal structures, which have planar geometry of perylene bisimides. These planes are arranged in parallel stacks. The distance between these planes is between 3.3 and 3.6 Å (for comparison, the distance between parallel planes of graphite is 3.35 Å).[15] However, the perylene planes do not fully overlap with each other. The offset

differentiates one perylene from another. Graser[15] and Kazmaier et al[17] set up a model (Figure 1.3). The model defined a transverse offset, which is the cross-shift of imide, and a longitudinal offset, which is the shift along the imide. The color of a dye is not only determined by the electronic properties of the individual molecular chromophores, but also is influenced by the electronic interactions with the vicinal molecules in the crystal. In perylene packing structure, the interaction between two planes is π-π stacking.

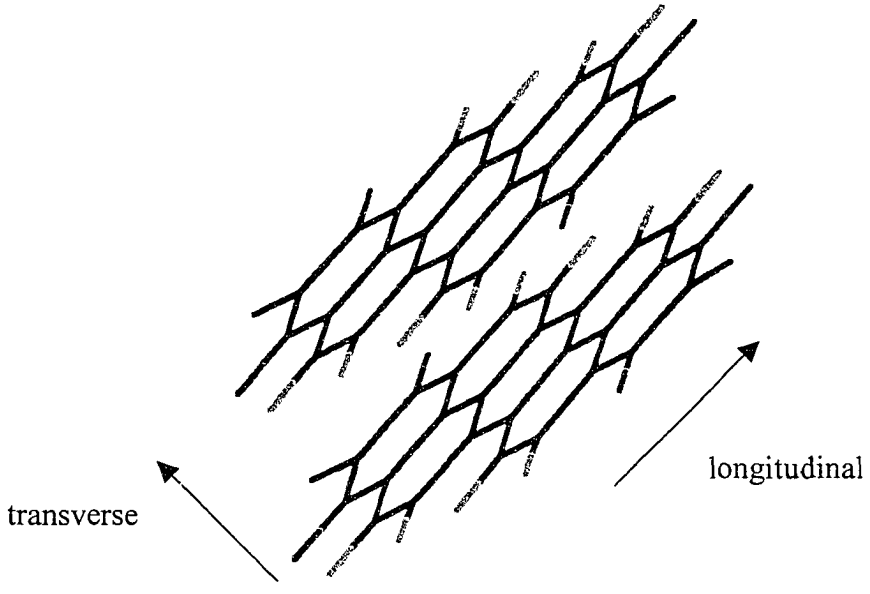

Figure 1.3 π-π stacking of perylene bisimides in the solid state involving longitudinal and transverse offsets.

Although the basic chromophore for perylene bisimide is identical, different substituents change the color of bisimides due to the difference of transverse offset and longitudinal offset. Thus, perylene bisimides may exhibit very different colors in the solid state depending on the packing of these bisimides, but they have almost identical absorption spectra in solution. According to Graser et al theory,[15] the color band depends on the overlap of neighboring perylene skeletons. An empirical model was established for

absorption maxima of the 18 perylene bisimides in solid state as functional of three crystal parameters: stacking perylene-perylene distance - *d*, transverse offset shift - *t*, and longitudinal offset shift - *l*. However, because most perylene bisimides in their crystal structures have similar interplanar d-spacing which is approximately 3.5 Å, *d* was not included in the empirical equation. As a result, the following equation giving the best determination of absorption maximum (λ_{max}):

$$\lambda_{max} = 9.718t^2 - 82.009t - 21.888l + 735.329 \qquad \text{(Equation 1.1)}$$

The longitudinal shift causes a linear change in the wavelength, while the change in absorption maximum has a much steeper dependence on the transverse shift. Therefore, the transverse shift in the stack is a more influential factor than longitudinal shift for the differences in color of the bisimides. As the width of perylene skeleton is around 4 Å, the transverse shift cannot be more than this distance. Otherwise, there is no overlap between neighboring molecules. Theoretically, the maximum of absorption will be 735 nm if the two molecules are superimposed. However, to avoid unfavorable interactions between the packed molecules in all compounds, a relative longitudinal and transverse shift was observed. For the 24 perylene bisimides,[15,16] the longest wavelength found was 625 nm.

1.1.3 Solution and Film Spectroscopic Behaviors

After the first discovery of the intense yellow-green fluorescence of perylene bisimides,[3] numerous perylene bisimides have been synthesized for applications as fluorescent dyes. However, the wavelength of fluorescence, like UV-visible absorption, does not depend on the nitrogen-substituents. Almost all perylene bisimides have the same yellow-green fluorescence. This can be explained by HMO-calculations (Hückel-approximation

molecular orbital) with usual hetero-atomic parameters[18] which showed that the wavefunctions have nodes in the orbitals at the nitrogens not only in HOMO (highest occupied molecular orbital) and LUMO (lowest unoccupied molecular orbital), but also in the orbital above LUMO and in the orbital below HOMO, i.e., perylene bisimides can be regarded as a closed chromophoric system with an S_0–S_1 transition (ground state to the first excited singlet state) which intensity and position remain unchanged by the respective imide substituents.[19] The frontier orbitals for the N,N' model compound are shown in Figure 1.4.[20]

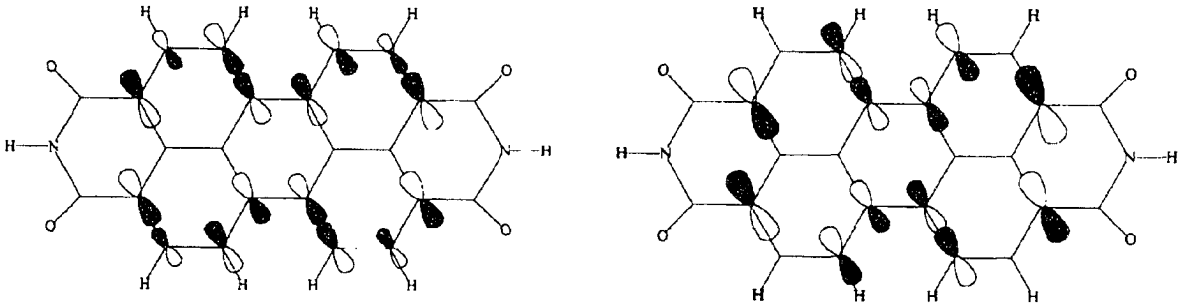

LOMO HOMO

Figure 1.4 Frontier orbitals for the N,N' model compound of perylene bisimide (reproduced from reference 20).

Perylene pigments in solid state have a red (or orange-red), red-brown, or purple blue appearance depending on the structure of the N-substituents. However, their solubility in common solvents is very low. In organic solvents, *N,N'*-dialkyl or N,N'-diaryl perylene bisimides exhibit UV-visible absorption at λ_{max} 510-530 nm with an extinction coefficient of (5-10) x 10^{-4} cm^{-1} M^{-1}.[21] The λ_{max} is not sensitive to the structure of the N-substituent. On the other hand, substituents in the perylene ring can induce either a bathochromic or a

hypochromic shift on the λ_{max}, depending on the nature and the position of the substituent. The magnitude of the ring-substituent-induced shift is in the range of 50 nm. The generally small spectral shift suggests that the π-π^* transition of perylene is localized in the perylene ring.

While the solution absorption wavelengths of N,N'-dialkyl perylene bisimides are independent of the N-alkyl group, the shapes of their solid-state UV-visible absorption bands are very sensitive to the structure of the N-alkyl group.[22,23] The appearance of thin films of N,N'-dialkyl perylene bisimides varies from red to red-brown to black. The effect of the N-alkyl group on the crystallographic properties and the solid-state absorption of N,N'-dialkyl perylene bisimides have been discussed in Section 1.1.2, which were studied by Graser and Hadicke,[15] and by Duff et al.[24] These authors have systematically shown that the solid-state absorption of N,N'-dialkyl perylene bisimides are dependent on the extent of the intermolecular interactions in the solid state. When the intermolecular interaction is strong, such as in the case of N,N'-di-n-propyl perylene bisimide, the absorption is panchromatic and the appearance is black. As the intermolecular interactions decrease, the absorbance of the long wavelength component decreases. Schematics of the three possibilities of intermolecular interactions are given in Figure 1.5. The color difference is due to displacements of the layers: black crystals are formed only if the longitudinal displacement is 27 to 30% of the length of a molecule and if the transverse displacement is less than 20% of the width of a molecule. The longitudinal displacement of 27 to 30% corresponds to a shift by the length of one

benzene ring. All red perylene imides exhibit larger transverse displacement and in part, different longitudinal displacements.

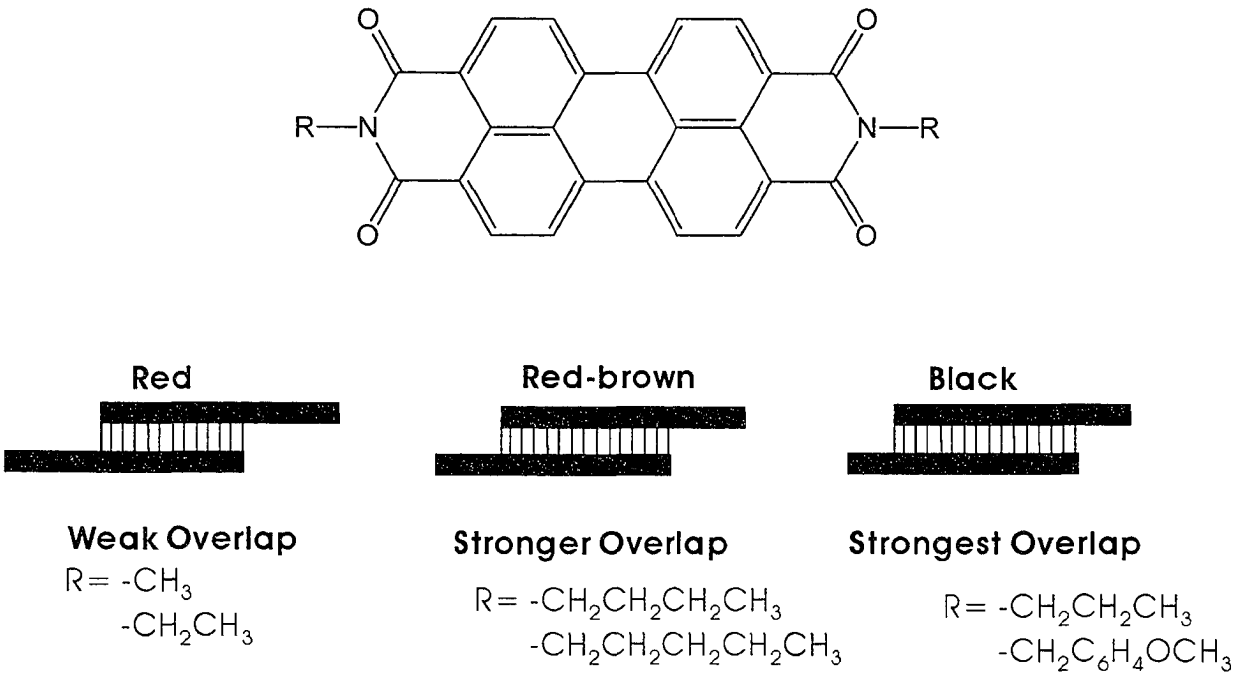

Figure 1.5 Molecular and simplified crystal structures for N,N'-dialkyl perylene bisimide pigments.

1.1.4 Liquid Crystalline Perylene Bisimides

Perylene derivatives are promising compounds for application in electronic devices such as molecular semiconductors. Most organic conducting materials can be described as p-type semiconductors, in which holes in the valence band are the majority charge carriers. In contrast, in *N,N'*-dialkyl-3,4,9,10-perylene tetracarboxylic acid bisimides the majority charge carriers are electrons in the conduction band, and this material is thus classified as an n-type semiconductor.[25,26]

Liquid crystals possess the ability to self-organize spontaneously into highly ordered structures. Due to the spontaneous ordering of the molecules in the liquid crystalline phase, very highly ordered films can be obtained after the liquid crystalline film is cooled to a crystalline phase. Therefore, the use of liquid crystalline perylene derivatives in organic p-n junctions is a promising method which may increase the efficiency of a solar cell. So far, only a few liquid crystalline perylene derivatives have been synthesized.[27-33]

1.2 Polyimides

Polyimides are polymers containing cyclic imide groups in the main macromolecular chain. Depending on the structure of the radicals attached to the imide group, polyimides can be aliphatic, alicyclic, or aromatic and linear or three dimensional. Since only aromatic linear polyimides have found wide practical application, most of the publications focus on them. The first synthesis of an aromatic polyimide was performed by Bogert and Renshaw in 1908.[34] However, a high molecular weight polyimide was not prepared until 1955 by Edwards and Robinson.[35] The first aromatic polyimides prepared and studied were polypyromellitimides obtained from pyromellitic dianhydride and various diamines by Sroog et al.[36] They described the synthesis of polyimides derived from the polycondensation of pyromellitic dianhydride (PMDA) with a variety of aromatic diamines. The synthetic approach to these highly insoluble polyimides was to make a precursor poly(amic acid) solution in either N,N-dimethylformamide (DMF) or N,N-dimethylacetamide (DMAc). The precursor solution was then cast into a film and thermally imidized to give the corresponding polyimide. Although this report is almost 40 years old, it is still commonly used today for polyimide synthesis, both in research and

production facilities. This early work led to the first commercial polyimide derived from PMDA and ODA (4,4'-oxydianiline) by DuPont, which is sold as a thin film as Kapton®.[37]

1.2.1 Synthesis of Polyimides

Synthesis of polyimides is similar to the synthesis of bisimides. Polyimides are usually synthesized by polycondensation of an aromatic dianhydride and a diamine. The polymerization can be done in one-step process or two-step process via a poly(amic acid). In the latter process, the poly(amic acid) is hydrolytically unstable and the molecular weight decreases with time, therefore, the use of two-step process is limited. On the other hand, polyimides obtained by melt polymerization or one-step process are more flexible and easily processable. So the one step process is more useful for research synthesis. Typically, the dianhydride and diamine are stirred in a high boiling organic solvent at 180-220°C.[38] Under these conditions, chain growth and imidization essentially occur spontaneously. The water generated from imidization is usually allowed to distill off from the reaction mixture. Nitrobenzene, chlorophenol, and *m*-cresol are the most widely used solvents. The one step method is especially useful in the polymerization of unreactive dianhydrides, such as perylene dianhydride, and diamines. Another interesting feature of the one step method is that it can yield a material with a higher degree of crystallinity than the one obtained from the two step method. The excellent solvation of the polymer at high temperature may allow it to obtain a more favorable conformation for packing.

The mechanism of polyimide formation is illustrated using a monofunctional species in Scheme 1.2.[39] Nucleophilic attack of the nitrogen of an amine to the carbonyl group of a dianhydride gives an intermediate amic acid which is then converted to the corresponding imide at elevated temperature or upon treatment with a chemical dehydrating agent such as acetic anhydride.

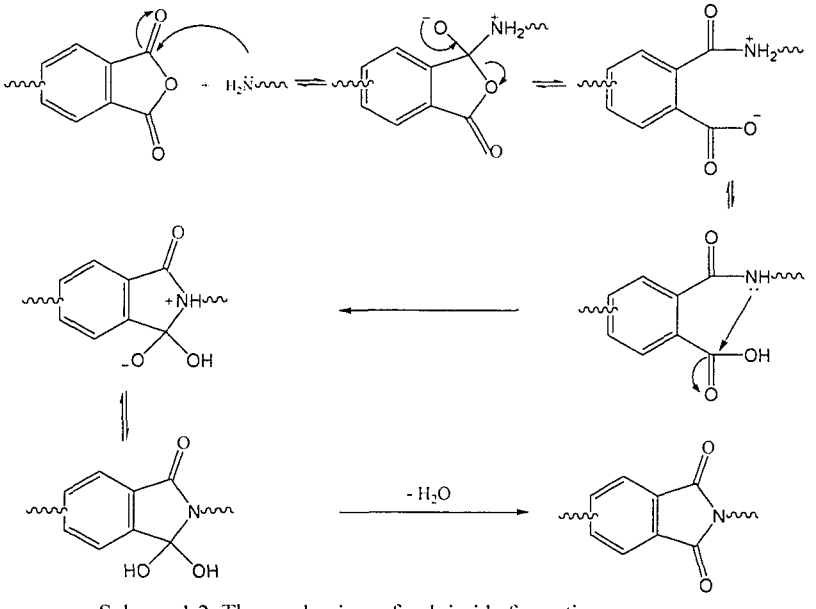

Scheme 1.2. The mechanism of polyimide formation.

1.2.2 Structure-Property Relationships of Polyimides

The chemical structures of aromatic polyimides and their derivatives are very varied, which corresponds to a great diversity in their physical properties. At the same time, such properties as chain conformation, the ability to crystallize and ordering of the molecular structure in bulk are determined only by the main features of the chemical structure of polyimide monomer units, such as the length of the rigid cyclic part, and the presence or absence of flexible joints and their location in the unit.

Data on the molecular structure of polyimides are mainly based on x-ray investigations. But, it is very difficult to obtain a highly ordered crystalline structure for many polyimides. In that case, theoretical model and calculation become more important. The success of the application of x-ray diffraction theory to the investigation of polymers depends not only on the structure of repeating units but also to a much greater extent on the degree of order of their arrangement in the real system. The latter alone determines the quantity of reflections on the diffraction pattern. For polymers, this quantity is small and insufficient for complete calculation of the structure up to the atomic coordinates in the unit cell. Hence, several models for the atomic structure of the theoretical x-ray diffraction patterns are calculated and compared with the experiment results. And additional confirmation of the correct choice may be obtained by other physical methods: UV-visible absorption, IR spectroscopy, NMR, measurement of density and other physical characteristics of samples.

1.2.3 Structural Modification of Polyimides

Since aromatic polyimides were developed in the 1960s, they have been of great technological importance due to their outstanding thermal and electrical properties. However, their applications have been limited in many fields because aromatic polyimides are normally insoluble in common organic solvents and have extremely high glass transition or melting temperatures, which preclude melt processing. This low solubility and poor processability has been proposed to be due to the strong polymer chain-chain electronic interaction occurring between the electron deficient pyromellitimide moieties and the electron rich phenyl rings within the polyimide

backbone.[39] The chain-chain interaction makes the polymer pack extremely well in the solid state. Evidence of this electronic interaction is often seen in enhanced color of polyimides.[40]

Modifications are necessary to increase solubility. The main approaches used for structural modifications include:

(1) Introduction of a flexible, thermally stable unit into the polymer chain.

Polyimides with aliphatic linkages, such as those derived from PMDA, usually have lower thermal stability. In order to maintain good thermal stability, it is common to use flexible units containing thermally stable groups, such as, "O", "C=O", "O=S=O", "S", and "$C(CF_3)_2$" (*6F*). The *6F* group is especially interesting, since incorporation of the *6F* unit into the polymer chain usually increases the solubility, thermal stability, flame resistance, and oxidation resistance, while decreasing the crystallinity.[39] High thermal stability of the *6F*-containing polyimides is attributed to the strong C-F bond. However, the *6F*-containg monomers are usually expensive, which consequently limits the scope of applications of *6F*-containing polyimides.

Although the rigidity and the inter-chain interaction of polyimides can effectively be reduced by incorporating flexible linkages into their polymer backbone, the high-temperature performance associated with the rigid parent polymer is compromised with the increased flexibility of the polymer chains.

(2) Incorporation of large polar or non-polar substituent into the polymer backbone. Incorporating bulky pendant groups along the polyimide chain can inhibit chain packing and therefore allow less interaction to occur between the polymer chains. As a result, the solubility of the polymers increases while the high temperature properties remain because the overall polyimide chain is still rigid. Both diamine and dianhydride monomers containing various non-polar and polar pendant groups have been synthesized and polymerized to produce soluble yet rigid polyimides.

(3) Disruption of symmetry and recurring regularity in the polymer backbone through copolymerization of two dianhydrides or two diamines.

Copolymerization is an alternative way to modify polymer properties to meet a specific requirement. The disruption of symmetry and recurring regularity through copolymerization of two dianhydrides or two diamines can reduce the chain-chain interaction and crystallinity of rigid polyimides. Consequently, copolymerization is one of the most convenient methods to improve the solubility of polyimides. It is especially desirable to use a copolymerization method for improving the solubility of poly(pyromellitimide)s derived from the stiff diamines (*p*-phenylenediamine or 4,4'-benzidine). In the past, all effects towards structural modifications on PMDA or on *p*-phenylenediamine and benzidine failed to result in organo-soluble poly(pyromellitimide)s without introducing flexible linkages within the polymer chain. To maintain the rigidity of poly(pyromellitimide)s, it is preferable to use a second dianhydride, with the smallest ratio of poly(pyromellitimide)s. However, the best results reported so far are poly(pyromellitimide)s containing at least 50% of the other flexible dianhydride with , in

most case, diamines containing flexible linkages. For example, copolyimides synthesized from PMDA, BPDA and 9,9'-bis(4-aminophenyl)fluorine were soluble in amide solvents and 1,1,2,2-tetrachloroethane (TCE), when the BPDA content reached above 50 mol%.[26] Another report described the synthesis of perfect alternating copolyimides via amic ester precursors, from PMDA and 6FDA with *m*-phenylenediamine and *p*-phenylenediamine.[41] The resulting alternating copolyimides were more soluble than the corresponding random ones.

1.2.4 Chain-Chain Interaction of Polyimides

It is proposed that polyimide chains interact with each other via a charge-transfer or electronic polarization mechanism. It is sufficient to take into account the strongest interchain, i.e., the dipole-dipole interactions between high polarity C=O groups. With such assumptions, the behavior of interacting polyimide chains can be illustrated by the schematic mechanical models in Figure 1.6. These dipole-dipole interactions as hinges prevent free rotation around them. This research was based on spectral absorption shifts in the UV-visible range. Figure 1.6 shows the interactions between polymer chains. This interaction should predominate in a linear aromatic polyimide, and will be primarily dependent on the electron affinity of the dianhydride-derived moiety and electron availability (ionization potential) of the diamines-derived moiety. This is caused by charge transfer between electron-donating diamines fragment and electron-accepting bisimide fragment. The charge transfer occurs either intra- or inter-molecularly.

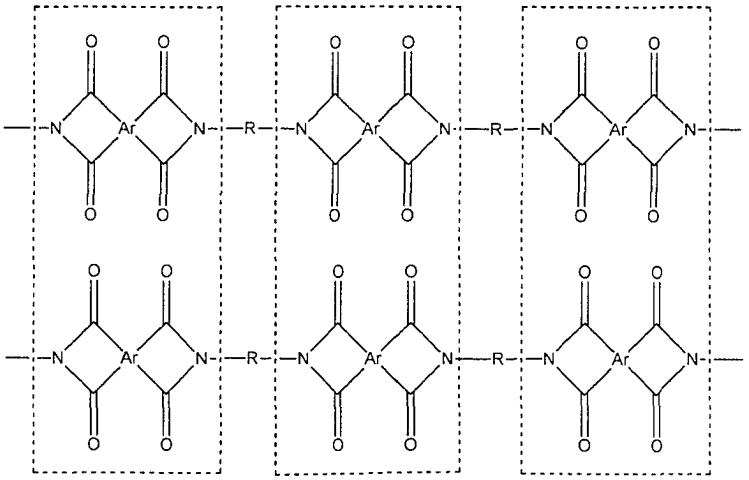

Figure 1.6 Chain-chain interactions between polyimides (*Ar* is aromatic ring, and *R* is spacer, either aromatic or aliphatic).

1.3 Perylene Polyimides

1.3.1 Synthesis of Perylene Polyimides

Little information is available on the synthesis of perylene polyimides (PPI), since 3,4,9,10-perylene tetracarboxylic dianhydride (PTDA) is a low-reactive monomer. This is explained, for example, by the fact that a six-membered anhydride ring has no strain.[42] Another reason is that the six-membered anhydride rings exhibit a lower electrophilic reactivity than their five-membered analogs.[43] In addition, PTDA is poorly soluble in organic solvents, and the introduction of rigid perylene moieties into polyimides hampers the formation of high-molecular-mass products. Like perylene bisimides, reaction in high boiling point solvents and base catalysts are necessary.

The first polymeric perylene dyes was reported by Langhals.[44] Afterwards, perylene copolyimides was reported by Ghassemi et al.[45] They synthesized bis(N-amino perylene imide) with dianhydride of 2,2-bis[4-(3,4-dicarboxyphenoxy) phenyl]propane (dianhydride A) and also with other dianhydrides in *m*-cresol or dichlorobenzene to form crystalline homopolymer or copolymers.

More interestingly, Icil et al[46] synthesized a PPI from PTDA and 1,12-diaminododecane in *m*-cresol in the presence of isoquinoline. Although this PPI contained long aliphatic fragments in the polymer chain, it exhibited thermal stability up to 475°C and had a softening temperature of 325°C. In this work, IR, UV, fluorescence spectroscopy and thermal properties were studied. More detailed work for the study of similar compounds was reported by Wang et al.[47] After annealing, PPI films showed a red-shift in UV-visible absorption and improved photosensitivity due to an increase in crystallinity, as indicated by wide-angle x-ray diffraction measurements.

Furthermore, in order to increase solubility and improve processability, few authors synthesized perylene-containing copolyimides. Yang M. et al[48] designed and synthesized a copolyimides by a one–step polycondensation of one cardo diamines, with PTDA and 4,4'-(hexafluoro-isoproplylidene)diphthalic anhydride (6FDA). The electroluminescence properties of that copolyimide were studied by fabricating and characterizing single layer electroluminescent devices using this copolyimide as active layer. However, the ratio of two dianhydride, PTDA and 6FDA is low, which is 5:95. Otherwise the copolymer will not dissolve in common solvents. Huang W. et al[49] synthesized a copolyimides by PTDA,

pyromellitic dianhydride (PMDA) and 4,4'-methylene-bis-(2-*tert*-butylaniline) (MBTBA). The properties, such as fluorescence, stability, and Tg, were studied. In their study, the mole ratio of PDTA remains very low, between 0.08 to 2.84 mole%.

1.3.2 Spectroscopic Properties of Perylene Polyimides

1.3.2a UV-visible absorption

Almost all perylene polyimides have the same patterns and very similar absorption positions compared to their monomers. Also those absorption peaks come from the conjugation of aromatic perylene rings. There are very few with conjugation with diamines fragments because the rigid perylene dianhydride has problems to react with aromatic diamines. Furthermore, in order to synthesize the processable polymers, peryelene dianhydride usually react with more flexible diamines, which results in lacking the conjugation of the polymer chains. Therefore, the absorption of most perylene polyimides has three peaks. For example, perylene-3,4,9,10-tetracarboxyl-bis-N,N'-dodecyl-polyimide (polymer PTDI) has the absorption peaks at 525 (peak 1), 489 (peak 2), 458 (peak 3) nm (Figure 1.7).[46] However, the relative intensities are strongly dependent on the N-substitution. This difference results from different aggregation in the solvents. Neuteboom et al[50] studied perylene polyimide including polytetrahydrofuran, which showed the length of polytetrahydrofuran change the relative absorption intensities due to forming H-type aggregates in o-dichlorobenzene. The longer polytetrafuran spacer had strong aggregates.

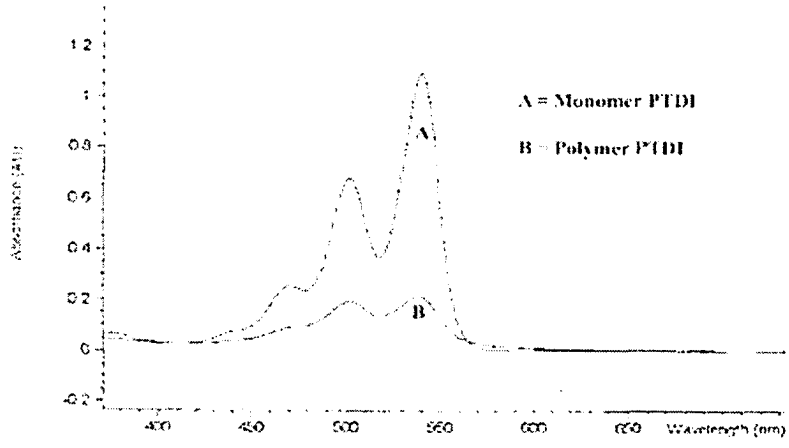

Figure 1.7 UV-visible spectra of monomer PTDI (a), polymer PTDI (b) in acetonitrile (Reproduced from reference 46).

1.3.2b Fluorescent Spectra

The fluorescence spectra show the mirror-image symmetry with the absorption spectra, such as, perylene-3,4,9,10-tetracarboxyl-bis-N,N'-dodecyl-polyimide shows three bands at 533, 553, and 651 nm from singlet excited states (Figure 1.8).[46] Most perylene polyimides are fluorescent. However, the intensities are weaker than their monomers.

Probably it is due to the aggregation of the polymers. It is apparent that the less soluble aromatic polyimide would show higher aggregation and weaker fluorescence. Furthermore, similar to the absorption, emission bands are also not influenced by the type of substituents.

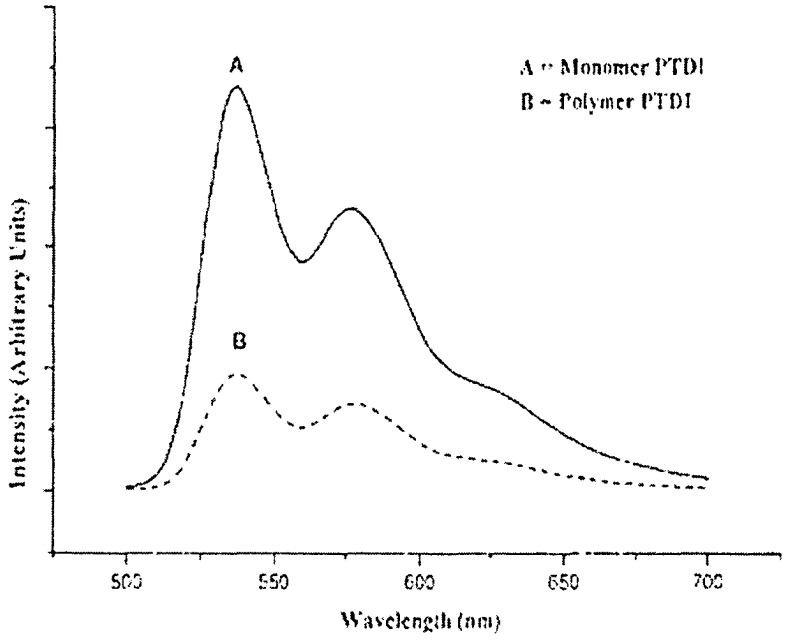

Figure 1.8 Fluorescence emission spectra of monomer PTDI (a), and polymer PTDI (b) in acetonitrile by excitation wavelength at 485 nm (Reproduced from reference 46).

1.3.2c Infrared Spectra

Vibrational spectroscopy is a unique technique to determination of the overall structure, chemical, mechanical and localized intermolecular interactions for materials, especially in thin film. In particular, the intensity in the vibrational spectrum of thin solid films can be explained in terms of the polarization of the incoming infrared beam and the directionality of the dipole moment derivatives. Transmission and reflection spectroscopic techniques can be used concurrently to enable a definitive account of the molecular orientation of perylene molecules.[51] Aroca et al[52] extensively studied infrared and Raman spectra by both transmission and refection absorption infrared spectroscopy

(RAIRS) for perylene bisimides. Vibrations of chromophore moiety can be limited to a few characteristic in-plane and out-of-plane vibrations. For instance, for perylene N,N'-bispropylimide,[53] the most characteristic in-plane molecular vibrations of perylene bisimides are the carbonyl stretching modes: the antisymmetric stretching at 1662 cm^{-1} and the symmetric stretching at 1697 cm^{-1}. The strongest in-plane C=C stretching vibration is 1595 cm^{-1}. The out-of-plane wagging vibrations of the perylene ring have a dynamic dipole perpendicular to the perylene plane and thereby perpendicular to components of the dipole moment derivatives of the carbonyl or C=C stretching vibrations. The out-of-plane modes are observed with characteristic wavenumber and relative intensity at 746 cm^{-1} and 810 cm^{-1}. Again, vibrational spectrum of polymer is similar to its monomer. The spectrum of perylene-3,4,9,10-tetracarboxyl-bis-N,N'-dodecyl-polyimide had only a little bit lower resolution than its monomer.[46]

1.3.3 Thermal Properties

Like other polyimides, perylene polyimides have superior thermal and photostabilities. Basically, polyimides coupling with long aliphatic chain diamines have less stabilities than aromatic diamines. Wang et al[47] studied a series of perylene polyimides including three to twelve methylene spacers. All of them were quite thermally stable in nitrogen. For 5% weight loss, the decomposition temperatures were range from 410 to 486 °C. It is noted that the long alkylene chains are responsible for the low thermal stability, i.e., as the number of methylene groups in the polymer chain increased, the decomposition temperature decreased.[54,55] Perylene polyimides with aromatic diamines segments have little better stabilities.[56]

The glass transition temperatures (T_g) of perylene polyimides with aliphatic spacers could not be detected by DSC.[47,55] This is probably due to the strong π-π stacking of perylene. Furthermore, in the case of rod-like polyimides, the transition became very weak or not detectable.[57] However, most polyimides with aromatic diamine segments have T_g between 300 to 400 °C.[56] Those extremely high transition temperatures made the polyimides difficult to process. Many researchers synthesized copolymers.[56] The transition temperatures of the copolymers can be reduced to 150 °C.

1.3.4 Solubilities of Perylene Polyimides

Solubilities of perylene polyimides are low in common organic solvents. Perylene polyimides with long aliphatic spacer, such as, twelve methylene units, can partially dissolve in some solvents, such as, chloroform, or *m*-cresol. The solution can easily be used for UV-visible absorption and fluorescence spectrum. However, the solubilities are still too low for casting films. Thus, copolymerization is necessary. 6FDA is the common dianhydride for increasing solubilities, in the case of copolymerization.[58]

1.4 Thesis Outline and Objective

Perylene bisimides are thermally and photochemically stable organic semiconductors. As molecules, they have been incorporated in electronic and optical devices such as field-effect transistors,[59] xerography,[10] and photovoltaic devices.[11] However, for many applications, processability and especially film formation is a pre-requisite. Blending is a common way to incorporate dyes into a polymer matrix. However, blending presents the

serious drawback of dye migration upon aging. To avoid the disadvantage of dye migration, chromophores must be covalently attached to polymers. The polymer structure brings the additional advantage of three-dimensional stability. The objective of this thesis is to find the structure and morphology of perylene based polymers. After surveying the perylene-based polymers, or copolymers, we try to make novel processable polyimides and self-assembly into morphologies and try to find potential application in photoconducting field.

Due to these requirements, some perylene polyimides, copolyimides, and endcapped PDMS were chosen for studying in this thesis. Three kinds of polymers were investigated:

(1) In Chapter 3, the crystalline conformations of perylene polyimides (PPIs), with alkyl spacers varying in length from C_3 to C_{12} are described. Although modeling of single chains would suggest the possibility that those with odd number of CH_2 groups adopt a flat helical shape, X-ray diffraction suggests that the chains with odd and even spacers have the same conformation, due to the necessity to pack the perylene units. Upon annealing, the UV-visible absorption maximum red-shifts by about 10 nm, indicating enhanced π-stacking between the perylenes. Several changes in the spectra are seen with an increase in annealing time, at a given temperature. With an increase in annealing time, X-ray diffraction patterns show changes in the number of reflections, indicative of a crystal to mesogenic transition. The time required for this transition increases with a

decrease in the spacer length, and annealing temperature, suggesting that the dynamics of this transition is very slow.

(2). Chapter 4 describes the work on a series of perylene-containing block copolyimides with different ratios of perylenetetracarboxylic dianhydride (PPI-12) and 4,4'-(hexafluoro-isopropylidene) diphthalic anhydride (6FDA). Copolymerization were studied to improve the solubility and the copolyimides with a low percentage (less than 20% of total dianhydrides) of perylene becomes highly soluble in conventional solvents, such as, $CHCl_3$, CH_2Cl_2, or THF etc. The positions of the absorption maxima in the UV-visible spectra do not change with 6FDA concentration, but the relative intensities do. Although the homopolymer PPI-12 does not show a distinct glass transition, its T_g was derived by extrapolation of the DSC results with the copolymers. The copolymers are semi-crystalline up to a concentration of 60% (mol) 6-FDA. It is of interest that the spacings of X-ray reflections also do not change with the addition of 6FDA. This is rationalized on the basis that the conformation of the 6FDA segment does not cause any significant difference in the preferred conformational shapes of the homopolymer of PPI-12. Due to this "*conformational* isomorphism" 6FDA is not a significant chain "kinker" in this case.

(3) In Chapter 5, we designed a new approach to novel perylene-based self-assembled structure. Self-assembly of the perylene segment leads to vesicle formation of perylene end-capped poly(dimethyl siloxane) (perylene end-cap-PDMS) in non-aqueous media. The perylene self assembles into crystalline aggregate, with a well-defined melting

temperature, and reversible melting and crystallization. The absorption spectra depend on the solvent used. TEM images of the vesicles show either a bilayer or a trilayer structure depending on the solubility parameter of the solvent. This initial attempt to prepare such vesicles in non-aqueous media may be applicable to similar systems.

References

1. Kardos, M. *Ber.* **1913**, *46*, 2068.

2. Herbst, W.; Hunger, K., *Industrial Organic Pigments: Production, Properties, Applications*, 2nd ed., WILEY-VCH: Weinheim, 1997.

3. Geissler, G.; Remy, H. (Hoechst) *Ger. Pat. Appl.* DE 1130099 (Oct. 14, 1959) (*Chem. Abstr.*, 1962, *57*, P11346f).

4. (a). Sadrai, M.; Bird, G. R. *Opt. Commun.* **1984**, *51*, 62–64; (b). Löhmannsröben, H.-G.; Langhals, H. *Appl. Phys. B* **1989**, *48*, 449–452; (c). Reisfeld, R.; Seybold, G. *Chimia* **1990**, *44*, 295–297.

5. Ford, W. E.; Kamat, P. V. *J. Phys. Chem.* **1987**, *91*, 6373–6380.

6. (a). Seybold, G.; Wagenblast, G. *Dyes Pigm.* **1989**, *11*, 303–317; (b). Seybold, G.; Stange, A. (BASF AG), *Ger. Pat.*, DE 35 45 004, 1987(*Chem. Abstr.*, **1988**, *108*, 77134c).

7. Gvishi, R.; Reisfeld, R.; Burshtein, Z. *Chem. Phys. Lett.* **1993**, *213*, 338–344.

8. Struijk, C. W.; Sieval, A. B.; Dakhorst, J. E. J.; Van Dijk, M.; Kimkes, P.; Koehorst, R. B. M.; Donker, H.; Schaafsma, T. J.; Picken, S. J.; vande Craats, A. M.; Warman, J. M.; Zuilhof, H.; Sudhölter, E. J. R. *J. Am. Chem. Soc.* **2000**, *122*, 11057–11066.

9. Dimitrakopoulos, C. D.; Malenfant, P. R. L. *Adv. Mater.* **2002**, *14*, 99–117.

10. Law, K.-Y. *Chem. Rev.* **1993**, *93*, 449–486.

11. (a). Schmidt-Mende, L.; Fechtenkötter, A.; Müllen, K.; Moons, E.; Friend, R. H.; MacKenzie, J. D. *Science* **2001**, *293*, 1119–1122; (b). Yakimov, A.; Forrest, S. R. *Appl. Phys. Lett.* **2002**, *80*, 1667–1669.

12. Langhals, H. *Chem. Ber.* **1985**, *118*, 4641.

13. Nagao, Y.; Misono, T. *Bull. Chem. Soc. Jpn.* **1981**, *54*, 1191.

14. Langhals, H. *Heterocycles* **1995**, *40*, 477–500.

15. (a). Graser, F.; Hädicke, E. *Liebigs Ann. Chem.* **1980**, 1994–2011; (b). Graser, F.; Hädicke, E. *Liebigs Ann. Chem.* **1984**, 483–494; (c). Hädicke, E.; Graser, F. *Acta Crystallogr., Sect. C* **1986**, *42*, 189–195; (d). Hädicke, E.; Graser, F. *Acta Crystallogr., Sect. C* **1986**, *42*, 195–198; (e). Klebe, G.; Graser, F.; Hädicke, E.; Berndt, J. *Acta Crystallogr., Sect. B* **1989**, *45*, 69–77.

16. Zugenmaier, P.; Duff, J.; Bluhm, T. L. *Cryst. Res. Technol.* **2000**, *35*, 1095-1115.

17. Kazmaier, P.M.; Hoffmann, R. *J. Am. Chem. Soc.* **1994**, *116*, 9684-9691.

18. Heilbronner, E. *HMO Model and Its Applications*, Wiley: London, 1976.

19. Langhals, H.; Demmig, S.; Huber, H. *Spectrochim. Acta* **1988**, *44A*, 1189–1193.

20. Mercadante, R.; Trsic, M.; Duff, J.; Aroca, R. *J..Mol. Struct. (Theochem)* **1997**, *394*, 215-226.

21. Iden, R.; Seybold, G.; Stange, A.; Eilingsfeld, H. *Forschungsber.-Bundesminist. Forsch. Techno.* **1984**, BMFT-FB-T, 84-164 (*Chem. Abstr.* **1985**, *102*, 150903k).

22. Borsenberger, P. M.; Regan, M. T.; Staudenmayer, W. J. U.S. Patent 4,578,334, **1986**.

23. Tamizhami, G.; Dodelet, J. P.; Cote, R.; Gravel, D. *Chem. Mater,* **1991**, *3*, 1046.

24. Duff, J. M.; Hor, A. M.; Melnyk, A. R.; Teney, D. *Hard Copy and Printing Materials, Media, and Process. Proc. SPIE-Znt. Soc. Opt. Eng.* **1990**, 183.

25. Meyer, J.-P.; Schlettwein, D.; Wöhrle, D.; Jaeger, N. I. *Thin Solid Film,* **1995**, *258*, 317-324.

26. Horowitz, G.; Kouki, F.; Spearman, P.; Fichou, D.; Nogues, C.; Pan, X.; Garnier, F. *Adv. Mater,* **1996**, *8*, 242-245.

27. Cormier, R. A.; Gregg, B. A. *Chem. Mater.* **1998**, *10*, 1309-1319.

28. Schlichting, P.; Rohr, U.; Müllen, K. J. *Mater. Chem.* **1998**, *8*, 2651-2655.

29. Pressner, D.; Göltner, C.; Spiess, H. W.; Mu¨llen, K. *Acta Polym.* **1994**, *45*, 188-195.

30. Göltner, G.; Pressner, D.; Müllen, K.; Spiess, H. W. *Angew. Chem.* **1993**, *105*, 1722-1724.

31. Müller, G. R. J.; Meiners, C.; Enkelmann, V.; Geerts, Y.; Müllen, K. J. *Mater. Chem.* **1998**, *8*, 61-64.

32. Rohr, U.; Schlichting, P.; Böhm, A.; Gross, M.; Meerholz, K.; Bräuchle, C.; Müllen, K. *Angew. Chem., Int. Ed. Engl.* **1998**, *37*, 1434-1437.

33. Liu, S.; Sui, G.; Cormier, R. A.; Leblanc, R. M.; and Gregg, B. A. *J. Phys. Chem. B* **2002,** *106,* 1307-1315

34. Bogert, T. M.; Renshaw, R. R. *J. Am. Chem. Soc.* **1908**, *30*, 1140

35. Edwards, M. W.; Robison, I. M. *U.S. Pat.* 2710853 to E.I. DuPont de Memours & Co. **1955.**

36. Sroog, C. E.; Endrey, A. L.; Abramo, S. V.; Berr,A. C. E.; Edwards, W. M.; Olivier, K. L. *J. Polym. Sci. A* **1965**, *3*, 1373-1390.

37. Hergenrother, P. M. *Angew. Chem. Int. Ed. Engl.* **1990**, *29*, 1262

38. Harris, F. W.; Norris, S. O.; Lanier, L. H.; Reinhardt, B. T.; Case, R. D., Varaprath, S; Padaki, S. M.; Torres, M.; and Feld, W. A. in *Polyimides*: *Synthesis, Characterization and Applications*, Vol. 1, Ed. Mittel, K.L., Plenum: New York, 1984, pp3-14.

39. Wilson, D.; Stenzenberger, H. D.; Hergenrother, P. M. *Polyimides*, Blackie and Son: Glasgow, 1990.

40. Fieser, L. F.; Fieser, M. *Organic Chemistry* 2nd, D. C. Heath and Co., 1980, p624.

41. (a) Rhee, S. B.; Park, J. W.; Moon, B. S.; Chang, J. Y. *Macromolecules* **1993**, *26*, 404. (b) Park, J. W.; Lee, M.; Lee M.-H.; Liu, J. W.; Kim, S. D.; Chang, J. Y.; Rhee, S. B. *Macromolecules* **1994**, *27*, 3459.

42. Eberson, L.; Landstrom, L. *Acta Chemica Scandinavica* **1972**, *26*, 239-249.

43. Sek, D.; Pijet, P.; Wanic, A. *Polymer* **1992**, *33*, 190-193.

44. Langhals, H. *Chemical Physics Letters* **1988**, *150*, 321-324.

45. Ghassemi, H.; Hay, A. S. *Macromolecules* **1994**, *27*, 4410-4412.

46. Icil, H.; Icli, S. *J. Polym. Sci. Part A: Polym. Chem.* **1997**, *35*, 2137-2142.

47. Wang, Z. Y.; Qi, Y.; Gao, J. P.; Sacripante, G. G.; Sundararajan, P. R.; Duff, J. D. *Macromolecules* **1998**, *31*, 2075-2079.

47. Yang, M.; Xu, S.; Wang, J.; Ye, H.; Liu, X. *J. Appl. Polym. Sci.* **2003**, *90*, 786-791.

49. Huang, W.; Yan, D.; Lu, Q; Huang, Y. *Europ. Polym. J.* **2003**, *39*, 1099-1104.

50. Neuteboom, E. E.; Meskers, S. C. J.; Meijer, E. W.; Janssen, E. A. J. *Macromol. Chem. Phys.* **2004**, *205*, 217-222.

51. Johnson, E.; and Aroca, R. *Appl. Spectrosc.* **1995**, *49*, 472.

52. (a). Rodriguez-Llorente, S.; Aroca, R.; Duff, J. *J. Mater. Chem.* **1998**, *8*, 629-632. (b). Rodriguez-Llorente, S.; Aroca, R.; Duff, J. *Spectro. Acta* **1999**, *A55*, 969-978. (c). Rodriguez-Llorente, S.; Aroca, R.; Duff, J.; de Saja, J.A. *Thin solid films* **1998**, *317*, 129-132.

53. Kam, A.; Aroca, R. *Chem. Mater.* **1998**, *10*, 172-176.

54. Karayannidis, G.; Stamelos, D.; Bikiaris, D. *Makromol. Chem.*, **1993**, *194*, 2789

55. Yao, D.; Wang Z. Y.; Sundararajan, P. R. *Polymer* **2005**, *46*, 4390-4396.

56. Rusanov, A. L.; Elshina, L. B.; Bulycheva, E. G.; Müllen K. *Polym. Sci. Ser. A* **1999**, *41*, 2-21.

57. Harris, F.W.; Hsu, S. C. C. *High Perf. Polym.* **1989**, *1*, 3.

58. Niu, H.; Wang, C.; Bai, X.; Huang, Y. *J. Mater. Sci.*, **2004**, *39*, 4053-4056.

59. Würthner, F. *Angew. Chem., Int. Ed*, **2001**, *40*, 1037–1039.

Chapter 2

Characterization Methods

2.1 Introduction

This chapter describes the characterization methods used in this thesis and the principle of operation of the various techniques. These include FT-IR, UV-visible and fluorescence spectroscopy, nuclear magnetic resonance spectroscopy (NMR), differential scanning calorimetry (DSC), thermogravimetric analysis (TGA), transmission electron microscopy (TEM), and X-ray diffraction, etc. Also molecular modeling and modeling software, i.e., Cerius[2] and HyperChem, are introduced in this chapter.

2.2 Instruments and Methods

2.2.1 Infrared (IR) Spectroscopy

Infrared spectroscopy is one of the most often used spectroscopic tools for the study of characterization of polymers. IR spectroscopy measures the vibrational energy level of molecules. The characteristic band parameters measured in IR spectroscopy are frequency (energy), intensity, band shape (environments of bonds), and the polarization of various modes, that is, the transition-moment direction in the molecular framework.[1] The position of an infrared absorption band is specified in frequency units by its wavenumber measured in reciprocal centimeter (cm^{-1}), or by wavelength measured in micrometer.

In IR spectra, the region from 4000 to 1400 cm^{-1} gives information about the functional group present in the structure. The region from 600 cm^{-1} to 1400 cm^{-1} is called the fingerprint region because the pattern of absorption in this region is unique to any particular compound.[2] The bands in this region can be used with great utility to assign the substitution pattern.[3]

Polymer vibrational spectroscopy may differ from spectroscopy of small molecules.[4,5] The foremost difference is that although a polymer molecule often consists of many thousands of atoms, the molecule does not observe the (3N-6) discrete vibrations expected for a small molecule. Instead, for a regular polymer chain, only vibrations in which the repeat units with specific phases give IR fundamental bands, greatly reducing the spectral complexity. In general, the interpretation of a polymer spectrum can be made on several levels. The simplest approach treats the polymer as a collection of individual functional groups and attempts to assign observed bands by using group frequency correlations. This can aid polymer identification (fingerprinting) or quantification of composition.[6] The second level correlates spectral features with specific conformations or phases, and is valuable in morphological studies.[7] The third approach attempts to assign the individual bands to their symmetry species by measuring their response to polarized radiation. This aids band assignments and helps to distinguish possible chain structures.[8] We see therefore that in terms of polymer characterization IR spectroscopy may be employed to identify unknown polymer and by means of conformational coupling effects, permit investigations of stereochemical structures, orientation and morphology of polymers. It also follows that the effect of variables which produce changes in these properties such as temperature, processing parameters, annealing times etc. may be monitored by following changes in the vibrational spectra.

In this thesis, FT-IR spectroscopic measurements were carried out at ambient conditions using an ABB Bomem MB100 Fourier Transform Infrared (FT-IR) spectrometer. All the data were collected using BOMEM GRAMS/386 software. The spectra of perylene-containing polymers and copolymers were obtained in the form of transparent KBr pellets.

A background spectrum was taken for each experiment with the identical sample holder. In our experiment, IR was mainly used to monitor the completion of reactions, and the changes of functional peaks after annealing, etc.

2.2.2 Nuclear Magnetic Resonance Spectroscopy (NMR)

Since the 1960s, NMR spectroscopy has become a major tool for the study of chain configuration, sequence distribution, and microstructure in polymers.[9] The NMR technique utilizes the property of spin (angular momentum and its associated magnetic moment) possessed by nuclei whose atomic number and mass number are not both even. Such nuclei include the isotopes of hydrogen (^{1}H) and ^{13}C, ^{15}N, ^{17}O, and ^{19}F. Application of a strong magnetic field to a material containing such nuclei splits the energy level into two, representing states with spin parallel and anti-parallel to the field. Transitions between the states lead to absorption or emission of an energy. The energy change is observed as a resonance peak or line in experiments where either fields of strength or frequency is varied. The positions of resonance lines on the scale of frequency or magnetic field depend on the local fields, which in turn result from the nature and location of the atomic groups in the vicinity of the protons. The displacements in the resonance, called *chemical shifts*, are measured in parts per million in frequency on a scale labeled δ. The zero of the δ scale is a reference point provided by the single resonance of the equivalent protons in a substance showing minimum chemical shift, such as tetramethyl silane (TMS).

In proton NMR, additional complexity and additional information result from coupling of the resonances of protons on adjacent carbon atoms, resulting in the splitting of their

resonances into $n+1$ peaks, where n is the number of equivalent neighboring protons. To aid in interpretation, two experimental modifications are useful. The first of these is the use of high magnetic field strength (present NMR is usually 400-500 M gauss). The second development, double resonance or spin decoupling, effects great simplifications in the spectra. A second radiofrequency field is used that has the effect of removing the coupling and collapsing multiplet spectra to much simpler ones.

In this thesis, a Bruker-400 instrument was used to record ^{1}H NMR spectra. For perylene end-capped poly(dimethyl siloxane)s, tetramethyl silane (TMS) was not used as internal reference due to similar chemical shift with PDMS. Instead, the chemical shift was determined by the peak of chloroform. Other compounds were used TMS as internal reference.

2.2.3 Differential Scanning Calorimetry (DSC)

Differential scanning calorimetry is one of the most common techniques for quantitative studies of thermal transitions in polymers, organic materials, metals, ceramics and composites. In DSC, the sample and an inert reference are heated, usually in a nitrogen atmosphere, and thermal transitions in the sample are detected and measured. Figure 2.1 is a schematic representation of the DSC cell. The sample and the reference in Figure 2.1 are provided with individual heaters, and energy is supplied to keep the sample and reference temperatures constant. The electrical power difference between sample and reference ($d\Delta Q/dt$) is recorded. This heat flow/temperature data provides valuable information of physical/chemical properties of the materials. For example, the crystalline

melting temperature (T_m), the crystallization temperature (T_c) and the heat of fusion (ΔH) of a crystalline or semicrystalline substance can be obtained from DSC. The glass transition temperature (T_g) and the specific heat capacity (C_p) of a polymer can also be determined from DSC. Polymorphic transitions are also detectible.[10] Among these DSC applications, glass transition temperature (T_g) is one of the most important ones. Glass transition is exhibited by amorphous polymers or the amorphous regions of partially crystalline polymers when a hard, brittle, glass-like state is transformed into a viscous or rubbery state. According to Fox and Flory's theory,[11] T_g is an iso-free-volume state and below T_g, the local conformational arrangement of the polymer segments is independent of both molecular weight and temperature. The glass transition temperature is a very important characteristic of a polymer. After the measurement of T_g, further studies, such as, annealing temperature (usually a little lower than T_g), blending with other materials, can be determined.

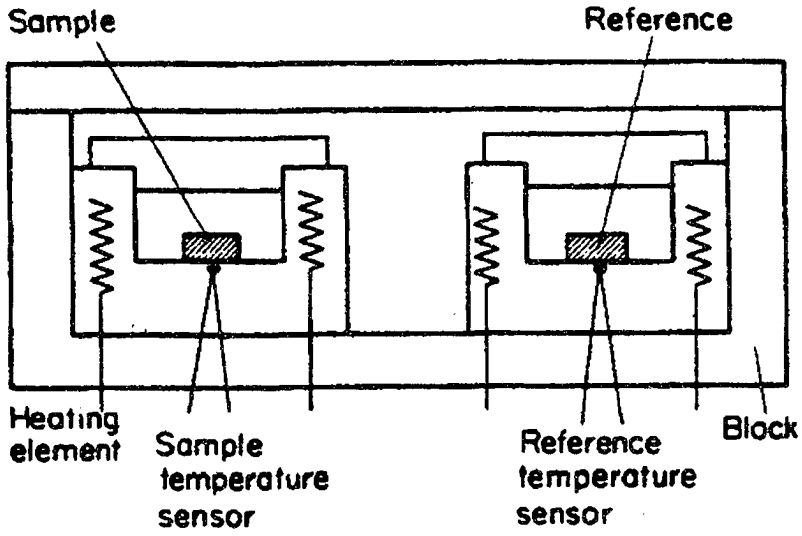

Figure 2.1 Schematic representation of DSC cell.

In this study, thermal analysis was performed using a TA Instrument DSC Q100 and 2010 differential scanning calorimeters at a heating rate of 10 °C/min. Both instruments were calibrated for temperature and energy with indium and tin reference samples. DSC traces were recorded with about 7-10 mg of sample, in a nitrogen or air atmosphere. The uncertainty in the measurement was ±1 °C for the melting point and ±2 J/g for the heat of fusion.

2.2.4 Thermogravimetric Analysis (TGA)

TGA is used primarily to determine the thermal stability of a compound. The weight loss from a compound due to the evaporation of the residual moisture or solvent or due to the decomposition of the compound (which usually occurs at high temperatures) can be easily determined by TGA. Two types of TGA methods are commonly used: non-isothermal and isothermal. Non-isothermal TGA is based on continuous measurement of weight on a sensitive balance (called a thermobalance) as the sample temperature is increased in air or in an inert atmosphere.[12] Data are recorded as a thermogram of weight versus temperature. Isothermal TGA records weight loss with time at a constant temperature.

The thermogravimetric analysis was carried out using a Seiko 220 TGA at a heating rate of 10 °C/min from 25 – 300 °C under nitrogen flow or air flow (50 ml/min). The onset temperature for decomposition for all the samples was taken at 5% weight loss.

2.2.5 Transmission Electron Microscopy (TEM)

The TEM provides detailed structural information at levels down to atomic dimensions. Under favorable conditions, the most capable instruments can resolve detail at the 0.1 nm level, but such high resolution examination is seldom possible with polymers. Nevertheless, it is possible to obtain information within the range 1-100 nm with varying degrees of difficulty. This is beyond the range of light microscopy and TEM can provide information that can rarely be obtained by any other means. Further advantage of the TEM is that it can be rapidly adjusted to provide an electron diffraction pattern from a selected areas, facilitating investigation of crystal structure and orientation, and enabling particular morphological features to be identified. The main disadvantage of the TEM is that it can be used only on thin samples, less than 1 μm thick, and preferably less than 100 nm thick. Problems are encountered as a direct consequence of the way in which the sample and the electron beam interact, because electron irradiation results in chemical changes,[13] destruction of crystallinity[14] and mass transport.[15] In addition, the electron beam may also cause heating, which increases the beam-sensitivity of the material still further. In those cases, the problems are often best overcome by the indirect examination of the sample. In effect, successful TEM depends on three skills: preparing a good specimen, acquiring good data, and adequate interpretation. TEM images are actually contrast images. Contrast is produced in the image if different sites within the specimen transmit electrons with different efficiencies. For example, if a very thick region of the specimen is adjacent to a very thin region, most electrons passing through the thick part will be scattered and will fail to pass through the aperture causing the corresponding part of the image to be dark, whereas a high proportion of the electrons passing through the

thin area will be undeviated and will reach the image making it bright. This is known a "mass-thickness" contrast, because a similar effect is obtained if two regions have the same thickness but contain atoms with different atomic mass and transmit electrons with different efficiencies as a consequence, i.e., the image from atom silicon (atomic weight is 28) is darker than that from atom carbon (atomic weight is 12). By this way, the conformation of polymer may be discovered by TEM.

However, staining is necessary if there are no or small mass differences in the molecules. Staining techniques rely upon incorporation heavy, electron-dense elements into the structure at particular sites, either through specific chemical reactions or simply through physical absorption. Of all available staining reagents, osmium tetroxide (OsO_4) is of particular importance, being one of the most widely used chemicals for staining polymers. OsO_4 reacts with carbon-oxygen double bonds and is therefore widely used as a means of enhancing contrast in unsaturated systems.[16] During this reaction cross-links are formed and the morphology present is therefore simultaneously stained and fixed. OsO4 may also be used in saturated systems.[17] In the simplest case, amplitude contrast may be induced in the TEM image by the preferential absorption of OsO_4.

In this thesis, direct examination was used for studying the samples described in Chapter 5. Transmission electron micrographs were recorded using a Philips CM20 TEM, operated at 120 kV. The samples were prepared by pipeting a small amount of the solution onto a carbon lacey grid. The solution was allowed to cascade down the surface of the tilted grid. This reduced the agglomeration of the material. The thin film formed in this manner was allowed to dry for a few hours before examination. All TEM

experiments were carried out by using the facility at Xerox Research Centre of Canada. TEM was used to study morphology of perylene end-capped poly(dimethyl siloxane)s in Chapter 5.

2.2.6 X-ray Diffraction

The X-ray diffraction method is a powerful tool for investigating orderly arrangement of atoms or molecules through the interaction of electromagnetic radiation to give interference effects with structures comparable in size to the wavelength of radiation.[18] The wavelengths of X-rays are comparable to interatomic distances in crystals. Most of our knowledge about atomic positions and intramolecular distances is gained from X-ray diffraction measurements. To get complete information of the molecular ordering in a crystalline or semicrystalline material, it is necessary to obtain a single crystal of the compound. The crystal is rotated at an angle perpendicular to the incident beam so that diffraction patterns at all possible angles are recorded. However, when a single crystal is not available, powder X-ray diffraction can provide valuable information regarding the interplanar distances between atomic planes (*d* spacing), crystallite size and crystallinity. In powder X-ray diffraction, the reflections are obtained from several microcrystals with different orientation. This method is more convenient, but gives less information than the single crystal method. It gives at best 20 reflections whereas single crystals can usually give >2000 reflections. Direct methods are available to determine the crystal structure using single crystals; this is not the case with the powder pattern.

The basic equation of X-ray diffraction is the Bragg formula:

$$2d \sin\theta = n\lambda \qquad (2.1)$$

Where λ is the wavelength of X-ray radiation, *d* the distance between atomic planes, θ the angle of incidence of the x-ray beam on the atomic planes and n (1, 2, 3 ..., n) is the order of the reflection.

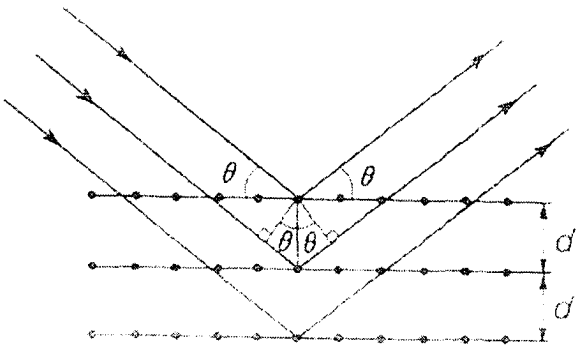

Figure 2.2 Bragg construction illustrating the principle of diffraction where *d* is the spacing between two atomic planes.

In real cases, higher order reflections corresponding to n>1 are extremely weak in intensity. Hence only those corresponding to n=1 are observed. Thus, the above equation reduces to

$$2d \sin\theta = \lambda \qquad (2.2)$$

Rearrangement of Bragg's equation gives the *d*-spacing as

$$d = \frac{\lambda}{2\sin\theta} \qquad (2.3)$$

Equation 2.3 shows that when the distance (*d*) between the two planes in the lattice is large, the scattering angle (2θ) has to be small to produce a diffraction pattern. The diffractions obtained at angles smaller than 2° (d > 44 Å) are called Small Angle X-ray

Diffraction (SAXD).[18] The diffractions obtained at all larger angles, theoretically extending up to 180° are called Wide Angle X-ray Diffraction (WAXD).[18] WAXD provides information about the spatial arrangement of atoms, whereas SAXD provides information about domain arrangements (e.g. long spacing).[19]

In our study, X-ray diffraction data were collected within the range of $2^{\circ} \leq 2\theta \leq 50^{\circ}$ using a Philips automated powder diffractometer, Model PW 1710. Nickel-filtered Cu K_{α} radiation (λ = 1.542 Å) was used. Figure 2.3 shows a schematic of the Bragg diffraction with this diffractometer.

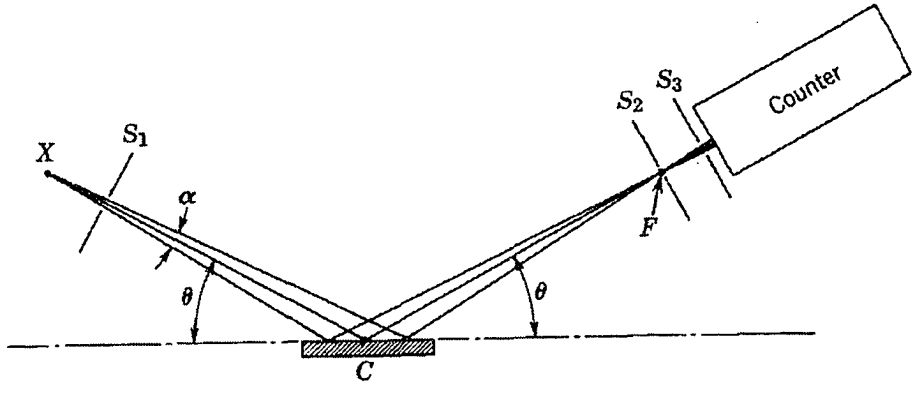

Figure 2.3 Schematic of the Bragg diffraction with the powder X-ray diffractometer used for the present study [from Alexander[18]]. Here, S_1, S_2 and S_3 are the divergence slit, receiving slit and scatter slit respectively; α = 1-4°.

The MDI Datascan 3.2 software (Materials Data Inc., Livermore, CA) was used for data collection. The results were analyzed using MDI Jade 5.0 XRD Pattern Processing software.

Percent crystallinity of the sample, X_c, was calculated using the formula

$$X_c = (I_c / I_{total}) \times 100 \qquad (2.4)$$

Where I_c is the area under the crystalline peak and I_{total} is the total crystalline and amorphous area. The reproducibility in the calculation was ± 2%.

When there was an overlap of peaks in the diffractogram, the profile was first fitted using the MDI Jade 5.0 XRD Pattern Processing software before calculating the crystallite size corresponding to a particular reflection. A diffractogram with overlap of peaks and the fitted profile is shown in Figure 2.4.

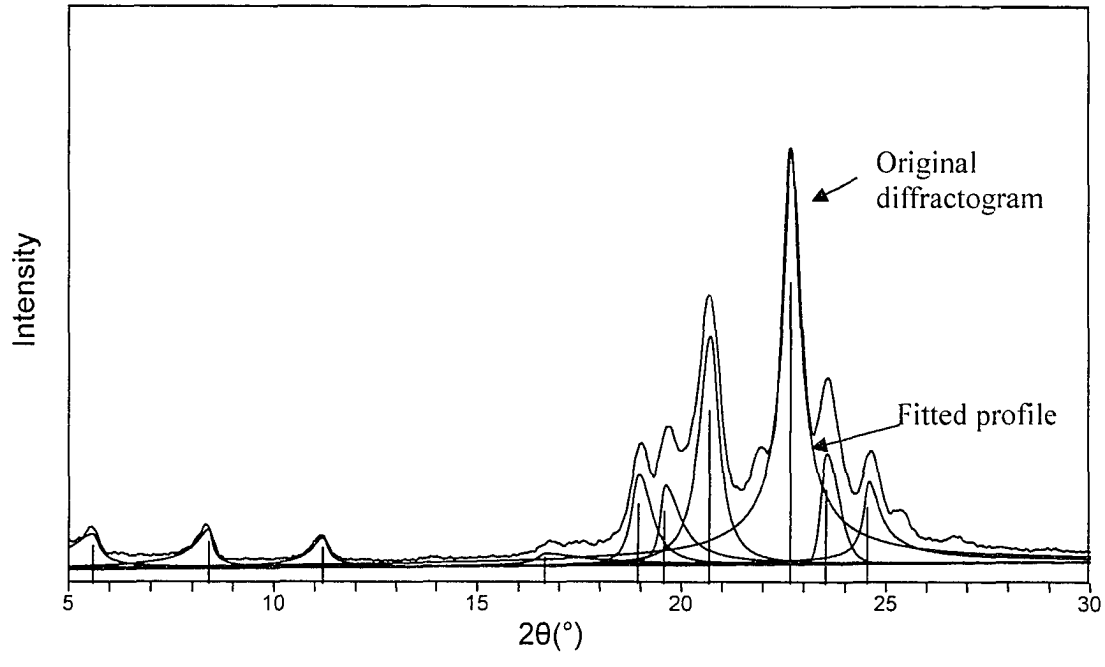

Figure 2.4 Fitted profile of a diffractogram with overlap of peaks.

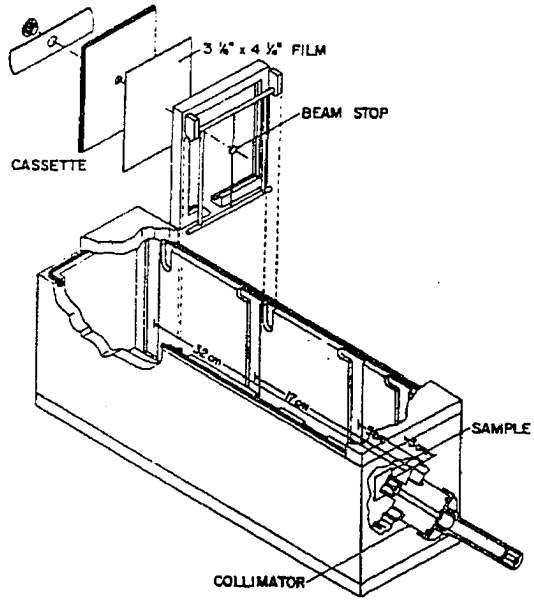

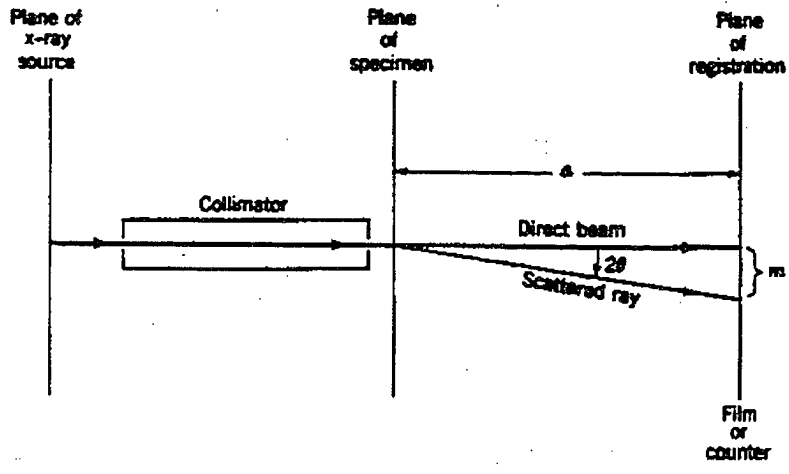

Figure 2.5 Schematic of a Statton-type Warhus flat film camera (top) and the Bragg diffraction (bottom).

Considering the molecular length of the polyimides, significant X-ray reflections were expected at $2\theta<5°$. The diffraction patterns obtained below 5° by the above diffractometer were not reliable; i.e., the peaks were not well resolved because of overlap with the background. Hence, additional diffraction patterns were recorded under vacuum with a Statton-type Warhus flat film camera (William Warhus Co., Wilmington, DE), using Cu K_α radiation (λ = 1.542 Å), with sample to film distance of 5.4 cm and 17.4 cm. A schematic of a Statton-type Warhus flat film camera and the Bragg diffraction is shown in Figure 2.5.

2.2.7 UV-visible Spectroscopy

The UV-Visible spectrum corresponds to electronic excitation and the energy levels depend on the chemical bonds within the specimen. σ electrons, involved in covalent bonds, absorb high energy photos in the UV region, where π electrons absorb low energy photos at longer wavelengths, often in the visible region. Although UV-visible spectroscopy is not capable alone of completely identifying an unknown compound, the advantage of using very small samples and rapid analysis makes it still a common routine analytical technique. One of the most useful applications of UV-visible spectroscopy to polymers is the measurement of the length of conjugation in unsaturated molecules. A modern application is in the analysis of rigid rod molecules with liquid crystal properties. The stiffness of the molecule derives from the presence of cyclic structures along the backbone. The uninterrupted conjugation lengths can be obtained using UV-visible spectroscopy. The π-electrons in a conjugated system are delocalized, which means that they are not restricted to an atomic orbit, but can move freely within the conjugated

region. The theory starts with the proposal that the behavior of a π-electron can be modeled by a particle in a square potential well with infinite side and whose length is chosen to coincide with the conjugation length within the molecule. Such a particle can exit anywhere within the well, but it cannot escape. This represents a good approximation because a π-electron has a very low probability of escape. Another application of the measurement of the conjugation length is in the study of *cis-trans* isomers.[20] The other application is in the analysis of copolymers. If the two (or more) monomers process characteristic absorptions that do not overlap, then the relative intensities of the absorption measured on the copolymer formed from them can be used to estimate composition.

In this study, The UV-visible absorption spectra were recorded on a Perkin-Elmer 900 Spectrophotometer. The concentration of samples is between 10^{-5} and 10^{-6} M.

2.2.8 Fluorescence Spectroscopy

Fluorescence occurs when some chromophores, after being electronically excited, reemit the energy. During the absorption of the UV photon, the chromophore is usually brought to a state that is excited both electronically and vibrationally. However, nonradiative relaxation very quickly brings the chromophore to its lowest vibronic level within the electronically excited state. When the remaining excitation energy is reemitted and the chromophore returns to the electronic ground state, the molecule usually retains some vibrational energy (which is subsequently also dissipated). Thus, the fluorescent radiation occurs at longer wavelengths than the exciting radiation; a whole fluorescence spectrum is observed because the molecules may end up in different vibronic states. The

reradiation process is slow as electronic phenomena go; the lifetimes of the excited states are measured in nanoseconds, while most transitions among electronic states are completed in picoseconds or faster. In macromolecular studies, the chromophore is either a part of the macromolecule itself or fluorescent probes are covalently attached to the macromolecules (e.g., on chain end).

Since most fluorescence occurs in solution, the environmental factors must be considered. [21] These factors include interactions with solvent and other dissolved compounds, temperature, pH, and the concentration of fluorescent species. The effects that these four parameters have upon fluorescence vary from fluorescent moiety to moiety. Both absorption and emission spectra as well as the quantum efficiencies of fluorescent molecules are influenced by these parameters.

In this study, the fluorescent emission data were collected using a Shimadzu RF 1501 fluorescence spectrophotometer. The concentration of samples is between 10^{-5} and 10^{-7} M.

2.3 Molecular Modeling

2.3.1 Introduction

The rapid development of powerful computers in the past decades has allowed chemists to investigate a wide range of chemical behavior without using a single test-tube. Easy-to-use software packages are now available based on a wide variety of ingenious computational methods. These can be used to build computer models that probe the intimate details of sample reactions, predict the characteristics of materials such as catalysts and polymers, and visualize the interactions of biological molecules and drugs.

There are three main reasons why computational chemistry is so widely used. First, it can help us to understand the behavior of a system at molecular level information that may be difficult if not impossible to obtain by any experimental technique. Second, it enables researchers to evaluate many possible choices, in terms of reactants, reaction conditions and so on, before undertaking any experimental work. Third, computational methods can be used to investigate systems under extreme conditions-such as very high pressures and/or temperatures-which cannot be reproduced in the laboratory.

Modeling study ranges from single isolated molecules to polymers containing thousands of atoms immersed in solvent molecules. Computational chemists have at their disposal a variety of methods but at the heart of all programs is some procedure for calculating the energy of the system. The programs then make small change to the system and recalculate the energy after each change. They then use the principle that a chemical system tends to adopt the lowest energy which it can attain to select the most likely configuration of the system.

Energies can be calculated using two basic methods: quantum mechanics and molecular mechanics. Quantum mechanics offers the most fundamental approach and is mostly used on simple atoms and molecules. Molecular mechanics is particularly useful for modeling large molecules and assemblies of molecules.

When we wish to model larger molecules, or assemblies of molecules, quantum mechanics is usually not feasible. Such systems can be studied by the molecular

mechanics, or force field method.[22] The molecular mechanics approach considers the energy of any arrangement of atoms to be made up of several distinct parts. These can be calculated separately and then added up.

One of the most common applications of molecular mechanics is in conformational analysis. This is the task of exploring all the ways in which the various parts of molecule rotate in relation to each other (their so-called conformational space), in order to identify the conformations with the lowest energy.

2.3.2 Molecular Simulation

The two major techniques used in molecular simulation are molecular dynamics and the Monte Carlo method. The molecular dynamics method solves Newton's equations of motion for the collisions between atoms in the system. In current molecular dynamics simulations, the calculation is broken down into many very small steps each of about 1 fermtosecond. At each time-step, the forces on the atoms are determined. From their positions at the next small time-step ahead are deduced, and so on. The restriction to small time-steps means that the length of a typical simulation is limited to picosecond or nanosecond timescales. Although these appear to be very short times in our everyday world, at the molecular level they are often sufficient to enable many interesting phenomena to be studied.

2.3.3 Cerius^2 Software

Computationally molecular dynamics simulation and conformational analyses were performed using Cerius^2 version 4.5, molecular simulation software for material

science,[23] developed by Accelrys, USA. The Cerius[2] molecular simulation software was run on a Silicon Graphics Inc (SGI) Octane2 workstation operating on an IRIX 6.4 platform. In order to carry out the computations, the following modules: 3D-Sketcher, monomer editor, polymer builder, energy minimizer, NPT molecular dynamics polymer properties, orientation function and conformational analysis were used.

The Dreiding 2.21 force field described by Mayo e al[24] was applied since it was found to be very suitable and reliable for the molecular simulation of polymers. The initial macromolecular conformation was optimized and the value of the total potential energy of the single chain was obtained. In order to search a local minimum conformational energy for each simulated molecules, several cycles of potential-energy minimizations and molecular dynamics runs were done. Each cycle of energy minimization was continued until convergence of the total potential energy. The criteria of energy convergence were to obtain a residual root-mean-square force in the simulated system of less than 0.01 Kcal/mole·Å. The minimization was performed using Conjugate-Gradient minimizer, algorithm described by Fletcher and Reeves.[25] Two main types of energy terms used in Dreiding 2.21 force field are bonded (E_b) and non-bonded (E_{nb}) interactions: $E_{total} = E_b + E_{nb}$. The bonded interactions include all terms arising from covalent bond formation, whereas the non-bonded interactions include the long-range non-covalent energies. The bonded terms typically include bond stretching (E_s), angle bending (E_a), torsional (E_t), and inversion (E_i) energies: $E_b = E_s + E_a + E_t + E_i$. Non-bonded terms typically contain van der Waals (E_{vdW}), electrostatic (E_q) and hydrogen bond (E_{hb}) interactions: $E_{nb} = E_{vdW} + E_q + E_{hb}$.

The molecular dynamics simulations were performed at 300K and/or 600K. The number of steps was 500,000 (500ps), and the output frequency was every 50 steps. . We set up 3-20 units of monomers and use polymer builder in Cerius[2] to build the polymers.

2.3.4 HyperChem Software

HyperChem is a desktop molecular modeling system developed by HyperCube Inc. (Waterloo, Ontario).[26] It is used to run on PC under Windows. Like most other molecular modeling programs, HyperChem is accessed through a graphical user interface with pull-down menus. It provides a molecular editor for constructing molecules on the screen or it can read molecular structure files in several formats, and it provides a variety of molecular mechanics and quantum mechanical computational methods together with various options for presenting and rendering different aspects of molecular structure, including isodensity surfaces, electron orbitals, and vibrational modes. HyperChem is more basic than Cerius[2]. It is more suitable for small organic molecules and natural polymers. In this thesis, HyperChem Version 7.0 was used and performed on Windows XP operation system. MM+[27] was used for force field, which is suitable for organics.

References

1. Koenig, J.L. *Spectroscopy of Polymers*, American Chemical Society: Washington, D.C. 1992.

2. Kalsi, P.S. *Spectroscopy of Organic Chemistry*, New Age International Ltd, 2000, 4th Ed., 60-63.

3. Pavia, D.L.; Lampman, G.M.; Kriz, G.S. *Introduction to Spectroscopy*, Harcourt College Publisher, 2001, 3rd Ed., 41.

4. Painter, M.C.; Coleman, M.M.; Koenig, J. *The Theory of Vibrational Spectroscopy and its Applications to Polymeric Materrials,* Wiley-Interscience: New York, 1982.

5. Siesler, H.W.; Holland-Moritz, K. *Infrared and Raman Spectroscopy of Polymers, Practical Spectroscopy Series 4*, Marcel Dekker Inc.: New York, 1980.

6. Hendra, P.J.; Maddams, W.F.; Royaud, I.A.M.; Willis, H.A.; Zichy V. *Spectrochim. Acta*, **1990**, *46A*, 747-56.

7. Stokr, J.; Schneider, B.; Dostocilova, D.; Lovy, J.; Sedalacek, P. *Polymer*, **1982**, *23*, 714-21.

8. Koenig, J.L. *Appl. Spectrosc. Rev.* **1971**, *4*, 233-306.

9. Mirau, P.A. in *Polymer Characterisation*, Hunt, B.J.; James, M.I. (Eds), Blackie A & P: Glasgow, 1993, Chapter 3.

10. Wendlandt, W.W. *Thermal Analysis*, Wiley Interscience: New York, 1986, 667.

11. (a) Fox, T.G.; Flory, P.J. *J. Appl. Phys.* **1950**, *21*, 581. (b) Fox, T.G.; Flory, P.J. *J. Polym. Sci.* **1954**, *14*, 315.

12. Stevens, M.P. *Polymer Chemistry an Introduction*, 3rd ed.; Oxford University Press: New York, 1999; Chap. 5.

13. Chapiro, A. *Radiation Chemistry of Polymeric Systems*, Interscience: London, 1962.

14. Grubb, D.T. *J. Mater. Sci.* **1974**, *9*, 1715-1736.

15. Breedon, J. E.; Jackson, J. F.; Marcinkowski, M. J.; Taylor, M.E. *J. Mater. Sci.* **1973**, *8*, 1071-82.

16. Weiss, R.A.; Sasongko, S.; Jerome, R. *Macromolecules*, **1991**, *24*, 3779-3787.

17. Sawyer, L.C.; Grubb, D.T. *Polymer Microscopy*, Chapman and Hall: Lodon, 1987.

18. Alexander, L.E. *X-Ray Diffraction Methods in Polymer Science*, Wiley-Interscience: New York, 1969.

19. Billmeyer, F.W. *Textbook of polymer science*, 3rd ed.; Wiley-Interscience : New York, 1984

20. Rao, C.N.R. *Ultra-Violet and Visible Spectroscopy: Chemical Applications*, 3th Ed. Butterworths: London, 1975, p 100.

21. Pesce, A.M.; Rosen, C.-G.; Pasby, T.L. *Fluorescence Spectroscopy*, Marcel Dekker Inc: New York, 1971

22. Eichinger, B.E.; Khare, R. *Molecular Modeling* in: *Encyclopedia of Polymer Science and Technology*, Interscience: New York, 2003.

23. *Cerius*^{2} *Simulation Tool User's Reference*, Version 4.5, Molecular simulation software for material science. Accelrys, San Diego, CA, USA, 2000.

24. Mayo, S.L.; Olafson, B.D.; Goddard, W.A. *J. Phys. Chem.* **1990**, *94*, 8897-909.

25. Fletcher, R.; Reeves, C.M. *The Computer Journal* **1964**, *7*, 149-53.

26. HyperChem Manual, Hypercube Inc., Waterloo, 2002

27. Allinger, N. *J. Am. Chem. Soc.* **1977**, *99*, 8127-8134.

Chapter 3

Time Dependent Crystal-Smectic Transformation in Perylene-Containing Polyimides*

(* D. Yao, Z.Y. Wang, P.R. Sundararajan, *Polymer*, **2005**, *46*, 4390-4396)

3.1 Introduction

Perylene 3,4,9,10-tetracarboxylic dianhydride and its bisimides are some of the most thoroughly studied classes of organic semiconductors with possible applications in photovoltaic cells,[1] light-emitting diodes,[2] xerography,[3] and field-effect transistors.[4] Perylene derivatives are remarkable in the diversity of colors that can be obtained by modifying the groups attached to the periphery of the chromophore. This essentially controls the extent of π overlap between the chromophores in the crystal structure. From the crystal structure data on a series of such substituted perylenes, Hädicke and Graser[5] related the color of the crystal to the molecular overlap. Liquid crystalline (LC) derivatives of perylene are also known.[6,7] Cormier and Gregg[6] recently reported self organization in thin films of liquid crystalline perylene bisimides, with linear and branched poly(oxyethylene) derivatives. Struijk[7] et al discussed the liquid crystalline behavior of N-alkyl-substituted perylene bisimide derivatives, with 7, 12 and 18 carbon atoms. Thus, perylenes substituted with flexible side chains generally form LC phase.

For device fabrication, the pigment is usually either vapor deposited to form thin films or dispersed in a polymer binder. The latter is typical of a photogenerator layer of xerographic photoreceptors. There have also been efforts to covalently incorporate the pigment as a part of the polymer, with a view to increase the robustness and flexibility of the device as well as to address the issue of phase separation of the small molecule from the polymer matrix.

Polyimides are thermally stable polymers that exhibit good mechanical properties, low dielectric constant, low coefficient of thermal expansion and high radiation resistance. Since the first commercial polyimide-Kapton was produced by DuPont, polyimides have been extensively used in microelectronics, photonics, optics and aerospace industries.[8,9] Wang et al[10] reported that the synthesis and xerographic characterization of polyimides containing perylene tetracarboxylic dianhydride and aliphatic diamines in the main chain (Figure 3.1). These polymers are insoluble in common organic solvents, and inherent viscosities were measured in concentrated H_2SO_4. It was found that with the perylene-containing polyimides with a C_{12} spacer (PPI-12), the UV-visible absorption maximum red-shifted upon annealing at 320°C, and the crystallinity improved as well. Based on the work of Hädicke and Graser,[5] this was attributed to the enhanced packing of the perylene units upon annealing. A molecular dynamics simulation of a single chain of PPI-12 also showed that intramolecular chain folding could occur, which is facilitated by the alkyl segment. [11] The possibility of aggregation of perylene units in solution, via such intramolecular chain folding has been proposed by Neuteboom et al,[12] in the case of perylene bisimide polymers with polytetrahydrofuran segments. This polymer, of course, is soluble in solvents such as *o*-dichlorobenzene.

Although the liquid crystalline behaviour of perylene derivatives (in monomeric form) has been reported, phenomena such as odd-even effect were not studied. In this chapter, we describe the structural characteristics of a series of perylene based polyimides (Figure 3.1) with different alkyl chain lengths ranging from C_3 to C_{12}, and changes induced by annealing of this series of polymers. The annealing induced changes are interpreted as a

transition from the crystalline to smectic state. An interesting aspect of this transition is that it is very slow and it depends on the time of annealing at a particular temperature. We believe that this is the first reported case in which the time of annealing plays a role in crystal-smectic transition.

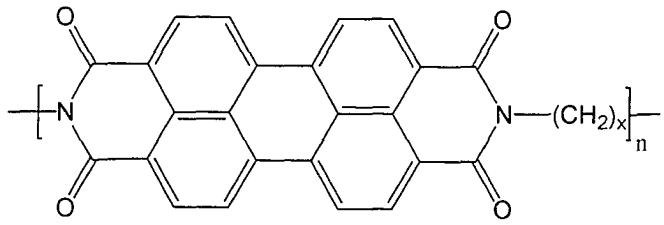

Figure 3.1 Schematic of the perylene-containing polyimide polymers studied here (x = 3-12, polyimide ID: PPI-3 to PPI-12, details in Table 3.1 in Section 3.3.2).

3.2 Synthesis

While some of the samples used in this study were provided by the group of Prof. Z.Y. Wang, Carleton University, most of the samples were synthesized by the author using the procedure described in reference.[10]

3.2.1 Raw Materials.

Aliphatic diamines including 1,3-diaminopropane, 1,5-diaminopentane, 1,7-diaminoheptane, 1,8-diaminooctane, 1,10-diaminodecane, and 1,12- diaminododecane, isoquinoline were purchased from Aldrich Chemical Co. and used as received. Perylene-3,4,9,10-tetracarboxylic dianhydride (PTDA, 1) was purchased from Aldrich Chemical Co. and converted to the tetrapotassium salt of the tetracarboxylic acid using aqueous potassium hydroxide solution (1M). After filtration, the filtrate was acidified with

aqueous hydrochloric acid solution (2 M) to yield a mixture of dianhydride and its tetracarboxylic acid, which was collected by filtration and dried in a vacuum oven at 150°C. *m*-cresol was purchased from Aldrich, distilled before used and kept in molecular sieve to prevent absorbing water.

3.2.2 Synthesis Procedure (Scheme 3.1)

Perylene-3,4,9,10-tetracarboxylic dianhydride (PTDA, **1**) (0.588g, 1.5 mmol), diamine 1,12- diaminododecane (**2**, 0.3 g, 1.5 mmol), *m*-cresol (25 ml), and isoquinoline (1 ml) were added to 100ml three-necked, round-bottomed flask equipped with a nitrogen inlet and outlet. The mixture was heated to 80°C and kept for 1 h under nitrogen, and then heated to 200 °C and kept for 24 h. After finishing the reaction, the solution was cooled down to room temperature. The resulting dark red solution was poured into acetone (300 ml). After filtering, the solid was washed repeatedly with aqueous sodium hydroxide (1 N) solution, in order to remove unreacted PTDA, followed by water and acetone. Then drying was under vacuum at 120 °C overnight. Finally, polyimide (compound **3**) was obtained as a dark red solid (0.70g, 83.3%). Completion of imidization was confirmed by infrared spectroscopy, which showed peaks of imide at 1695 cm^{-1} and 1655 cm^{-1} instead of anhydride at 1700 cm^{-1}.

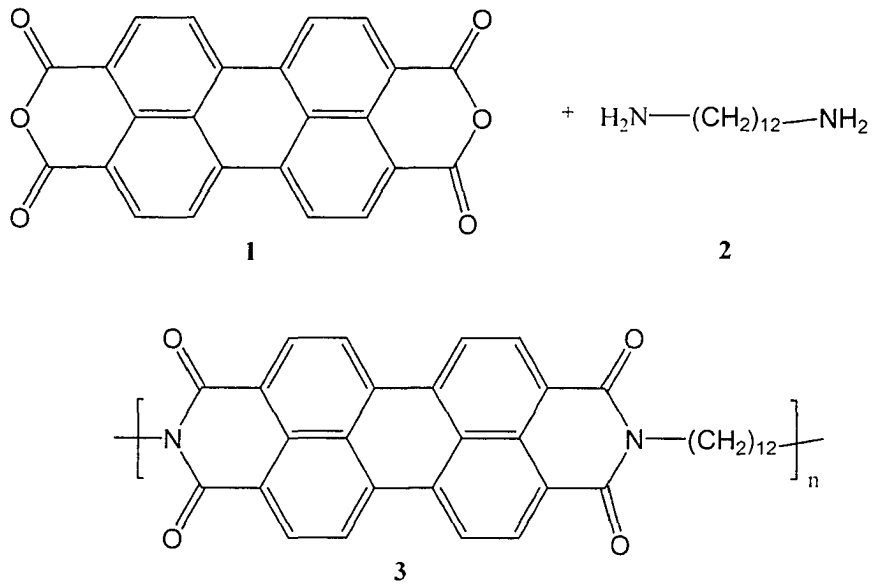

Scheme 3.1. One-step condensation polymerization of perylene tetracarboxylic dianhydride and aliphatic diamines.

3.3 Results and Discussions

3.3.1 Synthesis and Solubility

A series of linear aliphatic diamines were chosen for the preparation of perylene polyimides with perylene-3,4,9,10-tetracarboxylic dianhydride (PTDA, 1) (Scheme 3.1 in Synthesis Section 3.2.2). The polymerization was best carried out in *m*-cresol with a small amount of isoquinoline (1-2 weight % of PTDA) as catalyst at 200°C. Completion of imidization was confirmed by IR spectroscopy, which showed the absence of the peaks of perylene anhydride at 1700 cm^{-1}, and the presence of the peaks of carbonyl peaks for the imide at 1695 and 1655 cm^{-1}. Because the solubility is very low in common organic solvents, the molecular weights cannot be determined by gel permeation chromatography (GPC). Instead, viscosity was measured in concentrated sulfuric acid. The intrinsic viscosity of PPI-12 in concentrated sulfuric acid was 0.65 dl/g, which close to the

literature value of 0.70 dl/g.[10] Typically, the intrinsic viscosity of perylene polyimides (PPI-3 to PPI-12) ranged from 0.30 to 1.06 dl/g similar to the work of Wang et al.[10]

The solubility increased from PPI-3 to PPI-12 in *m*-cresol. In this homologous series, this could be attributed to the increased flexibility of the polymers with longer alkyl spacers. However, this increase in flexibility is not enough to let PPIs dissolve in common organic solvents. This led the study of perylene copolyimides described in Chapter 4.

3.3.2 Thermal Characteristics

The results of the thermogravimetric analysis are summarized in Table 3.1. These illustrate the good thermal stability of perylene-containing polyimides. The 5% weight loss in nitrogen was in most cases around 450-480°C and the maximum peak temperatures of derivative thermogravimetry (DTG) are in the range of 470-530°C. It is also seen from Figure 3.2 and Table 3.1 that the thermal stability generally decreases with an increase in the length of the (CH_2) spacer. This is in accord with the theory that the introduction of flexible swivel groups lowers the thermal stability. [13] However, a systematic trend is absent. The glass transitions (T_g) of these polyimides were not detectable (Figure 3.3). This is similar to the conclusion reported by other authors on similar polyimides.[14,15] In the case of rod-like polyimides, the transitions were very weak or not detectable. Such shallow transitions are also characteristic of liquid crystalline polymers.[16] Because of these constraints, it was not possible to derive the effect of odd and even spacer lengths on the glass transition temperatures.

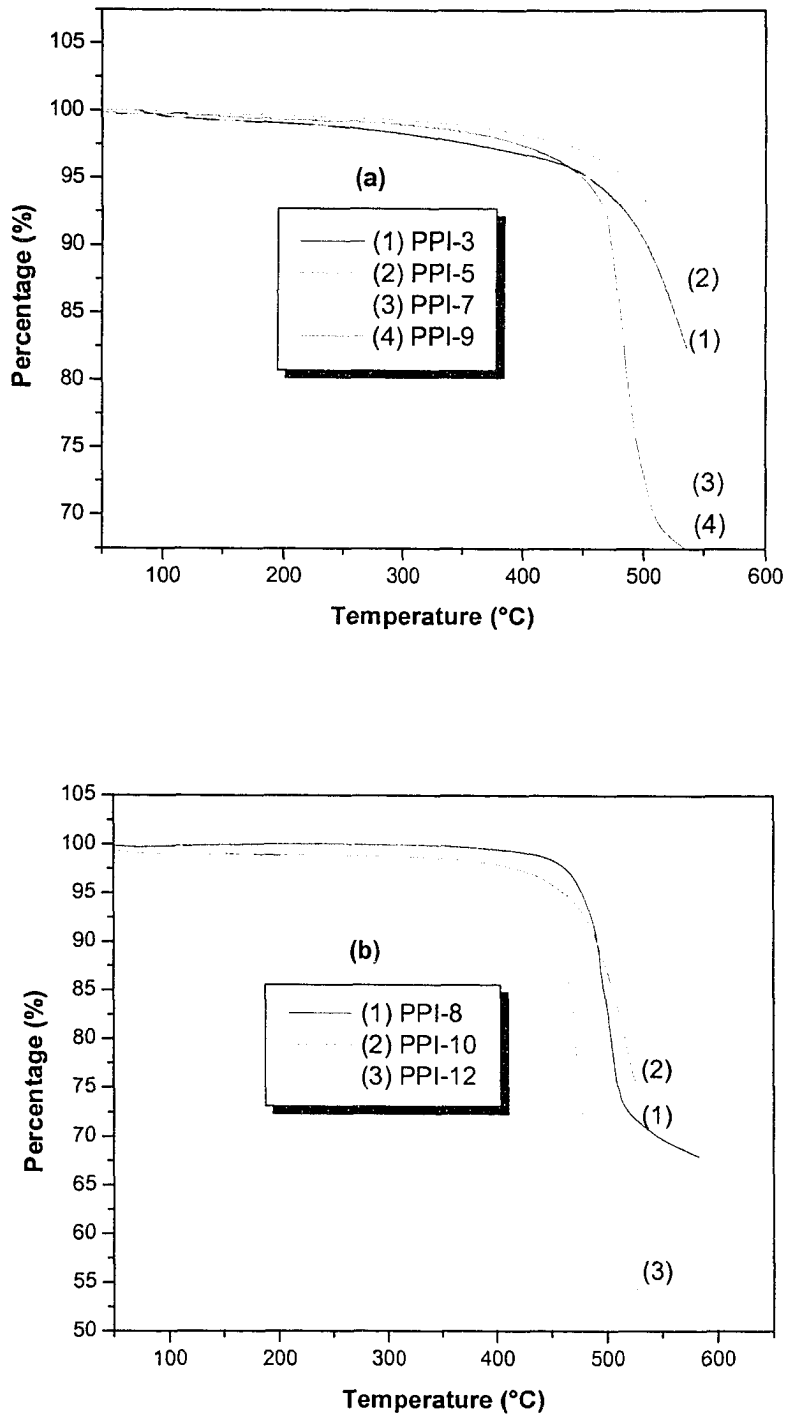

Figure 3.2 Thermogravimetric analysis curves of perylene polyimides with odd number spacers (a) and even number spacers (b).

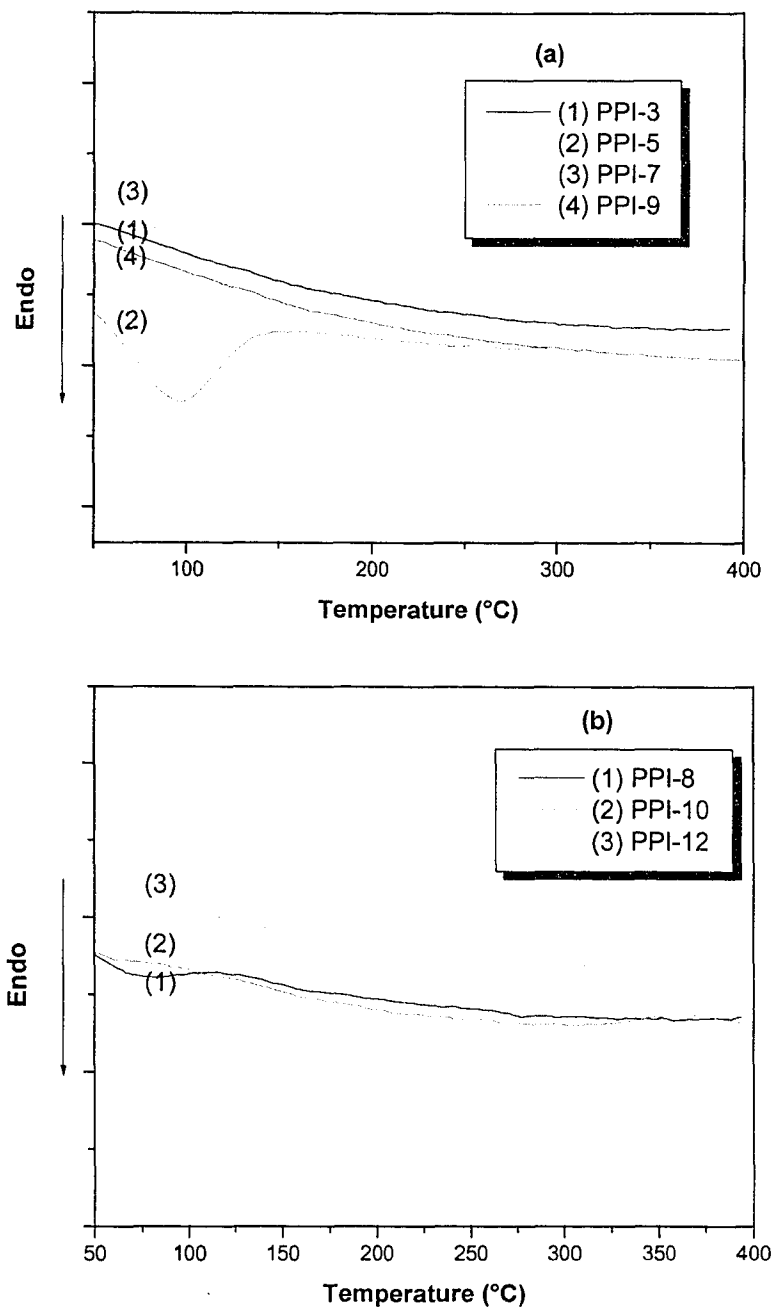

Figure 3.3 DSC thermograms of perylene polyimides with (a) odd-spacer and (b) even-spacer.

Table 3.1 Results of thermogravimetric analysis (TGA)

Aliphatic amine in PPIs	Polyimide ID	TGA (°C)	
		$T_{5\%}$[a]	T_{max}[b]
diaminopropane	PPI-3	456.1	526.6
diaminopentane	PPI-5	485.4	523.0
diaminoheptane	PPI-7	455.3	500.2
diaminooctane	PPI-8	449.6	484.8
diaminononane	PPI-9	477.8	501.8
diaminodecane	PPI-10	461.2	518.2
diaminododecane	PPI-12	424.4	474.9

a. $T_{5\%}$: temperature at which 5% of the sample weight was lost.
b. T_{max}: the temperature of maximum peak characterized by derivative thermogravimetry (DTG).

3.3.3 Effect of Annealing on the UV-visible Absorption Behaviors

As is well known, the extent of π overlap between the chromophores packed face to face in the crystal structure determines the color. With an increasing overlap, the absorption maximum shifts to longer wavelengths. It was noted before[10] that in the case of PPI-12, a red shift of the absorption maximum occurred when the polymer was annealed at 320°C for 2 h.

Figure 3.4 shows the effect of annealing at 320°C, for different times, on the UV-visible absorption of PPI-7 and PPI-12. In all cases there is a red shift of 6-10 nm upon annealing. We could not detect any correlation between the alkyl chain length and the

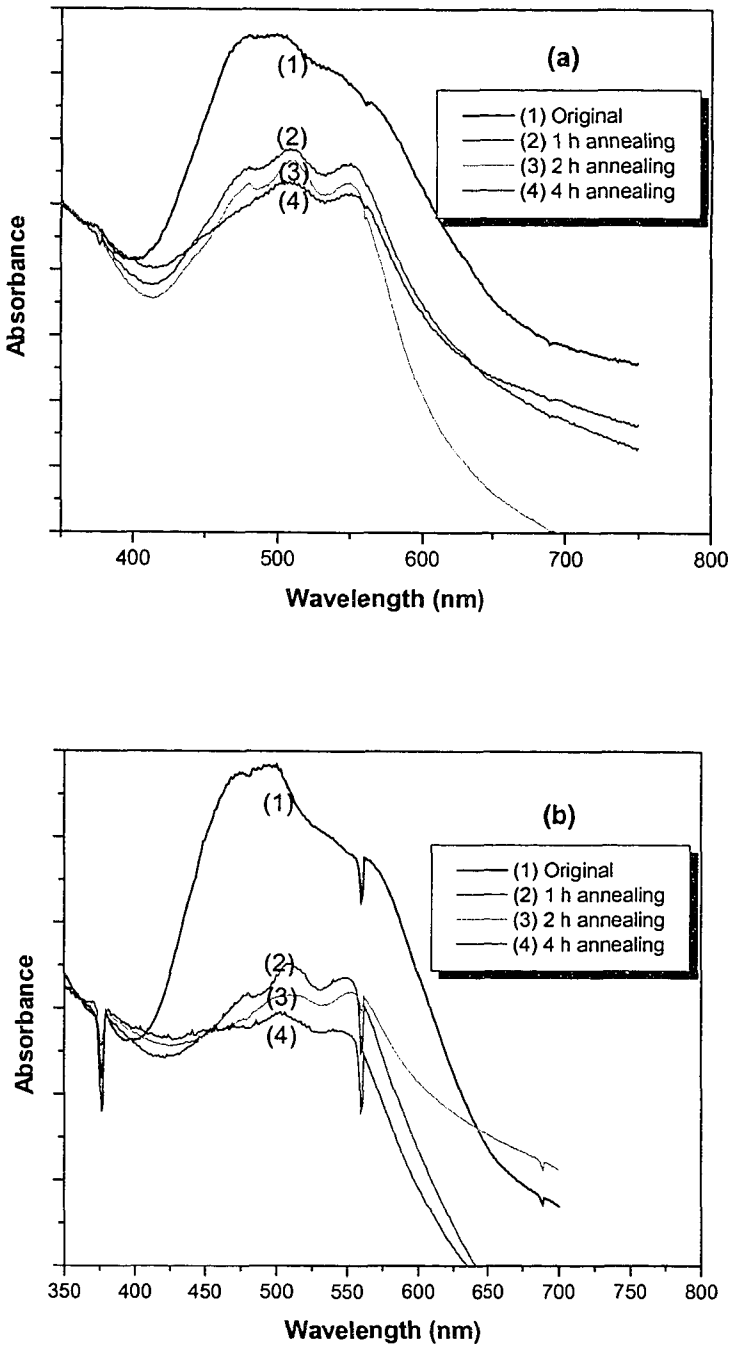

Figure 3.4 The effect of annealing for different times, on the UV-visible absorption spectra of (a) PPI-7 and (b) PPI-12 at 320°C.

extent of the shift. It was noted that there was no change in the absorption characteristics with annealing for PPI-3 and PPI-5. It is perhaps due to the short alkyl segments not having enough mobility to cause any structural changes. With PPI-7 (Figure 3.4a), initially a broad absorption is seen ranging from 450 to 600 nm, with a "maximum" at 492, and 527 nm. Upon annealing at 320°C for 1 h, three maxima are seen, at 475, 508 and 545 nm, with the absorption at 508 nm being more intense. The red and blue shifted bands are usually assigned to J-type and H-type aggregates.[17] J-aggregates are formed with the monomeric molecules arranged in one dimension such that the transition moment of the monomers are parallel and the angle between the transition moment and the line joining the molecular centers is zero (ideal case). The strong coupling of several self-similar monomers results in a coherent excitation at red-shifted wavelengths relative to the monomer. In addition, the spectrum gets narrower and the vibrational coupling to the molecular modes will be largely absent. H-aggregates are again a one-dimensional arrangement of strongly coupled monomers, but the transition moments of the monomers are perpendicular (ideal case) to the line of centers. In contrast to the side-by-side arrangement of molecules in J-aggregates, the arrangement in H-aggregates is face-to-face (Figure 3.5).[18] Theory predicts that the dipolar coupling between monomers leads to a blue shift of the absorption band. In the solid state, the process may take longer time for aggregates. However, the result is similar. Therefore, the red-shift of absorption is caused by J-aggregates. J-aggregates of perylene bisimides was found in the references by W. Würthner at al.[19] In that paper, they found J-type aggregates and columnar mesophases of perylene bisimide dyes by simple derivatization of the imide groups with mesogenic trialkoxyphenyl substituents.

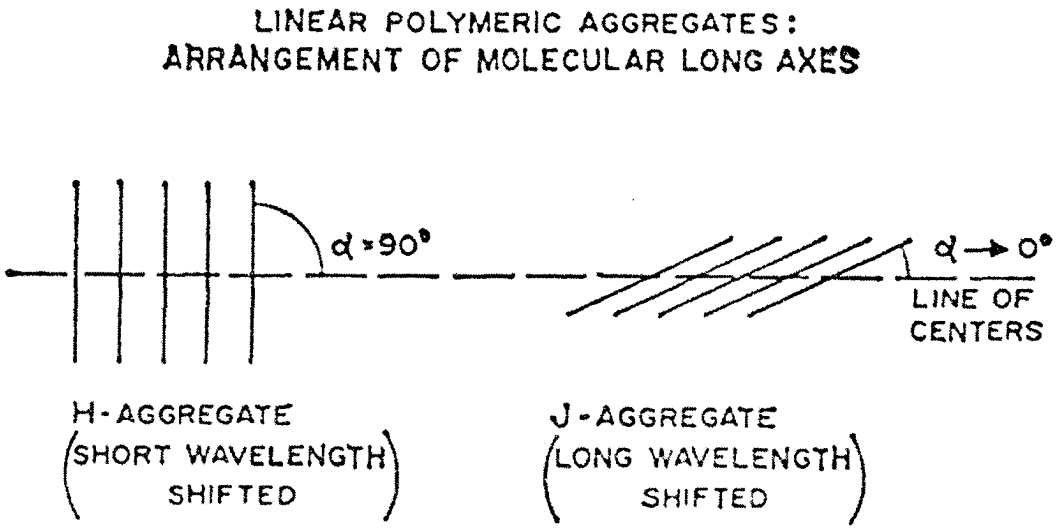

Figure 3.5. The orientation of transition dipole moments (or molecular long axes) for linear H and J aggregates (Reproduced from reference 18).

The relative intensities of these maxima remain the same with 2h of annealing. After annealing for 4h, the blue maximum (475 nm) vanishes. A similar trend is seen with PPI-12 as well (Figure 3.4b). Thus, annealing at 320°C for 1-2 h causes a structural change, and increasing the annealing time to 4 h results in yet another structural transition. The differences in the intensities between the spectra from the original samples and those after annealing could be due to the variation in the thickness of the samples and the roughness of the sample surface. These samples were dried dispersions rather than films. Partial oxidation of the chromophore can not be ruled out.

Struijk et al[7] compared the solution and thin film spectra of the perylene bisimide with a $(CH_2)_{18}$ side chain and concluded that the blue and red shifted absorption bands could be due to a rotation of the transition dipole moments of adjacent molecules and/or more than

one type of aggregate being present, with different orientations of adjacent molecules within the film. Note that the spectra shown in Figure 3.4 were obtained by placing a drop of solution in *m*-cresol on a glass slide and letting it dry. Annealing was also performed on these samples, which can be considered similar to thin films.

3.3.4 Chain Conformation

If the alkyl chain is in the all-trans conformation, and the torsion angle with the perylene unit C (perylene)—N—C(methylene)—C(methylene) is close to 0°, odd number of (CH_2) groups would lead to a helical conformation of the chain and the even number would lead to a zig-zag structure. This is illustrated in Figure 3.6, for the PPI-12 (Figure 3.6a) and PPI-9 (Figure 3.6b) polymers. For example, the Hyperchem and Cerius[2] software chooses this torsion to be 0° as default. Due to the length of the rigid perylene unit (11.2 Å), the helices would have a rather large cavity, ranging from 12 Å with PPI-5 to 30 Å, in the case of PPI-9. In addition, the perylene stacking distance in successive turns is more than 10 Å. Conceptually, this would create a rather large free volume, and due to the poor perylene stacking, the UV-visible spectra as seen in Figure 3.4 would not arise. However, if the above torsion angle is shifted to about 90° with respect to the perylene plane, the chain with odd number of (CH_2) groups also would adopt an extended conformation (Figure 3.6c). Such a model, with the torsion angle of 90° between the aliphatic carbon and the perylene plane was proposed by Aroca et al,[20] for the molecule 1,2-bis(propylimido perylene)ethane using AM1 for geometry optimization (essentially, this molecule is a perylene dimer, bridged by $(CH_2)_2$). Interruption of the all-trans sequence with a few *t-g* conformations would also lead to a zig-zag shape for the chains

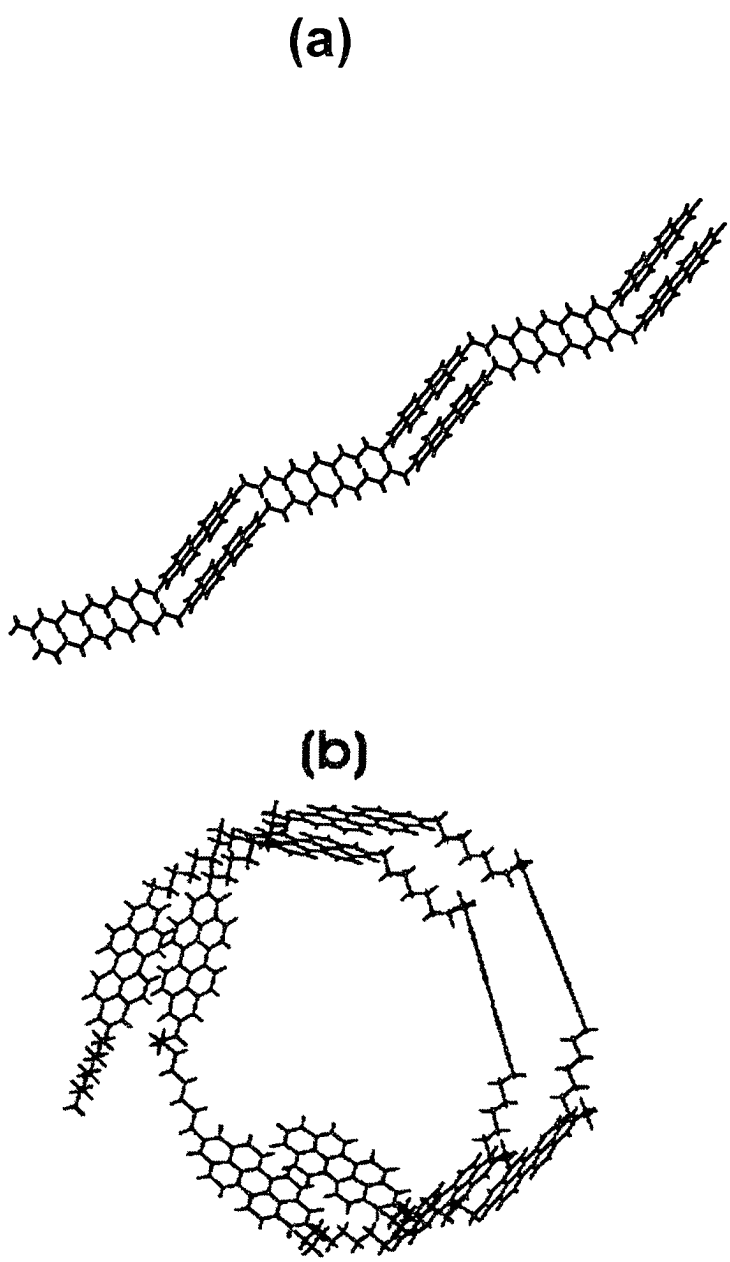

Figure 3.6. (a) Extended zig-zag conformation of PPI-12 with 3 monomer units (b) helical conformation of PPI-9 with 10 monomer units.

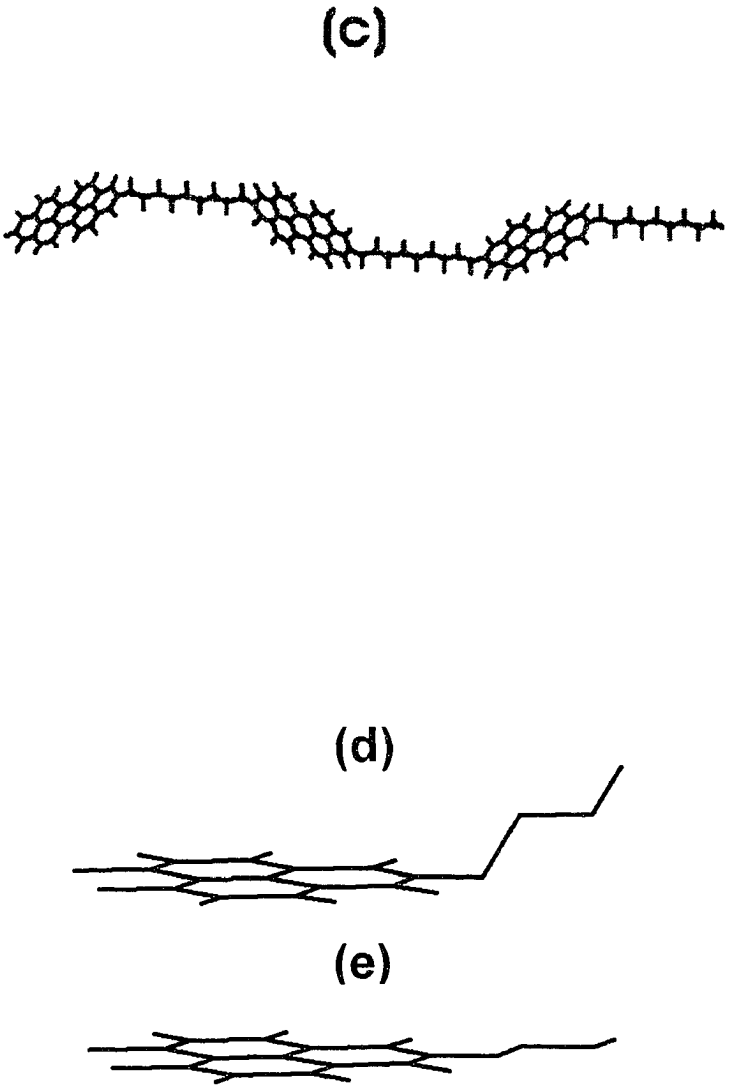

Figure 3.6. (c) extended conformation of PPI-9 when the aliphatic C-C bond is at about 90° with respect to the perylene plane; (d) and (e): schematics of the aliphatic C-C bond at 90° and 0° respectively, with respect to the perylene plane.

with odd number of (CH_2) groups. Figure 3.6e shows the scheme of aliphatic C-C bond at 90° and 0° respectively, with respect to the perylene plane.

Since films could not be prepared with these polymers, and due to the low molecular weight, oriented X-ray diffraction patterns to derive the crystalline conformation could not be obtained. The discussion hence will be limited to some of the features of the powder diffraction patterns, and the effect of annealing.

Figure 3.7 shows the longest d-spacing (in the wide angle region) recorded for each of the polymers. It is seen that this spacing increases almost linearly with the number of CH_2 groups in the spacer, and parallels the monomer length, as calculated from energy minimized models, with an all-trans conformation for the alkyl segment. If the alkyl spacers are in the all-trans conformation, successive pairs of CH_2 groups will add about 2.5Å to the length of the perylene unit. Of course, defects in the alkyl spacer conformation would reduce this distance. Deviations from the all-trans conformation is indicated by Figure 3.7, in which the longest *d*-spacing is 4-6Å less than the monomer length in all cases. The systematic increase in the longest *d*-spacing with the number of CH_2 groups supports the proposal that polymers with odd numbered CH_2 groups also adopt an extended conformation, to facilitate stacking of the perylene units. Thus, in the case of these polymers, the chain is extended for both even and odd number of CH_2 groups in the spacer, being dictated by the π stacking.

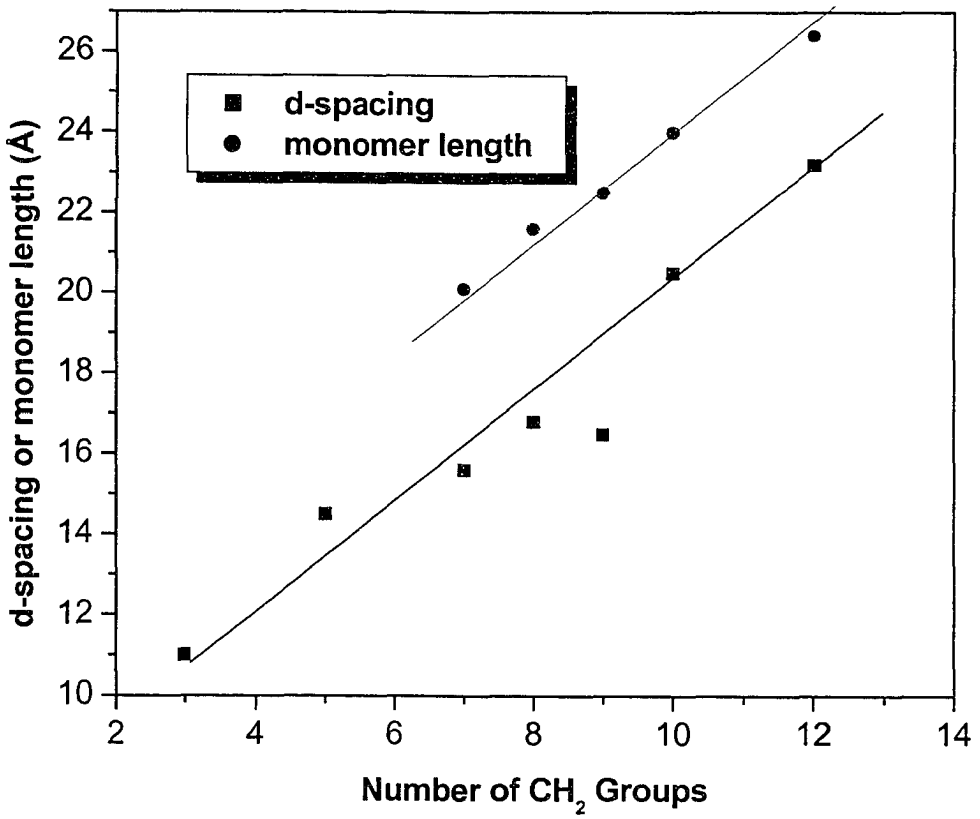

Figure 3.7. Variation of the longest d-spacing with the number of CH_2 groups in the spacer (■); and the lengths of the monomers, with the spacers in the extended conformation (calculated using HyperChem) (•).

We could not record the second or third order reflections corresponding to these spacings even in the powder sample. Hence, the repeat distance of the chain and the crystalline chain conformation could not be deduced, except to say that these are extended helices. Table 3.2 lists the d-spacings recorded for the polymers PPI-7, PPI-8, PPI-9, PPI-10 and

PPI-12, by X-ray powder diffraction. It is seen that most of the reflections are common to both odd and even number alkyl groups. This also confirms that the packing of these chains in the crystalline lattice is similar.

The length of the CH_2 spacer plays a role in the efficiency of packing of the perylene units. Figure 3.8 shows the X-ray crystallinity (see Equation 2.4 in Chapter 2) as a function of the number of CH_2 groups, for the as-prepared polymers. Although the crystallinity is small, an increase with the length of the spacer is seen. Also, the crystallinity increases after annealing if the number of CH_2 spacer is more than 5. Neuteboom et al[21] observed that in the case of perylene bisimide-polyTHF copolymers in *o*-dichlorobenzene solutions, enhanced aggregation occurs with the shortest polyTHF segments. The crystallinity in the solid state was not measured in this reference. The opposite trends noted between these two cases could be attributed to the differences in the flexibility of short polyTHF segment compared to a short alkyl segment. The presence of the solvent could play a role as well.

Table 3.2. Comparison of the d-spacings and the relative intensities observed in the X-ray diffraction patterns for the various perylene polyimides

PPI-7		PPI-8		PPI-9		PPI-10		PPI-12	
d (Å)	I (%)	*d* (Å)	I (%)	*d* (Å)	I (%)	*d* (Å)	I (%)	*d* (Å)	I (%)
				2.48	11.5				
				2.61	9.5				
				2.82	12.1				
						3.21	20.4	3.13	19.7
		3.32	53.1	3.37	39.3	3.37	27.1	3.29	56.4
3.41	42.9					3.49	25.6		
								3.65	41.1
		3.88	49.8					3.80	28.9
3.93	37.5	3.94	48.6	4.05	34.6	4.10	25.6	4.16	25.3
		4.34	41	4.39	32	4.37	24	4.42	30.5
4.62	29.2	4.65	34.7	4.67	31.8	4.7	20.7	4.71	24.3
								5.22	15.4
				6.28	33.8	6.17	18.1	6.10	16.2
6.48	46.8	6.41	40.5						
								7.29	63.9
8.33	71.0	8.16	69.3	8.08	62.8	7.92	35.8		
								8.56	26.2
								9.53	28.4
15.67	100								
				16.5	100				
		16.85	100						
								20.27	100
						20.50	100		
								23.23	94.4

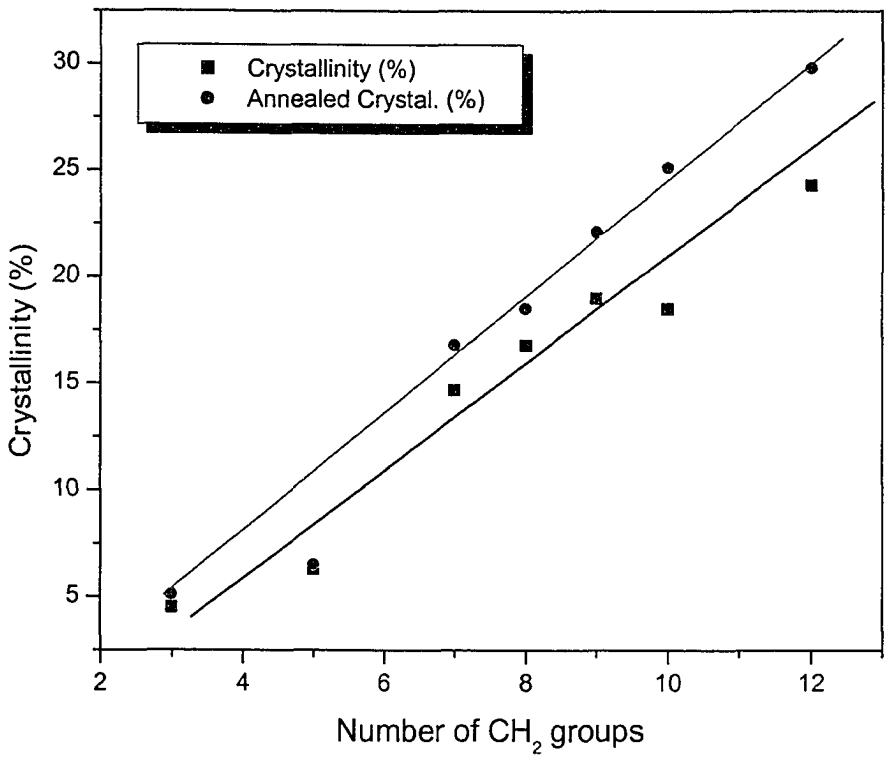

Figure 3.8. The variation of crystallinity of perylene polyimides, with the number of CH_2 groups in the spacer, for the as-prepared and annealed (for 4 h at 320°C) samples.

3.3.5 Mesomorphic Transition

Previous studies[10] on PPI-12 showed a red shift of the absorption maximum, upon annealing at 320°C for 2 h. To examine the changes, if any, upon prolonged annealing at this temperature, X-ray diffraction patterns were recorded after annealing for 4 and 6 h. The changes in the diffraction profile of PPI-12 are shown in Figure 3.9. It is seen that after annealing for 4 h, a number of reflections decrease in intensity, and only those corresponding to 3.29, 3.65, 7.29 and 9.58 Å remain. This is reminiscent of a partial transformation to a smectic state. The 3.65 Å diffraction can be assigned to the π-stacking of the perylene units. Polymers with shorter alkyl spacer lengths (below PPI-7) also

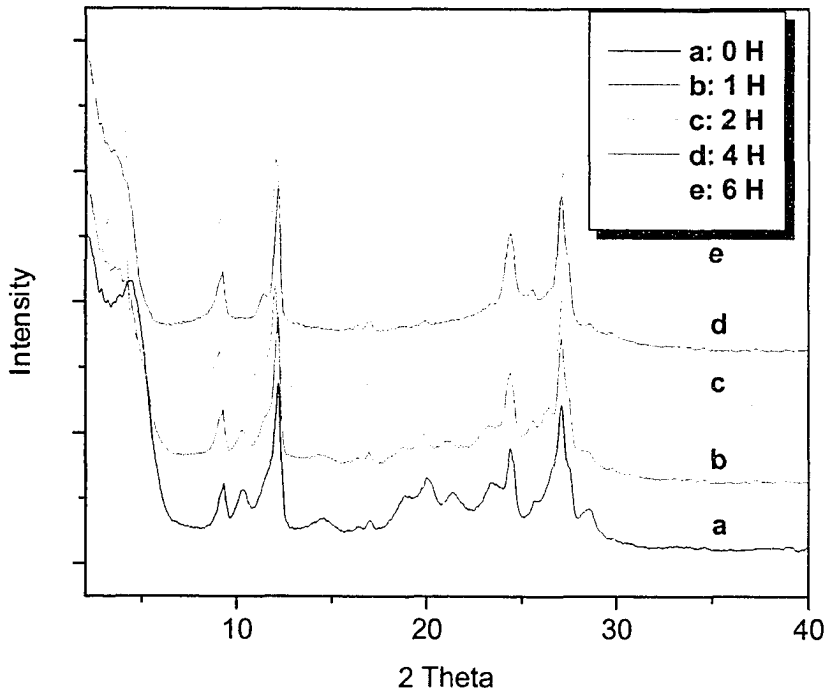

Figure 3.9. X-ray diffraction patterns of PPI-12 annealed for different times at 320°C.

shown the same behavior, although the time required for the transformation was longer. For example, when PPI-7 was annealed for 4 h, the diffraction pattern was still similar to original one. After 16 h annealing, the diffraction pattern finally shows the transformation (Figure 3.10). It was also found that with lower annealing temperatures, the time required for the transformation was longer. Figure 3.11 shows that the diffraction pattern of PPI-10 annealed for 6 h at 300°C is same as the one annealed for 4 h at 320°C. Thus a mesomorphic transformation occurs, for all perylene polyimides, with alkyl spacers of seven or more CH_2 groups. The time taken for the transformation

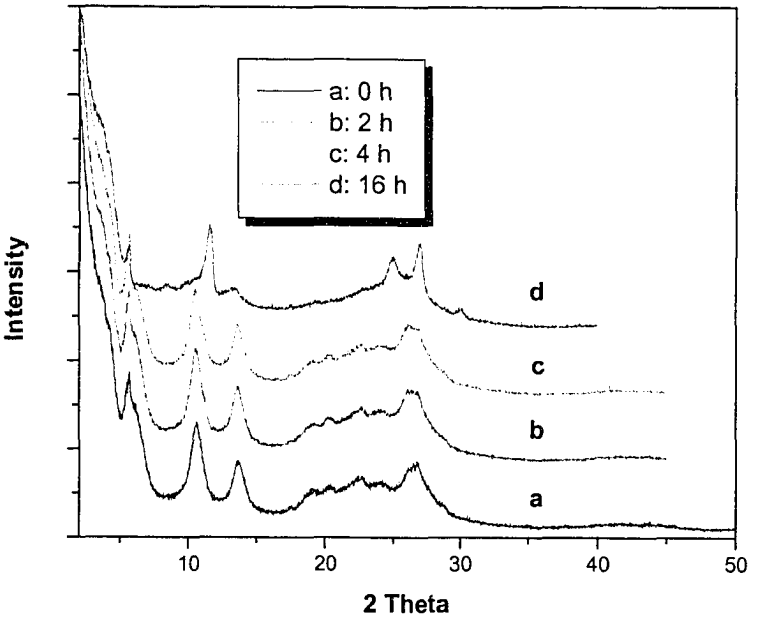

Figure 3.10. X-ray diffraction patterns of PPI-7 annealed for different times at 320°C.

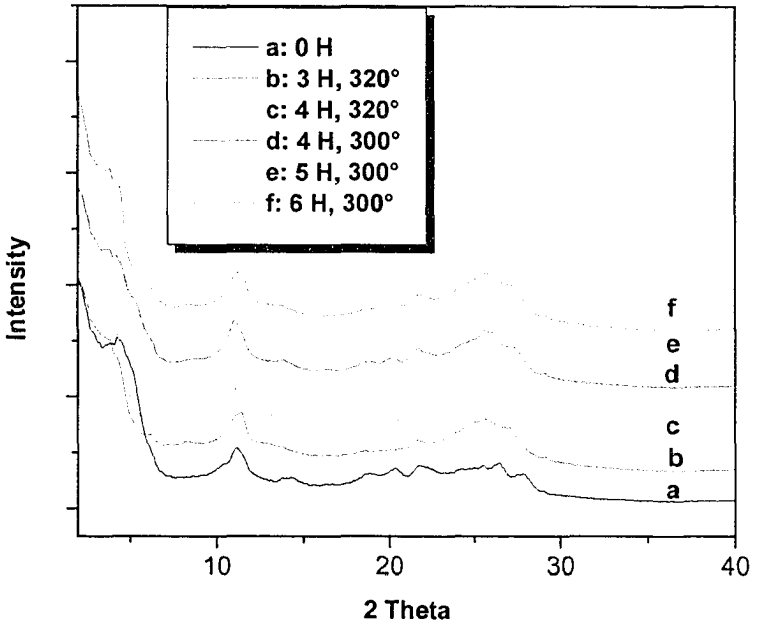

Figure 3.11. X-ray diffraction patterns of PPI-10 with annealed at different temperatures and for various times.

increases with a decrease in the spacer length. This also parallels the changes in the absorption spectra with increasing annealing times. Normally, such mesogenic transitions of polymers can be easily detected during the usual scan rate in DSC measurements. However, in the case of perylene based polyimides, this is a slow phenomenon.

This unusual behavior could not be followed with oriented films since these could not be prepared. Because of the inability to form films, the crystal-smectic transformation could not be studied by optical microscopy. In addition, due to lack of clarity of the thermal transitions (e.g., T_g), the DSC technique was also unable to provide confirmation of this transition. Thus, X-ray diffraction was the only technique that shows such a transformation, along with changes observed in the UV-visible spectra. In addition to the powder diffractometer, a flat-film camera was also used to record the diffraction traces for these transformations. These are shown in Figure 3.12.

Based on the premise that the strong interactions between the perylene moieties cause such a slow transformation, we attempted to blend short chain alkanes or perylene in the hope of providing mobility to the chains and reduce the time or temperature required for the transition. However, because of the poor solubility, these attempts were not successful. Even physical blending did not prove useful.

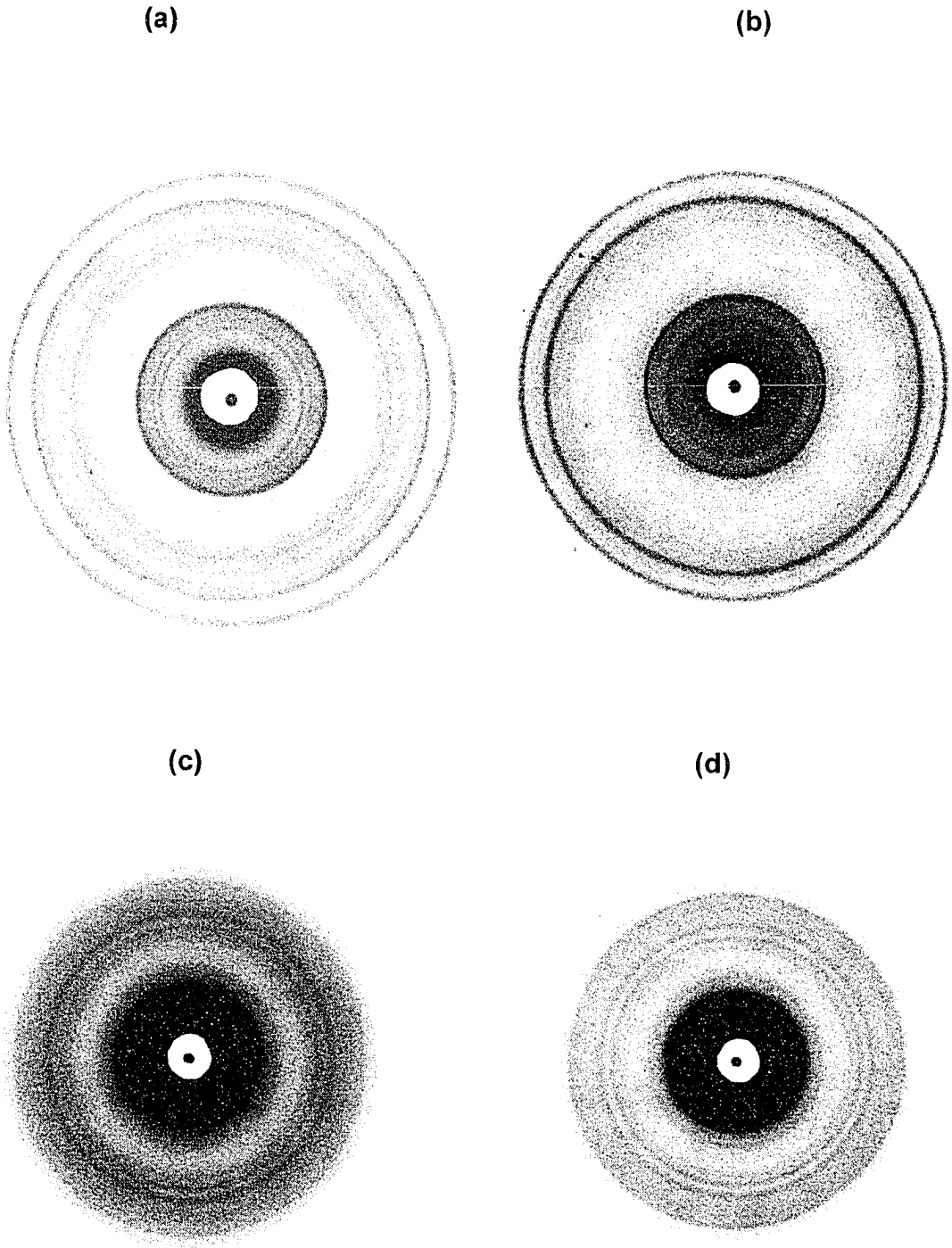

Figure 3.12. X-ray diffraction recorded on films: (a) diffraction of PPI-12, (b) diffraction of PPI-12 annealed for 4h at 320 °C; (c) diffraction of PPI-10, (d) diffraction of PPI-10 annealed for 4h at 320°C.

The question naturally arises as to if these changes are due to the degradation of the polymer upon prolonged annealing at temperatures over 300°C. From Table 3.1 it is seen that with PPI-12, a weight loss of 5% begins at 424°C. An isothermal TGA analysis was performed without the nitrogen flow, i.e., in the air flow, holding the sample at 320°C for 9 h. The weight loss was only 3% (Figure 3.13). Thus, if degradation occurs, it is not appreciable. The fact that the d-spacings of the prominent reflections do not change, also supports the conclusion that degradation is not the cause of the mesogenic transition.

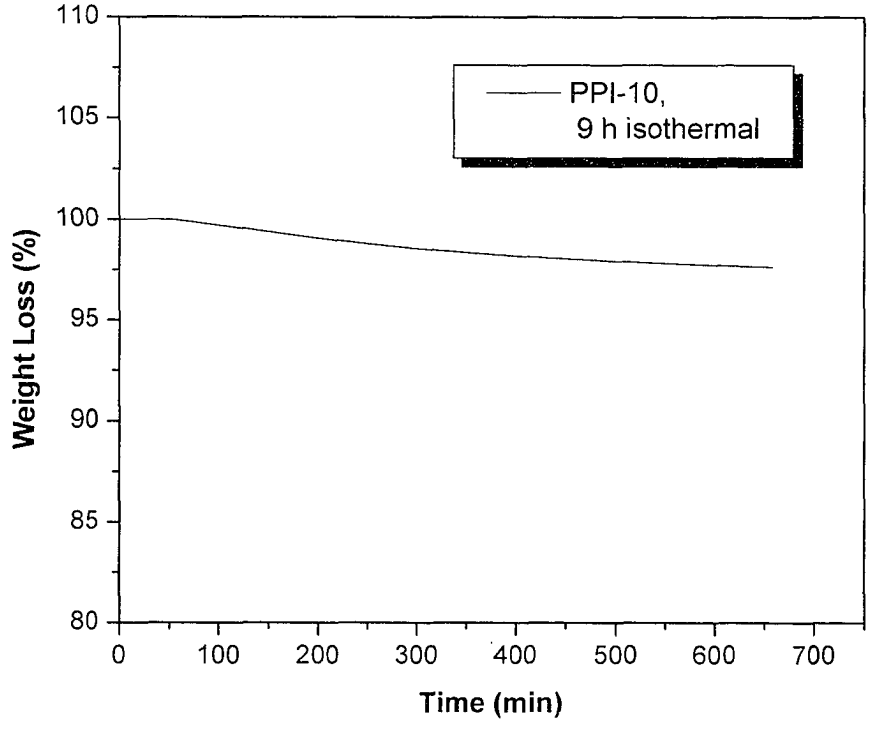

Figure 3.13. Isothermal thermogravimetric analysis curves of PPI-10 held for 9h at 320°C.

The degradation did not happen can be confirmed by another method. The annealed sample was dissolved in *m*-cresol, and X-ray diffraction was recorded on the dried precipitate. Most of the original reflections (i.e., as from samples prior to annealing) were observed again (Figure 3.14), which also confirms that the structural transformations observed above are not due to degradation. The low intensity of the reflections in Figure 3.14a is due to the small quantity of the sample used. This is because of the poor solubility of PPI-12 in *m*-cresol. However, the diffraction pattern is more like original one (Figure 3.14b) than annealed one (Figure 3.14c).

However, the flow of nitrogen does have an effect in slowing down the transformation. The PPI-12 was annealed in the DSC instrument, under nitrogen flow, for various times, and X-ray diffraction was recorded. It took nearly 15 h for the transition to occur. Figure 3.15 shows the diffraction from PPI-12, and after annealing in air for 5 h and under nitrogen flow for 15 h. It is seen that annealing in air and nitrogen leads to the transformation, although the time taken is longer in the latter case.

IR spectra also show changes in the absorption bands, corresponding to the carbonyl and CN bonds, upon annealing. The spectra are shown in Figure 3.16 and the peak assignments are given in Table 3.3. The most relevant molecular vibrations of PPIs are the two strong carbonyl stretching vibrations at 1655 and 1695 cm^{-1} which correspond to the anti-symmetric and symmetric C=O stretches,[20] respectively. Upon annealing at

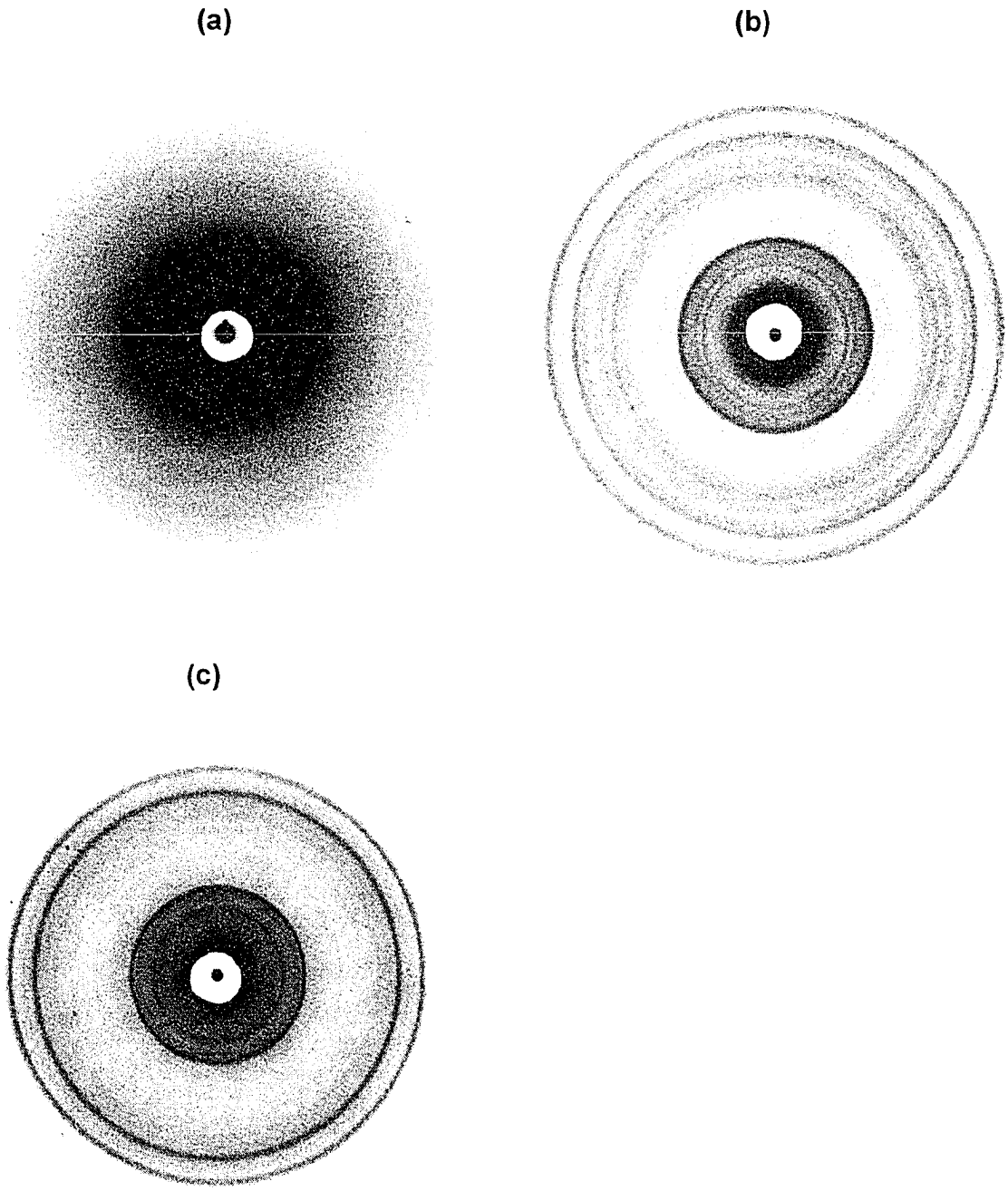

Figure 3.14. X-ray diffraction of PPI-12: (a) PPI-12 annealed 4 h at 320°C, then dissolved in m-cresol, and dried; (b) original PPI-12; (c) PPI-12 annealed 4h at 320°C.

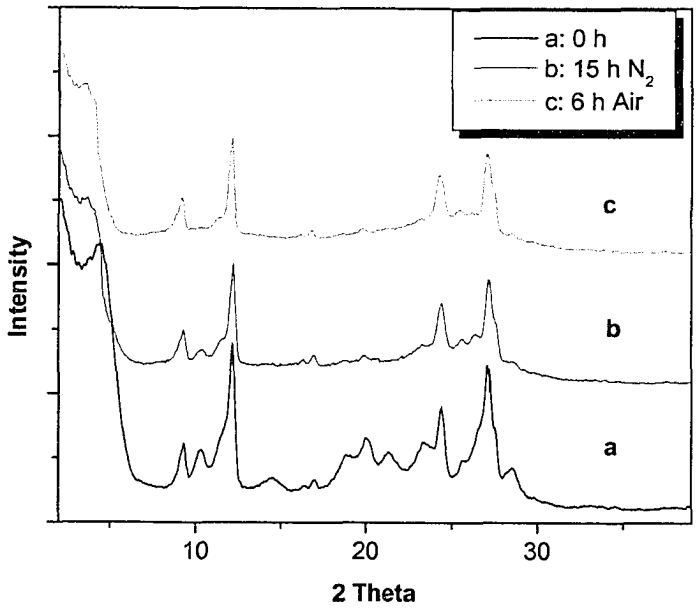

Figure 3.15. X-ray diffraction patterns of PPI-12 annealed at 320°C in nitrogen and air atmosphere.

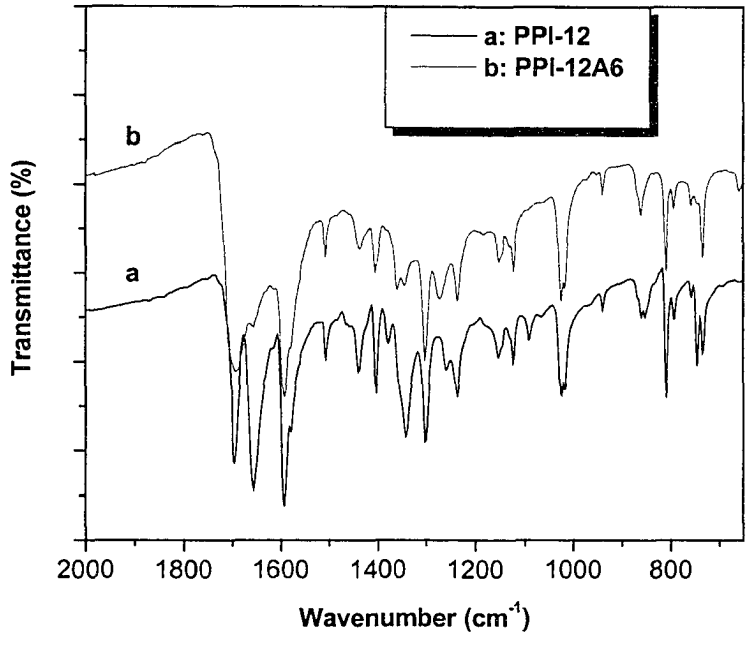

Figure 3.16. IR spectra of PPI-12: (a) original sample, (b) annealing for 6 h at 320°C.

320°C for 6 h, the relative intensities of these bands change drastically, with the 1655 cm^{-1} band becoming weak, and broadening of the one at 1691 cm^{-1}. The absorption at 1342 cm^{-1} corresponding to C—N stretch, splits into a doublet, with shifting to higher frequencies, at 1345 and 1359 cm^{-1}. This can be explained by an increase in crystallinity. There is no change in the positions of the absorption bands corresponding to the alkyl groups. Thus, annealing causes changes in the packing of the perylene moieties and increases the crystallinity.

Table 3.3. Observed IR wave numbers (cm^{-1}) and their assignments for PPI-12.

PPI-12	PPI-12 Annealed at 320°C for 6 hr	Assignment
746	735	C-H perylene wag
810	810	C-H perylene wag
852	860	C-H perylene wag
939	939	C-H bending
1024	1024	C-H bending
1122	1122	C-H bending
1155	1151	C-H bending
1236	1236	alkyl bending
1302	1302	alkyl bending
1342	1345	C-N stretch
	1360	
1404	1406	ring stretch
1441	1438	CH2 scissors
1593	1593	C=C ring stretch
1655	1691	C=O, stretch
1695		

3.3.6 Chain Folding

As noted in the Introduction, a molecular dynamics simulation of an isolated PPI-12 chain suggested the possibility of intra-molecular chain folding of these polymers, and the smectic ordering of the perylene units.[11] However, the results presented here show that in the real system, the mesomorphic transition is very slow, due to the predominant intermolecular interactions between the chains. This rules out the possibility of intra-molecular chain folding in the solid state, as suggested by simulations on single chains. Figure 3.17 shows that perylenes stack parallel to each other and the distance between two perylene is about 3.6Å. Local aggregates of perylene are seen, upon chain folding.

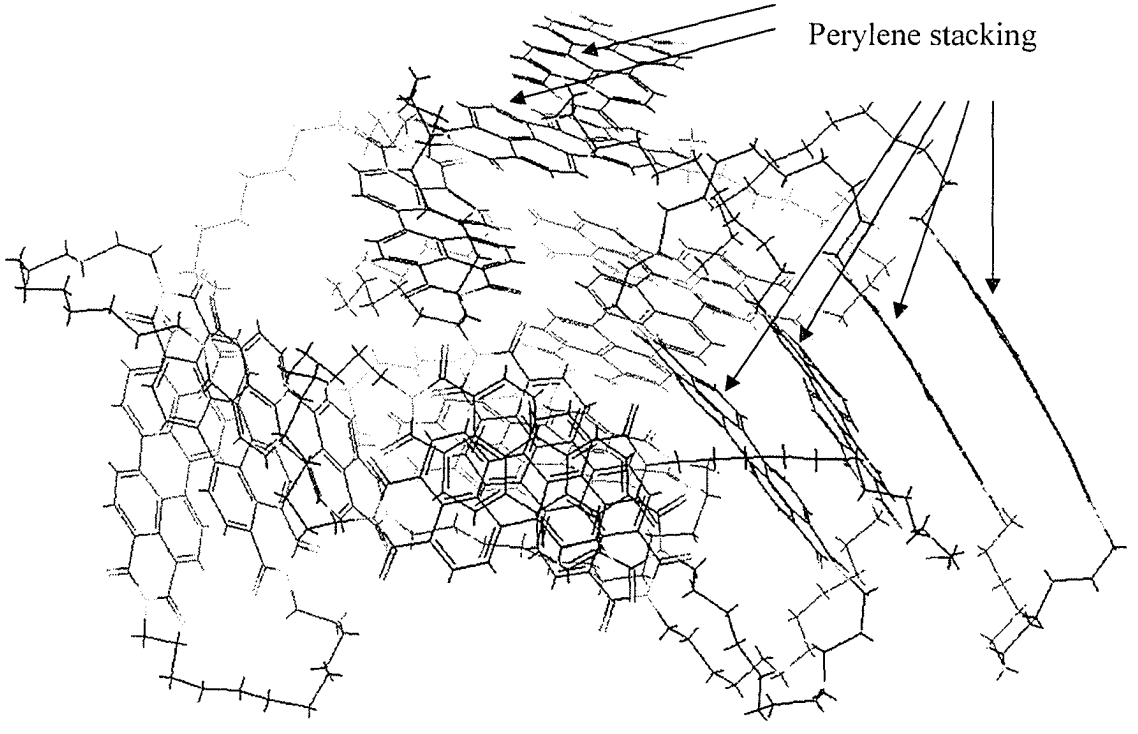

Figure 3.17. Chain conformation of PPI-12 after dynamics 500ps by Cerius[2].

As seen from Figure 3.7, the maximum *d*-spacing in the wide angle region increases with the length of the alkyl spacer, and parallels the calculated monomer length with the extended conformation of the spacer. This again confirms that intra-molecular chain folding, if any, is not predominant in this case. However, such intra-molecular chain folding has been suggested by Neuteboom et al[21] in the case of alternating perylene bisimide-poly THF copolymers in solution. Wang et al[22] reported folding of alternating conjugated chromophores and single stranded DNA in aqueous solution. The chromophore in this case was also the perylene tetracarboxylic bisimide. Thus, while the intra-molecular chain folding as suggested by the molecular dynamics simulations has been observed[12, 22] with perylene containing polymers in solution, such a possibility could not be examined for PPI-12 due to its poor solubility.

3.4 Conclusions

Perylene-containing polyimides with alkyl chain spacers of different lengths adopt an extended conformation, irrespective of whether the chain contains odd or even number of CH_2 groups. This is attributed to the tendency for stacking of the perylene units, which would not be possible if the chain with odd number of CH_2 groups were to take a helical shape. Insolubility of these polymers in common solvents and the inability to prepare films prevented us from obtaining oriented X-ray diffraction and deriving the detailed chain conformation in the crystalline state. The crystallinity of the as-prepared samples increases with the alkyl chain length. Annealing causes time dependent structural transformations, indicated by changes in UV-visible spectra, and X-ray diffraction. The former shows progressive changes with annealing time. The broad absorption maximum

splits into three well-defined maxima with about 1 h of annealing, and further annealing results in the broadening of the blue shifted maximum. Prolonged annealing results in a smectic-like transition as indicated by X-ray diffraction and the time for such transition depends on the temperature of annealing and the length of the spacer.

References

1. Ferrere, S.; Zaban, A.; Gregg, B.A. *J. Phys. Chem. B*, **1997**, *101*, 4490-4493.

2. Ranke, P.; Bleyl, I.; Simnerer, J.; Haarer, D.; Bacher, A.;, Schmidt, H.W. *Appl. Phys. Lett.* **1997**, *71*, 1332-1334.

3. Law, K.Y. *Chem. Rev.* **1993**, *93*, 449-486.

4. Horowitz, G.; Kouki, F.; Spearman, P.; Fichon, D.; Nogues, C.; Pan, X.; Garnier, F. *Adv. Mater.* **1996**, *8*, 242-245.

5. (a). Graser, F.; Hädicke, E. *Justus Liebigs Ann. Chem.* **1980**, 1994-2001. (b). Graser, F.; Hädicke, E. *Justus Liebigs Ann. Chem.* **1984**, 483-494. (c). Hädicke, E.; Graser, F. *Acta Crystallogr.* **1986**, *C42*, 189-195. (d). Hädicke, E.; Graser, F. *Acta Crystallogr.* **1986**, *C42*, 195-198. (e). Klebe, G.; Graser, F.; Hädicke, E.; Berndt, J. *Acta Crystallogr.* **1989**, *B45*, 69-77.

6. (a) Cormier, R.A.; Gregg, B.A. *Chem. Mater.* **1998**, *10*, 1309-1319. (b) Gregg. B.A.; Cormier, R.A. *J. Am. Chem. Soc.* **2001**, *123*, 7959-7960.

7. Struijk, C.W.; Sieval, A.B.; Dakhorst, J.E.J.; van Dijk, M.; Kimkes, P.; Koehorst, R.B.M.; Donker, H.; Schaafsma, T.J.; Picken, S.J.; van de Craats, A.M.; Warman, J.M.; Zuilhof, H.; Sudhoelter, E.J.R. *J. Am. Chem. Soc.* **2000**, *122*, 11057-11066.

8. Ghosh, M.K.; Mittal, K.L. Editors. *Polyimides: fundamentals and applications.* Marcel Dekker: New York, **1996.**

9. Wilson, D.; Stenzenberger, H.D.; Hergenrother, P.M. Editors. *Polyimides*. Blackie & Son: Glasgow, **1990.**

10. Wang, Z.Y.; Qi, Y.; Gao, J.P.; Sacripante, G.G.; Sundararajan, P.R.; Duff, J.D. *Macromolecules* **1998**, *31*, 2075-2079.

11. Sundararajan, P.R. *Comp. Theo. Polym. Sci.* **2000**, *10*, 219-220.

12. Neuteboom, E.E.; Meskers, S.C.J.; Meijer, E.W.; Janssen, R.A.J. *Macromol. Chem. Phys.* **2004**, *205*, 217-222.

13. Bessonov, N.A. *Polyamic Acids and Polyimides*, Chapter 4. CRC Press: **1993.**

14. Harris, F.W.; Hsu, S.C.C. *High Perf. Polym.* **1989**, *1*, 3-16.

15. (a) Icil, H.; Icli, S. *J. Polym. Sci. Polym. Chem.* **1997**, *35*, 2137-2142. (b) Ghassemi, H.; Hay, A.S. *Macromolecules* **1994**, *27*, 4410-4413.

16. Drappel, S.; Sundararajan, P.R.; Rudin, A. *Polymer* **1997**, *38*, 1259-1272.

17. Bohn, P.W. *Annu. Rev. Phys. Chem.* **1993**, *44*, 37-60.

18. Emerson, E.S.; Conlin, M.A.; Rosenoff, A.E.; Norland, K.S.; Rodriguez, H.; Chin, D.; Bird, G.R. *J. Phys. Chem.*, **1967**, *71*, 2396-2403.

19. Würthner,F.; Thalacker,C.; Diele,S.; Tschierske,C. *Chem. Eur. J.* **2001**, *7*, 2245-2253.

20. Rodriguez-Llorente, S.; Aroca, R.; Duff, J. *Spectrochim. Acta A* **1999**, *55*, 969-978.

21. Neuteboom, E.E.; Janssen, R.A.J.; Meijer, E.W. *Synth. Met.* **2001**, *121*, 1283-1284.

22. Wang, W.; Wan, W.; Zhou, H-H.; Niu, S.; Li, A.D.Q. *J. Am. Chem. Soc.* **2003**, *125*, 5248-5249.

Chapter 4

Effect of 4,4'-(Hexafluoroisopropylidene)diphthalic Anhydride (6FDA) on the Structural Features of Perylene Containing Copolyimides*

(* D. Yao, P.R. Sundararajan, *Eur. Polym. J.* **2005**, Article in Press)

4.1 Introduction

In Chapter 3, we described the annealing induced structural changes in polyimides containing perylene tetracarboxylic dianhydride and aliphatic diamines in the main chain with alkyl spacers of different lengths. With these perylene-containing polyimides (PPI), the crystallinity increased with the length of the spacer, and red-shift of the UV-visible absorption maxima was also seen upon annealing. From X-ray diffraction and molecular modeling, it was concluded that these polymers adopt the same conformation, with both odd and even number of methylene groups in the alkyl spacer. For polymers with $(CH_2)_{10}$ and $(CH_2)_{12}$ spacers, a mesomorphic transition was observed upon annealing at 320°C or higher, for more than 4h.

Perylene bisimides have been used in various fields for decades.[1,2] The color of these pigments depends on the extent of aromatic overlap. This offered the benefit of tunability of the color of the pigment by peripheral substitution, to control the π overlap. Although they were initially used by pigment industries, modification of their properties through novel materials design led to applications in areas such as electrophotography (e.g., xerographic photoreceptors)[3], photovoltaics[4] etc. as electron conductors. However, most of the perylene bisimides are insoluble and therefore the preparation of films requires vapor deposition or dispersing them in polymer matrices. This limited their applications. Recently, a number of authors[5-11] synthesized perylene-containing polyimides in order to avoid the problem of pigment aggregation and phase separation that would occur when dispersed in a polymer matrix.

Polyimides are known for their high thermal stability, good mechanical properties, low dielectric constant, low coefficient of thermal expansion and high radiation resistance.[1,2] Perylene-containing polyimides are an interesting class. For example, Ghassemi and Hay[6] reported red pigmentary polyimides made from N,N'-diamino-3,4,9,10-perylene tetracarboxylic acid bisimide. Icil and Icli [7] synthesized a photostable polymer based on perylene-3,4,9,10-tetracarboxylic acid-bis-(N,N'-dodecylpolyimide). Wang *et al* [9-11] prepared perylene containing polyimides and investigated their xerographic electrical properties, voltage dependent fluorescence etc. However, most of these materials dissolved or partially dissolved only in strong polar solvents, such as, *m*-cresol or concentrated H_2SO_4 because of the strong π-π stacking between perylene moieties. Therefore, improving the solubility became an important consideration. For the preparation of soluble perylene bisimides or polyimides, three different strategies proved to be successful. Langhals and coworkers[12,13] developed an approach in which the pristine perylene bisimide chromophore was dissolved by introducing solubilizing substituents, such as, 2,5-di-*tert*-butyl-phenyl, at the imide nitrogen. The dyestuffs obtained by this approach exhibit usually indistinguishable absorption and emission properties because nodes in the HOMO and LUMO at the imide nitrogen reduce the coupling between the perylene bisimide units and the imide substituents to a minimum.[13] Another strategy was to introduce substituents at the carbocyclic scaffold in the so-called bay-area (see Figure 1.1). This approach was first devised by Seybold and Wagenblast[14]. Yet another approach is copolymerization with other monomers. Niu et al[5] prepared aromatic copolyimides from 3,4,9,10-perylenetetracarboxylic dianhydride (PTDA), 4,4'-(hexafluoroisopropylidene)diphthalic anhydride (6FDA) and the aromatic diamines

containing 4,4'-diaminetriphenylamine and 4,4'-methylenedianiline and characterized the thermal stability and UV-visible absorption characteristics in solution and in the solid film. Yang et al[7] prepared copolyimides by one-step polycondensation of one cardo diamine, 4,4'-(9H-fluoren-9-ylidene)-bisphenylamine with two dianhydrides, PTDA and 6FDA and discussed the solubility, thermal stability, photoluminescence and electroluminescence. A previous study[9] on the alternating perylene-containing copolyimides with 6FDA showed annealing-induced red shift of the absorption maximum.

In most of the above studies, an alternating or a block copolymer was used. In addition, the discussions were focused on solubility. With copolymerization, properties such as the absorption spectra, crystallinity etc are expected to change with composition. However, the manner in which these changes occur depends on the particular system. In this chapter, we discuss the solubility, X-ray crystallinity, UV-visible and fluorescent spectra and thermal properties of random perylene containing copolyimides with perylenetetracarboxylic dianhydride and 6FDA, and effect of the copolymer composition on the these properties. The structural features and X-ray results are interpreted in terms of the adaptable conformation of the 6FDA segment and conformational isomorphism.

4.2 Experimental

4.2.1 Materials.

1,12-diaminododecane , 4,4'-(Hexafluoroisopropylidene)diphthalic anhydride (6FDA), isoquinoline, and other solvents were purchased from Aldrich Chemical Co. and used as

received. 3,4,9,10-perylenetrtracarboxylic acid dianhydride (PTDA) was purified by using the method in the literature.[9] *m*-cresol was stored over 4 Å molecular sieves and distilled before use.

4.2.2 Characterization.

Instruments used for characterization, (x-ray diffraction, UV-visible, FT-IR spectroscopy etc.) were described in Chapter 2.

4.2.3 Synthesis of Diamine 4 (Scheme 4.1)[9]

1,12-Diaminododecane (153.2 g, 0.76 mol) was dissolved in 240 mL of *m*-cresol with 1.0 g of isoquinoline, and the solution was heated to 200 °C. To this mixture, 20.0 g (51.0 mmol) of perylene-3,4,9,10-tetracarboxylic dianhydride (PTDA) was added as 4 portions over 40 min. The reaction mixture was stirred at 200 °C for 5 h, cooled to room temperature, and poured into 600 mL of methanol. The precipitated solid was then filtered off, washed with methanol, and dried in air to yield 30.1 g (80%) of crude product. The crude product was extracted by Soxhlet extraction system with *o*-dichlorobenzene under nitrogen atmosphere to give pure diamine **4**: 15.4 g (51%); mp >300 °C.

4.2.4 Synthesis of Alternating Copolyimides (Scheme 4.1)[9]

In a three-necked, round-bottomed flask, diamine **4** (2.269 g, 3.000 mmol), 6FDA (1.326 g, 3.000 mmol), and 0.5 g of isoquinoline were dissolved in 60 ml of *m*-cresol. The reaction solution was heated to 200 °C for 24 h, and during the course of the reaction, small amount of *m*-cresol was distilled off. The mixture was then cooled to 100 °C and poured into 300 ml of methanol. The precipitated polymer was collected by filtration and washed with methanol several times. The polymer was then dissolved in TCE (150 ml)

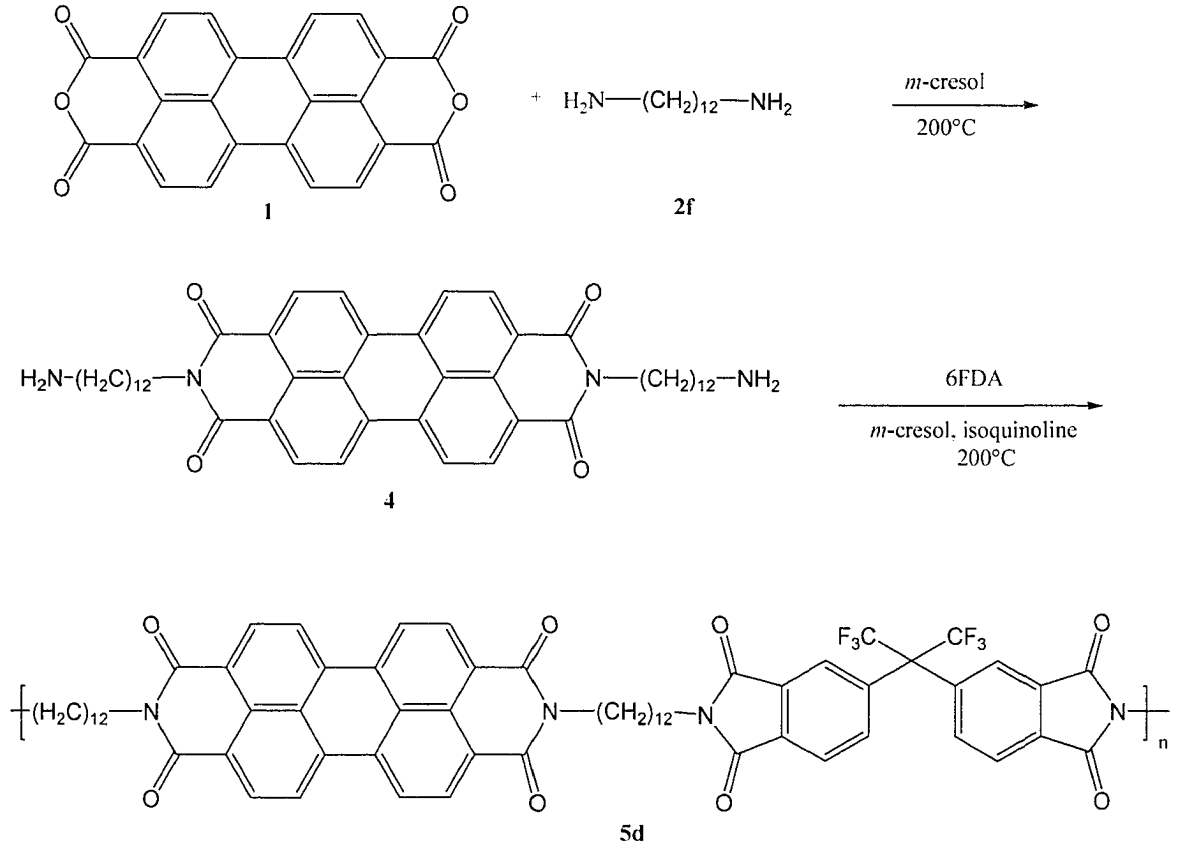

Scheme 4.1. Synthesis of alternating perylene-containing copolyimide.

and precipitated by adding 100 ml of methanol dropwise into the stirred TCE solution. The sticky precipitate was then dissolved in 40 ml of TCE and precipitated into 300 ml of methanol. Polymer **4d** was filtered off, washed with methanol, and dried at 120 °C for 24 h under vacuum (5 mmHg). Yield: 3.07 g (85%).

Other alternating copolymers were prepared following the same procedure.

4.2.5 Synthesis of Perylene-containing Copolyimide with 6FDA (Cop80) (Scheme 4.2).

The synthesis route of copolymers is similar to the earlier literature,[9] and the typical procedure is as follows: 1276.8mg(3.2mmol) of PTDA(99%), 816.3 mg(4mmol) of 1,12-diaminododecane (98%), and 0.4g isoquinoline as a catalyst were added into 35ml *m*-cresol in a 100ml three necked flask equipped with a nitrogen inlet and a magnetic stirrer. The mixture was stirred at 80° for 1 hr, then heated up to 120°C for 4 hrs. After cooling to the room temperature, 359.0mg (0.8mmol) of 6FDA(99%) was added to the mixture and heated again to 120°C for 2 hrs, and 200°C for overnight. The red clear solution was cooled to 80°C, and poured into 250ml acetone with vigorous stirring. The precipitate was collected by filtration, washed with methanol and dried under vacuum at 100°C and 1.95g was collected. The crude product was treated with acetone in a Soxhlet apparatus for 10 hrs, in order to remove high boiling solvents, i.e., *m*-cresol and isoquinoline. Acetone was replaced with chloroform in the Soxhlet apparatus, and the extraction was carried on for another 24 hrs. All the crude was chloroform-soluble, and 1.90 g was collected after dried. The characteristics are as follows: UV-visible(in $CHCl_3$):

526, 490, and 460 nm. IR (KBr pellet): 1778, 1721, 1694, 1656, 1594, 1440, 1393, 1342, 1256, 809, 746 and 721cm^{-1}.

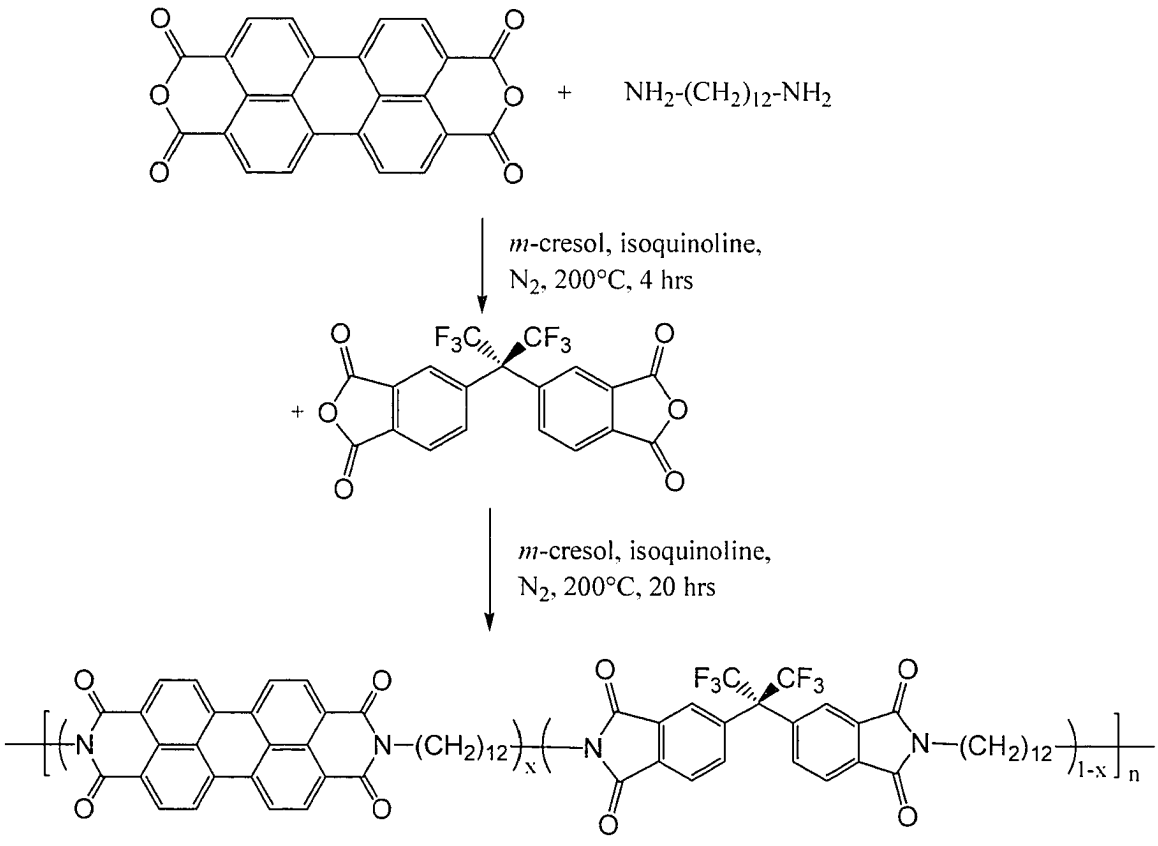

Scheme 4.2. Synthetic route of Perylene-containing Polyimide co-6FDA

4.3 Results and Discussions

4.3.1 Synthesis

Scheme 4.1 shows the procedure of alternating copolymerization (Alt-PPI-6FDA). First, to prevent polymerization, high ratio of aliphatic amines to perylene dianhydride (4 times) was used. Furthermore, because purification is critical for polymerization, Soxhlet

extraction with *o*-dichlorobenzene was used for this purpose. During extraction, inert gas atmosphere is very important due to the possibility of oxidation of amino groups.

Scheme 4.2 is shown the synthetic route of copolymers. Copolyimides were prepared with five different percentages of 6-FDA. The mol% perylene chromophore in the main chain was varied from 10 to 40mol% of polymers. The molar amount of diamine 1,12-diaminododecane was kept constant (50 mol%) and the amounts of PTDA and 6FDA were varied, keeping the total mole number of two dianhydrides equal to that of 1,12-diamino-dodecane. The percentage of perylene chromophore was from 20 to 80% of the sum of the two dianhydrides. The abbreviation Cop X refers to the percentage of 6-FDA. Due to the different reactivity of the five-membered pyromellitic dianhydride and the six-membered perylene dianhydride, a stepwise polymerization was necessary to achieve a random incorporation of the comonomers. First, 1,12-diamino-dodecane was reacted with the less reactive six-membered dianhydride PTDA in the presence of isoquinoline as a catalyst at 120 °C for 4h, resulting in a mixture of unreacted diamine 1,12-diamino-dodecane and amino-terminated perylene intermediate. In the second step, the more reactive five-membered dianhydride 6FDA was added when the reaction mixture was cooled to room temperature. Then the reaction mixture was heated again and kept at 120°C for 4 h in order to obtain high molecular weight poly (amic acid)s. In the final step the poly (amic acid) was kept at 200 °C for 10 h to imidize completely by elimination of water via purging dry nitrogen. The conventional approach of co-polymerization[9] by adding all comonomers together at one time did not lead to perylene-containing copolymers with exact amounts of perylene content because the more reactive five-

membered 6FDA reacted with diamine, and it was difficult to react the resulting oligomer with the six-membered PTDA. Furthermore, even when PTDA reacted with the oligomer, the distribution of molecular weight would be large. Finally, the completion of imidization of these copolymers was monitored with the IR shift[16] of C=O vibration band of the anhydride from a broad band between 1780 and 1730 cm^{-1} to new bands at about 1690 and 1650 cm^{-1} of the imide C=O anti-symmetric and symmetric stretching vibrations.

Previous studies[9] used the first step reaction of 6-membered dianhydride with diamine at a higher temperature of 200°C. However, we did not find any difference between the reactions at a medium temperature of 120°C or the higher temperature. The reason is that at the lower temperature, polyamic acid may not transfer to form imide totally. However, after the second dianhydride was added, the new dianhydride will only react with the unreacted diamine and the amino group on polymic acid, so the copolymer still formed as designed. Finally, the cyclization happened and the copolyimide formed.

It is difficult to integrate the number of hydrogens on perylene in the ^1H NMR spectrum. However, hydrogens on the methylene groups (CH_2) and on 6FDA are easy to map: 24 hydrogens for the methylenes and 6 for 6FDA. In that case, the copolymer composition can be calculated from ^1H NMR. In the present case, the percentages were 71.6 and 68.4 for Cop80 and Cop60, respectively. These numbers are reasonable compared to the theoretical values of 80% and 60% respectively.

4.3.2 Viscosity and Solubility

The viscosity of the copolyimides was measured at concentrations 0.05, 0.1, 0.2, and 0.4 g/dl at 30°C in H_2SO_4 so that the intrinsic viscosity can be extrapolated. The intrinsic viscosity is the limit of the reduced viscosity as the polymer solute concentration approaches zero. The intrinsic viscosity is also the limit of the inherent viscosity, as the solution polymer concentration approaches zero. Both methods should lead to same results, which have a common intercept that is the intrinsic viscosity. Table 4.1 shows the result of intrinsic viscosity of copolymers. Because of the limitation of solubility, the molecular weight cannot be measured by GPC for the copolymer with 6FDA ratio lower than mole 80%. However, in comparison with perylene homopolymers, the solubility of copolymers increases. It is well known that due to the strong π-π interactions, the homopolyimides from PTDA are usually insoluble in organic solvents. However, with increasing the percentage of 6FDA, the π-π interactions become weaker and the solubility in common solvents increases. Cop40 partially dissolves in *m*-cresol, TCE, and dichlorobenzene, and Cop60 can totally dissolve in *m*-cresol, and partially in TCE. Finally, Cop80 can dissolve in most common solvents such as $CHCl_3$, CH_2Cl_2 (Table 4.1).

The viscosities lie in the 0.31-0.66 dL/g range, similar to those of the homopolymers[9] and indicate that the polymers have medium to a reasonably high molecular weight. Note that the [η] decreases significantly with Cop80. The viscosity of the homopolymer, perylene-containing polyimide with dodecane spacer (PPI-12), was 0.65 dL/g at 30°C. This indicates that copolymerazation does not increase the molecular weight, but only the solubility. Thus, perylene-containing copolyimides can be processed easily from solution to form transparent, flexible and tough films when the PTDA content was lower than 20mol% of total dianhydrides. If we assume that the molecular weights are in the same range, the similarity of [η] up to a concentration of 60mol% FDA would indicate that the overall chain contour (e.g., the end-to-end distance) is similar even upon copolymerization, until the concentration of 6FDA reaches 80mol%. This is discussed later.

The solubility of alternating copolyimides is a little better than the block copolymers, such as Alt-PPI-6FDA has the similar solubility as Cop60. However, 50% of perylene inside the molecule is still too much to let the copolymers have good solubility in common solvents. Until the ratio of perylene is reduced to 20%, the solubility of copolymer becomes soluble.

Table 4.1. Intrinsic Viscosities and Solubilities.

	[η] (dL/g)[(a)]	Solubility[(b)]							
Polymer		H_2SO_4	$CHCl_3$	CH_2Cl_2	THF	*m*-Cresol	TCE	DCB	NMP
Cop20	0.505	+	+ –	–	–	+ –	+ –	–	–
Cop40	0.554	+	+ –	–	–	+ –	+ –	+ –	–
Cop60	0.66	+	+ + –	+ –	–	+	+ + –	+ –	+ –
Cop80	0.31	+	+	+	+	+	+	+	+
Alt-PPI-6FDA	-	+	+ –	+ –	–	+ –	+ –	+ –	–
PPI-12*	0.65	+	–	–	–	+ –	–	–	–

(a) Intrinsic viscosities were measured in different concentration in H_2SO_4 at 30°C.

(b) + Soluble in room temperature, + + – almost soluble in room temperature, + – slightly soluble at least in higher temperature, – insoluble in any cases.

* PPI-12: perylene-containing homo-polyimide with dodecane spacer.

4.3.3 Thermal Analysis

The TGA curves of the copolyimides, shown in Figure 4.1, confirm that these are stable up to 460 °C (5% weight loss) as expected (479, 480, 470 and 460°C for Cop80, Cop60, Cop40, and Cop20, respectively). It is noted that the decomposition temperature increases with FDA content and level off at 60%. This also shows that polyimides with 6FDA are more stable than with PTDA. The latter decompose at 425°C. Figure 4.1 shows that a first weight loss occurs for Cop20 to Cop60 between 260-300 °C, which maybe attributed to aliphatic chain scission.

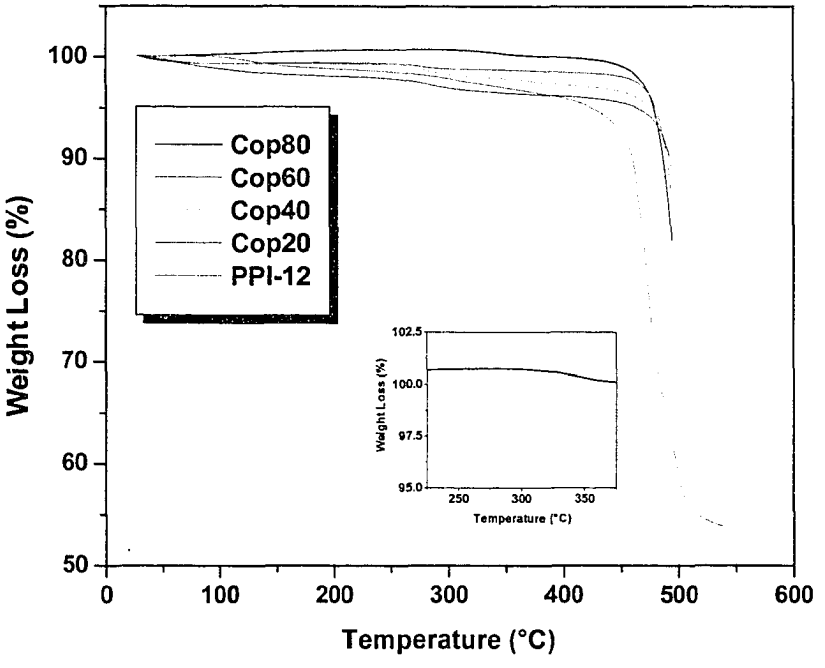

Figure 4.1. Thermogravimetric analysis (TGA) thermograms of copolymer Cop20, Cop40, Cop60, Cop80 and homopolymer PPI-12.

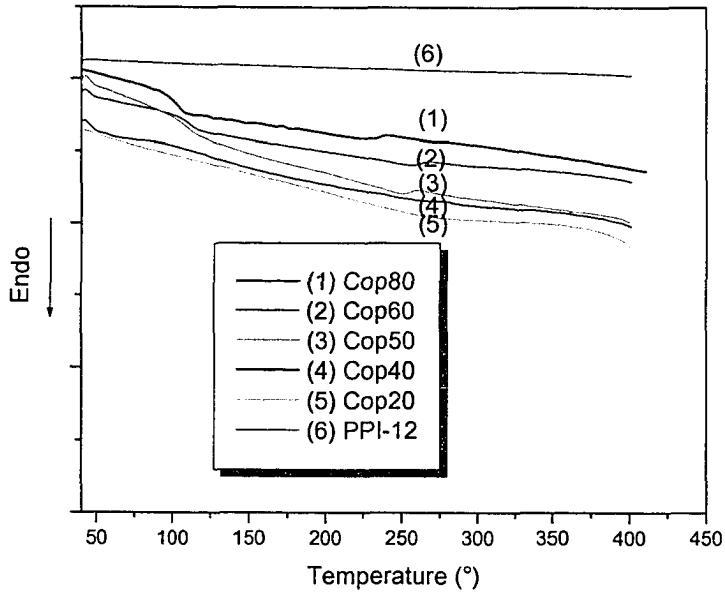

Figure 4.2a. Differential scanning calorimeter (DSC) thermograms of copolymer Cop20, Cop40, Cop50, Cop60, Cop80 and homopolymer PPI-12.

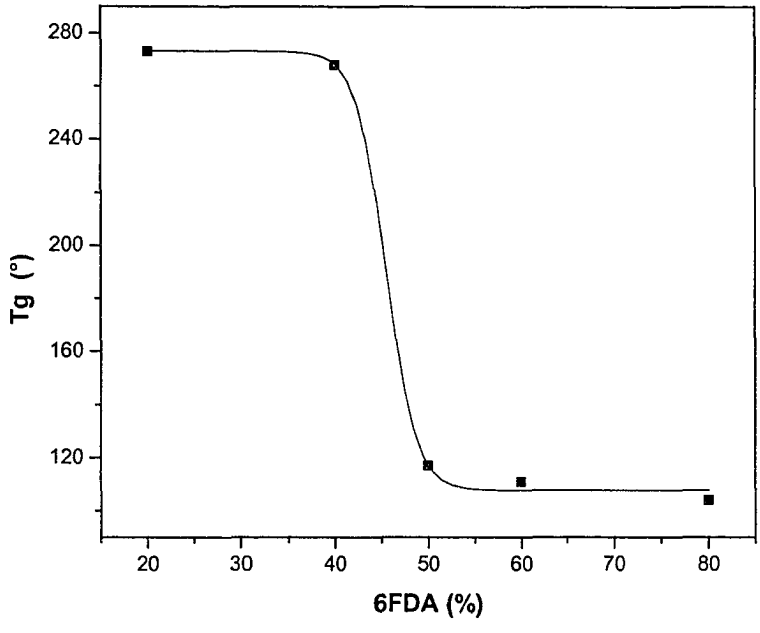

Figure 4.2b The relationship between Tg and the ratio of 6FDA in copolymers.

The DSC traces in Figure 4.2a show that Cop20 and Cop40 do not have a clear transition temperature, but the baseline shifted at the temperatures of 273 and 268°C respectively. Cop60 and Cop80 show T_gs at 111 and 104 °C, respectively. The DSC thermogram of Cop50 is close to the curves of Cop60 and Cop80. It is significant that the T_g is reduced so drastically with 6FDA content, between Cop40 and Cop50. Zhu et al[16] reported that 6FDA-containing oligomers may have a T_g as low as 97°C. Assuming that the baseline shift for Cop20 and Cop40 is indicative of glass transition, a plot of T_g versus 6FDA concentration is shown in Figure 4.2b. Extrapolation to 0% 6FDA leads to a T_g of about 280 °C for PPI-12. This is reasonable since the mesomorphic transformation that we discussed before in Chapter 3 occurs only upon annealing at temperatures of 320 °C or above. Thus by extrapolation, we were able to estimate the T_g of PPI-12, which could not be detected directly from DSC measurements.

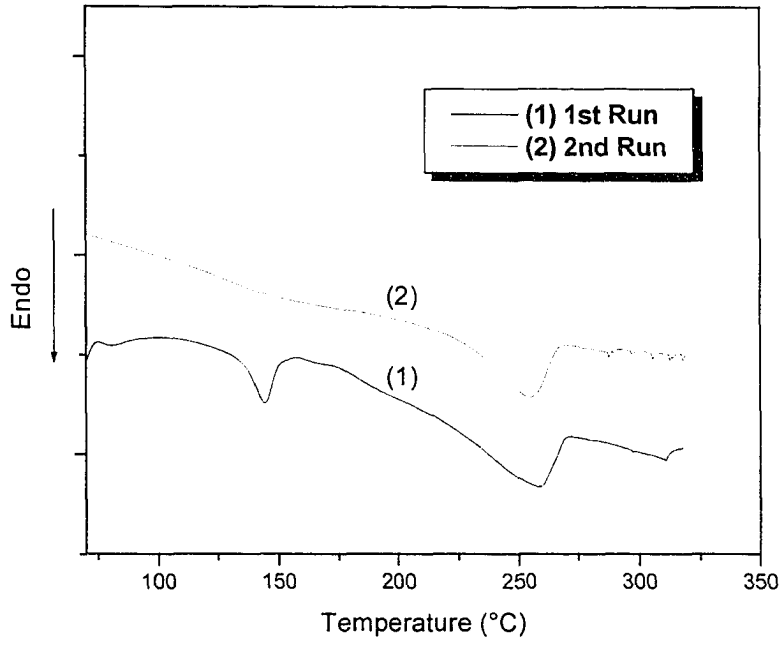

Figure 4.3. Differential scanning calorimeter (DSC) thermograms of alternating polymer — PPI-6FDA.

Alternating polyimide with 6FDA (PPI-6FDA) has the similar result (Figure 4.3). However, the peaks are more like melting points. The first melting peak is at 143 °C, and the second melting peak is at 259°C for the first run. At the second run, the first peak disappear, which means the imperfect crystal contains in the materials.

4.3.4 UV-Visible & Fluorescence spectra

The UV-visible absorption spectra of copolyimides in $CHCl_3$ solution are shown in Figure 4.4a. All these copolyimides show absorption maxima at 526, 490, and 460nm. These are similar to the behavior of N,N'-bis-(aminododecyl)-3,4,9,10-perylene-bis(dicarboximide)[18], which have absorption maxima at 525, 489, and 457nm. It is to be noted that the homopolymer of PPI-12 showed peaks at the same wavelengths as the above monomer.

The vibronic structure of the absorption bands corresponds to the characteristic perylene π-π^* electronic transition. In general, the wavelength of absorption maximum λ_{Abs} of perylene bisimides depends on the substitution pattern of the perylene core as well as on the interaction of the chromophore units.[18] However, there are no substituents on the perylene chromophore in the present case. The fact that there is no shift in the absorption maximum, indicates the absence of any contribution from the 6FDA chromophore to the chain conjugation. That the introduction of 6FDA does not cause any significant conformational change in the perylene segment is also supported by X-ray diffraction data and conformational modeling as discussed below. Further, these perylene copolyimides have the same absorption pattern and positions in other common solvents,

such as, NMP, THF, CH_2Cl_2, dichlorobenzene, and TCE etc. The only exception is a hydroxylic solvent, *m*-cresol, in which the absorptions were at 549, 509, and 475 nm. These positions are similar to absorption peaks of perylene bisimides with C_5, C_{10}, C_{15} and C_{20} alkyl chains in trifluoroacetic acid,[19] which were at 540, and 500 nm for the fist two major peaks. The 15-23 nm red-shift is due to protonic solvent surrounded molecules and parallels Langhals' explanation that all perylene dyes in sulfuric acid cause a 80 nm red shift, yet neither the structure of the spectrum nor the coefficient of extinction was noticeably altered.[12] It is to be noted, however, that the relative intensity of the 526, 490 nm peaks changes when the concentration of 6FDA is 40 mol% or higher, with the former being more intense.

The absorption of spectrum of a film of Cop80 (Figure 4.4b), which was cast from chloroform, shows maxima at 531, 490, 471 nm. The difference between the solution and solid state spectra can be ascribed to the extended state of order in the chain (the crystal structure) resulting in different degree of π overlap of adjacent molecules.[20] Alternating PPI-6FDA has the same absorption as block PPI-6FDA.

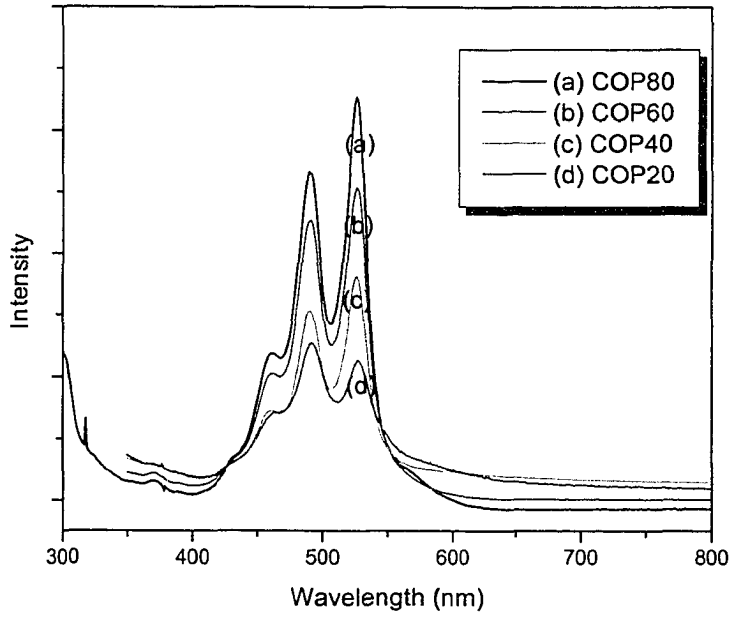

Figure 4.4a. UV-Vis absorption of copolymers in $CHCl_3$.

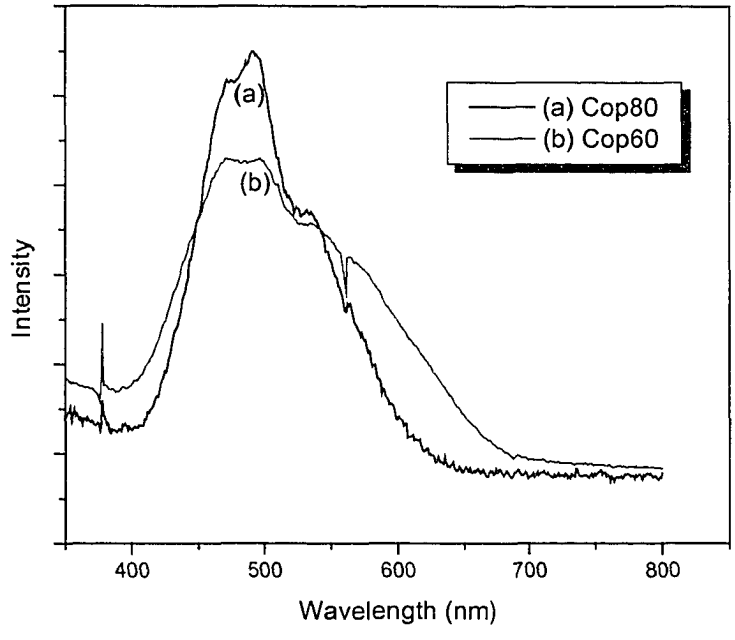

Figure 4.4b. UV-Vis absorption of Cop80 and Cop60 as films.

All these copolymers show that the solutions have strong green-yellow fluorescence. This fluorescence comes from perylene chromophore. This chromophore shows fluorescence at 536.0, 577.8 and 624.1 nm.[17] The fluorescent spectrum of Cop80 is showed in Figure 4.5a, which has peaks at 540, 574 and 621nm, which is quite similar to the monomer. However, the third peak is weak. This may be the reason that fluorescence is weaker for polymer.[21] The alternating copolymer has the same pattern as block copolymer, which has the position of 526, 574, and 521nm respectively (Figure 4.5b). This is reasonable, because they have the same chromophore, and the difference is only order of two monomers.

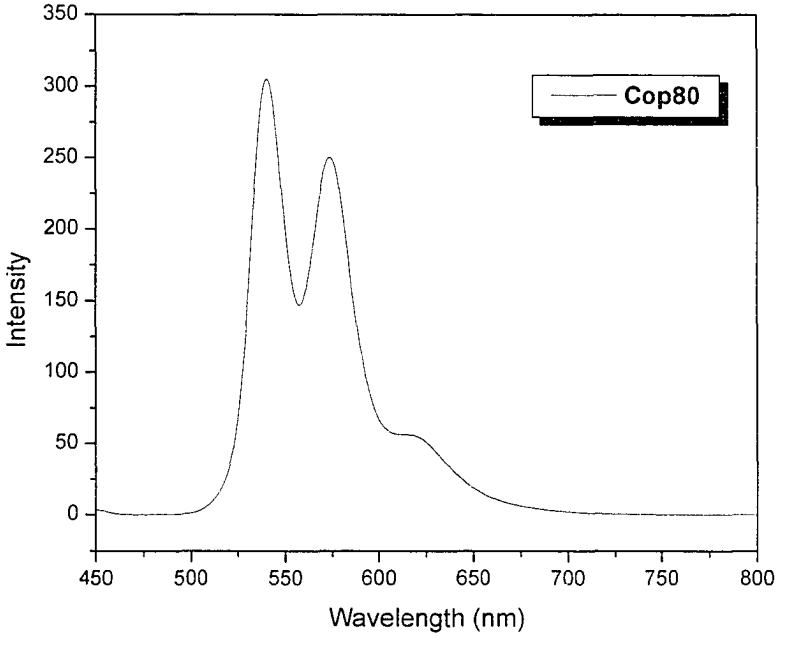

Figure 4.5a. Fluorescent emission (λ_{exc} = 450nm) spectrum of Cop80 in chloroform.

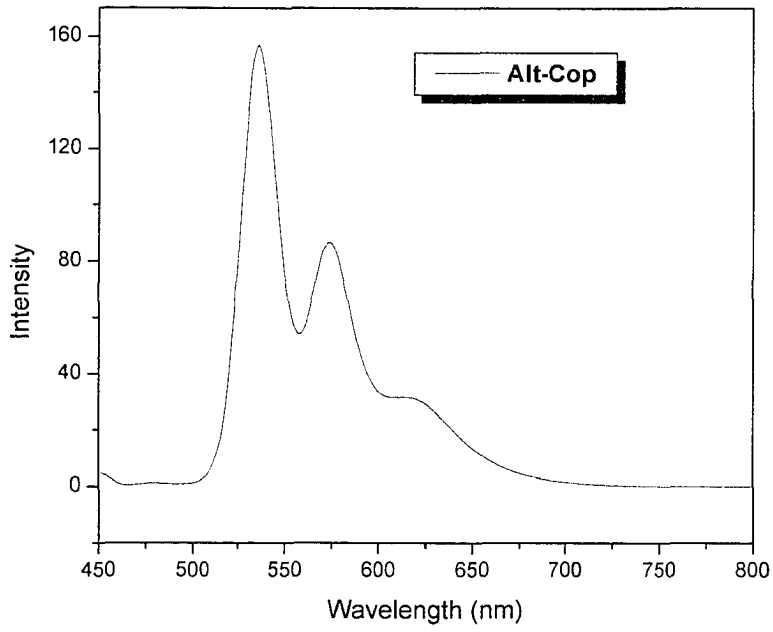

Figure 4.5b. Fluorescent emission (λ_{exc} = 450nm) spectrum of alternating copolyimide – PPI-6FDA in chloroform.

4.3.5 X-ray Diffraction

The wide-angle X-ray diffraction patterns and the crystallinity of the copolymers are shown in Figure 4.6a and 4.6b, respectively. It is seen that the crystallinity of the homopolymer PPI-12 is 24%, and that of Cop20 is 19%. As expected, the crystallinity decreases with an increasing ratio of 6FDA. However, the copolymers are still semi-crystalline until the ratio of 6FDA increases to 80% at which composition, the polymer becomes amorphous. It should also be noted that the reflection corresponding to the d-spacing of 17.9Å, (which is about the length of the perylene unit with 6 CH_2 groups) is not present in the diffraction from Cop80. In contrast to the abrupt decrease in T_g (Figure 4.2b) between 40 and 50% ratio of 6FDA, the crystallinity decreases linearly. The d-

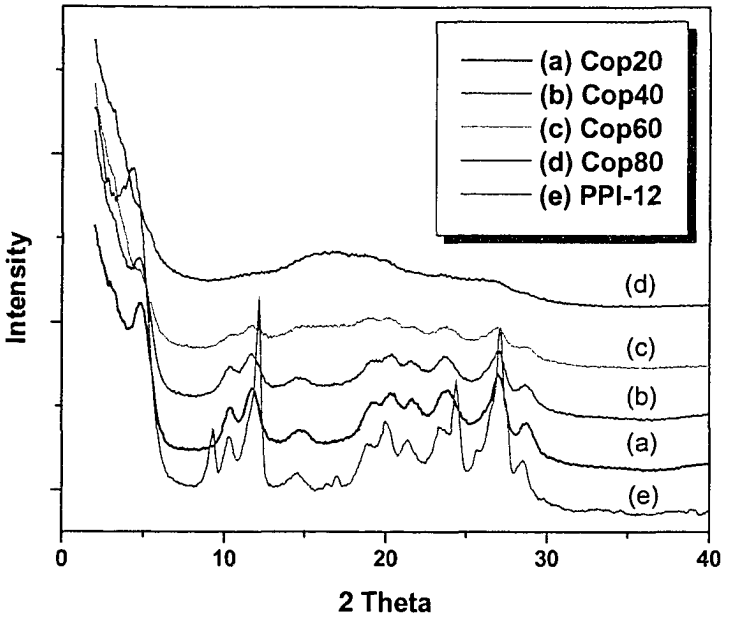

Figure 4.6a. Powder-wide-angle X-ray diffractograms of copolymers.

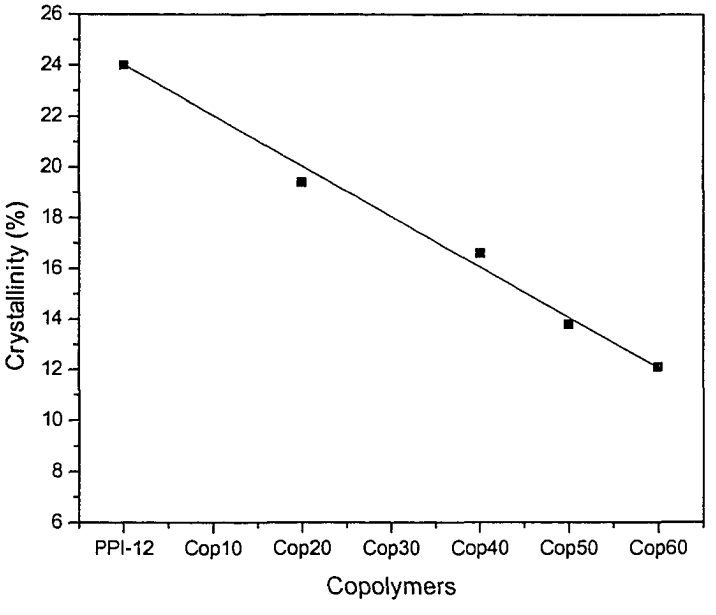

Figure 4.6b. Comparision of crystallinity of different ratios of copolymers with homopolymer PPI12.

spacings of Cop20, Cop40 and Cop60 are compared with PPI-12 in Table 4.2. It is noted from Figure 4.6a and Table 4.2, that the *d*-spacings of most of the reflections are similar to those of the homopolymer PPI-12. Prominent peaks in each case are graded 1 to 6 (given in parentheses) in terms of the intensity. While the reflection at d = 3.3Å is of medium intensity with PPI-12, Cop20 and Cop40, it becomes the most intense reflection with Cop60. The stacking distance varies from 3.3 to 3.6 Å with the perylene systems. The persistent intensity of the reflection at 3.3 Å (similar to graphite) shows that although the crystallinity decreases due to the presence of 6FDA, the perylene packing is hardly affected. Thus, the crystalline packing of the chains would be similar, although the defects introduced by 6FDA would disrupt the crystallinity.

Introduction of 6FDA in the polymer reduces the number of perylene units that participate in π-stacking relative to the degree of polymerization. As mentioned above, the *d*-spacings from the copolymers are similar to those of the homopolymer. Conformational analysis shows that 6FDA can disrupt the stacking, without changing the chain contour significantly. The 6FDA segment can be considered to be similar to that of bisphenol A segment of polycarbonate, with two phenyl groups flanking the isopropylidene moiety. The conformational behaviour of the latter has been discussed before[21]. Figures 4.7a and 4.7b compare the conformational maps in terms of the dihedral angles φ and ψ, in the two cases (the torsion angles φ and ψ are shown in Figure 4.7c). It is seen that similar to the polycarbonate segment, the 6FDA has several symmetrically related minima. One of the energy-minimized conformations of 6FDA is shown in Figure 4.7c, and the conformation of two segments of the copolymer is illustrated in Figure 4.7d.

Table 4.2. Comparison of the X-ray *d*-spacings of the copolymers with the homopolymer PPI-12

Cop20		Cop40		Cop60		PPI-12	
d (Å)	I (%)	*d* (Å)	I (%)	*d* (Å)	I (%)	*d* (Å)	I (%)
2.14	5						
3.10	17 (6)	3.11	12 (6)	3.1	33	3.13	20
3.30	46 (2)	3.29	33 (2)	3.29	100 (1)	3.29	56 (3)
3.72	23 (4)	3.73	19 (4)	3.75	73 (3)	3.65	41 (4)
						3.80	29
4.10	10	4.10	7	4.06	33	4.16	25
4.37	12	4.34	9	4.38	57 (4)	4.42	30 (5)
4.63	10	4.62	6	4.69	44 (6)	4.71	24
						5.22	15
5.88	8	5.89	6				
		6.10	8			6.10	16
						7.29	64 (2)
7.53	37 (3)	7.54	25 (3)	7.54	86 (2)		
8.53	19 (5)	8.52	14 (5)	8.46	32	8.56	26
						9.53	28
17.95	100 (1)	18.32	100 (1)	18.30	55 (5)		
						20.27	100 (1)
						23.23	94 (1)

It was reported before that although there are symmetrically related minima, the chain shapes corresponding to these could differ due to the differences in the torsion angles φ and ψ.[21] Comparison of Figures 4.7d and 4.7e shows that e.g., when both the torsion angles φ and ψ are 135° in 6FDA (corresponding to one of the minima in Figure 4.7a) the overall contour of the chain is not affected by the introduction of the 6FDA segment. This conformational isomorphism forms the basis for the d-spacings to be similar between the PPI-12 homopolymer and the copolymers.

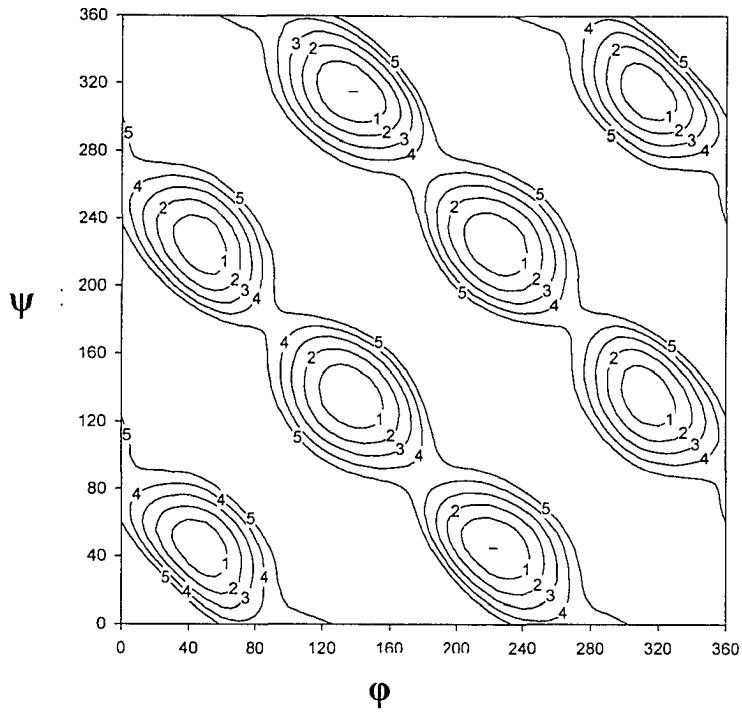

Figure 4.7a. Conformational map of 6FDA

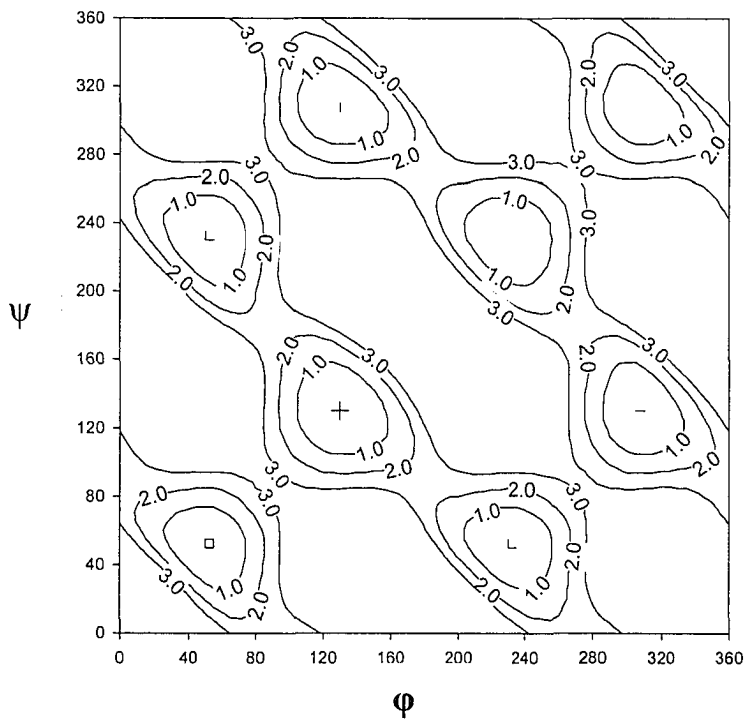

Figure 4.7b. Conformational map of bisphenol-A.

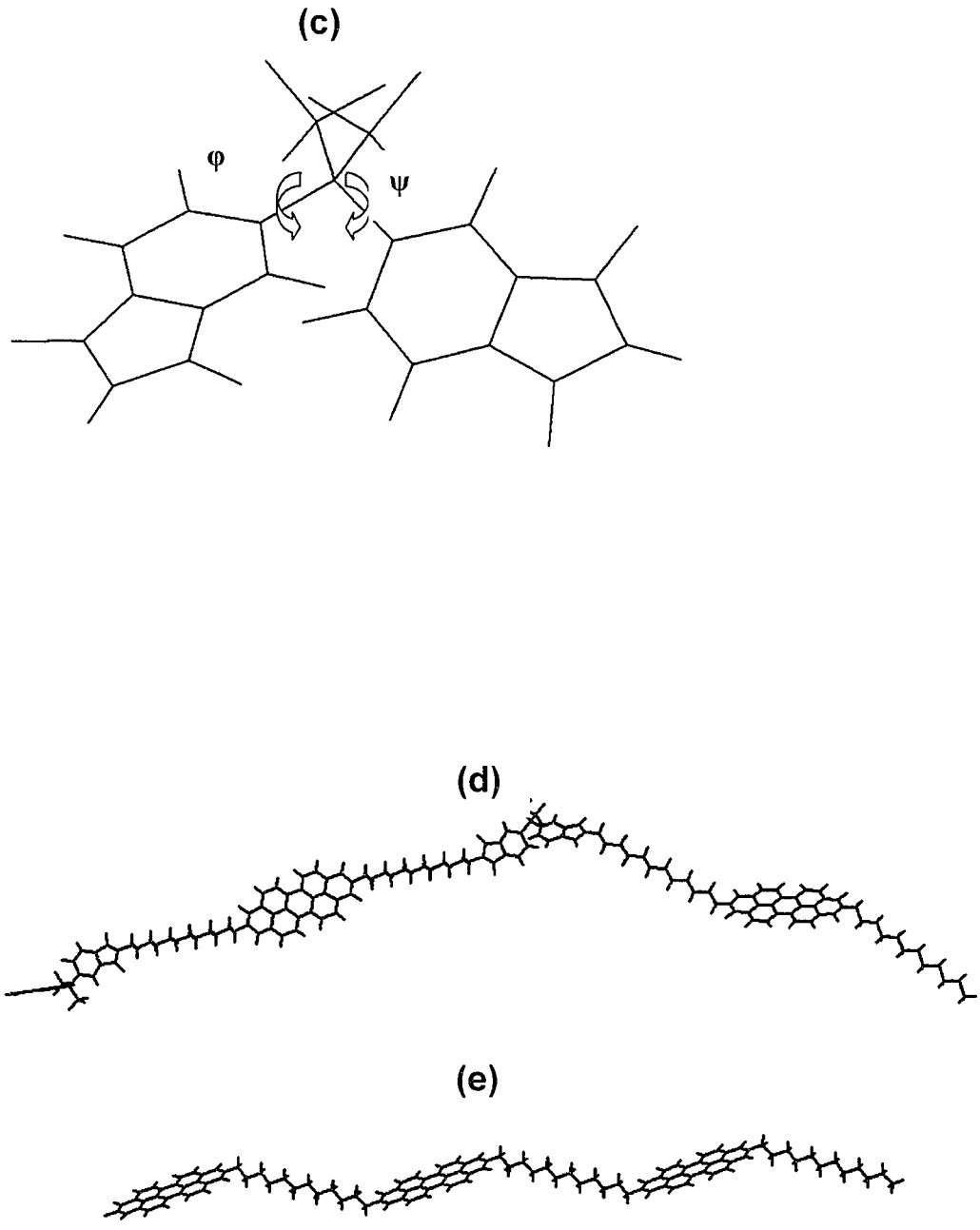

Figure 4.7. (c) Structure of 6FDA after using Ramachandran map and the energy minimized conformation; (d) conformation of two units of the copolymer by using Ramachandran map and the energy minimization; (e) conformation of 3 units of the homopolymer PPI-12.

All alternating copolymers are amorphous, though there are melting peaks. Basically, this due to another dianhydride (i.e., 6FDA) breaks the packing system of perylene.

4.4 Conclusions

The present study indicates that copolymerization of diaminododecyl perylene tetracarboxylic dianhydride (PPI-12) with 6FDA leads to "*conformational* isomorphism". The latter does not change the chain contour of PPI-12 significantly, and as a result, the d-spacings in the X-ray diffraction pattern remain the same. The X-ray reflection at 3.3Å corresponding to the perylene π overlap persists throughout. The crystallinity decreases linearly with increasing the content of 6FDA, due mainly to the decreasing ratio of the perylene units with respect to the degree of polymerization and finally becomes amorphous when the percentage of 6FDA is more than 80%. In contrast, the T_g decreases significantly between 40 and 50% of 6FDA. . The positions of the absorption maxima in the UV-Vis spectra do not change. The solubility increases with 6FDA ratio, and Cop80 can dissolve in most conventional solvents, such as, chloroform, dichloromethane, THF, etc. Thus, the desired solubility and processibility can be achieved with 6FDA-based copolymers of perylene polyimides.

Alternating copolymers have the similar properties to the block copolymers. However, another dianhydride disrupts the packing of the system, and leads to reduction in the crystallinity.

References

1. Ghosh, M. K.; Mittal, K. L. (Eds.) *Polyimides: fundamentals and applications*, Marcel Dekker: New York, 1996.
2. Wilson, D.; Stenzenberger, H.D.; Hergenrother, P.M. (Eds.), *Polyimides*, Blackie & Son: Glasgow, 1990.
3. Law, K.-Y. *Chem. Rev.*, **1993**, *93*, 449–486.
4. (a) Schmidt-Mende, L.; Fechtenkötter, A.; Müllen, K; Moons, E.; Friend, R. H.; MacKenzie, J. D. *Science*, **2001**, *293*, 1119–1122; (b) Yakimov, A.; Forrest, S. R. *Appl. Phys. Lett.*, **2002**, *80*, 1667–1669.
5. Niu, H.; Wang, C.; Bai, X. D.; Huang, Y. *J. Mater. Sci.* **2004**, *39*, 4053-4056.
6. Ghassemi, H.; Hay, A. S. *Macromolecules* **1994**, *27*, 4410-4412.
7. Icil, H.; Icli, S. *J. Polym. Sci., Part A: Polym. Chem.* **1997**, *35*, 2137-2142.
8. Yang, M.; Xu, S.; Wang, J.; Ye, H.; Liu, X. *J. Polym. Mater.* **2003**, *20*, 43-50.
9. Wang, Z. Y.; Qi, Y.; Gao, J. P.; Sacripante, G. G.; Sundararajan, P. R.; Duff, J. D. *Macromolecules* **1998**, *31*, 2075-2079.
10. Lu, W.; Gao, J. P.; Wang, Z. Y.; Qi, Y.; Sacripante, G. G.; Duff, J. D.; Sundararajan, P. R. *Macromolecules* **1999**, *32*, 8880-8885.
11. Mackinnon, S. M.; Wang, Z. Y. *J. Polym. Sci. Part A: Polym. Chem.* **2000**, *38*, 3467-3475.
12. Langhals, H. *Heterocycles* **1995**, *40*, 477-500.
13. Langhals, H.; Demmig, S.; Huber, H. *Spectrochim. Acta* **1988**, *44A*, 1189–1193.
14. Seybold, G.; Wagenblast, G. *Dyes Pigm.*, **1989**, *11*, 303-317.
15. Li, W. S.; Shen, Z. X.; Zheng, J. Z.; Tang, S. H. *Appl. Spectrosc.* **1998**, *52*, 985-9.
16. Zhu, S., Zhao J., Zhang Y. *J. Fluor. Chem.* **2003**, *123*,221–225.
17. Icil, H.; Arslan, E. *Spectrosc. Lett.*, **2001**, *34*, 355-363.
18. (a) Dotcheva, D.; Klapper, M.; Mullen, K. *Makromol. Chem. Phys.* **1994**, *195*, 1905. (b) Langhals, H.; Jona, W. *Angew. Chem. Int. Ed.* **1998**, *37*, 952-955.
19. Duff, J.; Hor, A. M.; Melnyk, A. R.; Teney, D. *SPIE*, **1990**, *1253*, 183-191.
20. (a) Graser, F.; Hädicke, E. *Liebigs Ann. Chem.* **1980**, 1994-2011. (b) Cormier, R. A.; Gregg, B. A. *J. Phys. Chem. B* **1997**, 101, 11004-11006.
21. Sundararajan, P. R. *Macromolecules*, **1987**, *20*, 1534-1539.

Chapter 5

Self-Assembled Vesicular Nanostructures of Perylene End-capped Poly (dimethylsiloxane)*

(*D. Yao, T. P. Bender, P. J. Gerroir, and P. R. Sundararajan, *Macromolecules*, **2005**, *38*, 6972-6978)

5.1 Introduction

There has been significant activity on the self-assembly of amphiphilic block copolymers in solution.[1,2] One of the blocks is usually water soluble, and a variety of morphologies such as spheres, rods, vesicles, lamellae have been observed, depending on the composition of the polymer and the polarity of water. In a number of cases, the amphiphilic block copolymer has to be highly asymmetric. Such architecture involves a long, hydrophobic core-forming block and a short, hydrophilic corona block. It has been shown that for the case of polystyrene-b-poly (acrylic acid), with a relatively long PAA block, micelles are seen initially. With a progressive decrease in the length of the PAA segment, successive transitions were seen from micelles to large spheres to rod-like micelles and then to vesicular structures.[1-7] The latter have hollow spherical shape, with walls composed of bilayers of the polymers.

Formation of such micelles or vesicles in non-aqueous media has not been explored so far. In this chapter, we discuss the synthesis, morphology and spectral properties of perylene end-capped poly(dimethyl siloxane) (perylene end-cap PDMS). This is essentially an oligomeric PDMS linked at one end to a perylene unit, whereby the macromolecular structure resembles that of a surfactant. However, in this case the surfactant has a large planar π-system (whose stacking tendency and hence insolubility is well known) attached to a long flexible, elastomeric and soluble PDMS chain. The micelle or inverse micelle formation in surfactant systems, depending on the nature of the head group, is well known. It was expected that in non-aqueous media, the self-assembly

of the perylene units would lead to morphologies similar to those observed in the case of polystyrene-b-poly (acrylic acid), and similar block copolymer systems.

Among the various classes of pigments, perylene bisimides are remarkable in the diversity of colors that can be achieved in the solid by derivitization, and the resulting changes in the π overlap and the crystal structure.[8] Perylene derivatives exhibiting liquid crystalline[9] or supramolecular polymer[10] characteristics have been studied. Perylenes have also been incorporated in polyimide polymers and copolymers.[11-14] Perylene derivatives are also candidate photogenerators and n-type organic semiconductors for opto-electronic applications.[8] It is expected that vesicle formation of perylene derivatives could lead to interesting and useful properties as such an assembly is analogous to the arrangement of perylene derivatives in a molecular crystal. This work is an initial attempt in this regard.

I. Perylene End-capped Poly(dimethyl siloxane) (Perylene End-cap PDMS)

5.2 Experimental

5.2.1 Materials

3,4,9,10-Perylenetrtracarboxylic acid dianhydride, 2,5-di-*tert*-butylaniline, zinc acetate dehydrate, imidazole, isoquinoline and *tert*-butyl alcohol were purchased from Aldrich Chemical Co. and used as received. Amine terminated polydimethylsiloxanes (DMS-A11, DMS-A12 and DMS-A15) were purchased from Gelest Inc. and used as received.

The molecular weights of PDMS terminated with primary amine end group were obtained by end group titration, with aqueous 0.01M HCl solution. The PDMS (0.1 milliequivalents) was stirred in 75 ml isopropanol, and an automated titrator was used. The molecular weight of each was determined as an average of three such measurements. The average molecular weights of A-11, A-12 and A-15 were determined to be 875 amu, 1500 amu and 3035 amu respectively.

Transmission electron micrographs were recorded using a Philips CM20 TEM, operated at 120 kV. The samples were prepared by pipeting a small amount of the solution onto a carbon lacey grid. The solution was allowed to cascade down the surface of the tilted grid. This reduced the agglomeration of the material. The thin film formed in this manner was allowed to dry for a few hours before examination. This is similar to the protocol used for the TEM analysis of vesicular morphologies of block copolymers in aqueous media.[1-6] For cryo-TEM, the sample was placed on the grid as above, and the grid was then loaded into the cryo holder and immediately inserted into the microscope. The reservoir of the cold stage initially at room temperature, was filled with liquid nitrogen and kept filled throughout the duration of the sample examination. Once the temperature had dropped to -40° C the high tension was turned on and filament current increased to saturation. Micrographs were acquired between -40 and -55° C.

The other instruments are described in Chapter 2.

5.2.2 Synthesis of N-(2,5-di-*tert*-butylphenyl) Perylene-3,4-dicarboximide (2)[17]

Perylene dianhydride (9.15g, 23.3mmol, **1**), 2,5-di-*tert*-butylaniline (2.625g, 12.8mmol), zinc acetate dihydrate (3.3g, 15mmol), imidazole (46.75g, 686.7mmol) and water (20ml, 1.11mol) were placed in a 250ml autoclave equipped with a manometer. The mixture was stirred at 190°C for 24hrs. The manometer showed from the beginning 100 to 200 psi at the end. After reaction, the mixture was cooled down, 200ml water was added to the reaction mixture. The resulting mixture was filtered and the filtered solid obtained was washed with 200ml of 2N aqueous HCl/methanol (1:1), then 200 ml of H_2O/methanol (1:1) and dried in an oven at 130°C overnight. The crude product was 9.0g (75.9%). The crude solid was dispersed in 200ml of chloroform, then filtered. Repeated this 2 times, combined all filtrate. The filtrate was concentrate to 200ml and then chromatographed with chloroform over silica gel. The first fraction was yellow with a blue fluorescence, then red with a yellow fluorescence, which is our target material. After evaporating the solvent, 4.72g (39.8%) of N-(2,5-di-*tert*-butylphenyl) perylene-3,4-dicarboximide **(2)** (Figure 5.1). –IR (KBr): ν=2961 cm^{-1}(sharp, the followings will use s instead), 1699.8 cm^{-1} (s, C=O), 1664 cm^{-1} (s, C=O), 1590.2 cm^{-1}(s), 1570.7 cm^{-1}(s), 1354.5 cm^{-1}(s), 1293.6 cm^{-1}(s), 1246.8 cm^{-1}(s), 810.8 cm^{-1}(s), 756.1 cm^{-1}(s). ^{1}H NMR($CDCl_3$): 1.32(s*, 9H, 26, 27, 28-H), 1.35(s, 9H, 29,30,31-H), 7.04 and 7.05(d*, 1H, 22-H), 7.46 and 7.48(d-d, 1H, 23-H), 7.60 and 7.62 (d, 1H, 25-H),7.66, 7.68, and 7.70 (t*, 2H, 9,11-H), 7.94 and 7.96 (d, 2H, 8,12-H), 8.49, 8.50, and 8.51(t, should be d-d, 4H, 4,7,13,16-H), 8.67 and 8.69 (d, 2H, 3,17-H) (* s – singlet, d – doublet, and t – triblet). (Figure 5.7) –MS (EI), m/z(%): 510 (3.8), 509 [$M^{+\bullet}$] (9.6), 452(38.1), 452[$M^{+\bullet}$ -$C(CH_3)_3$](100), 437 (6.2), 436(12.9).

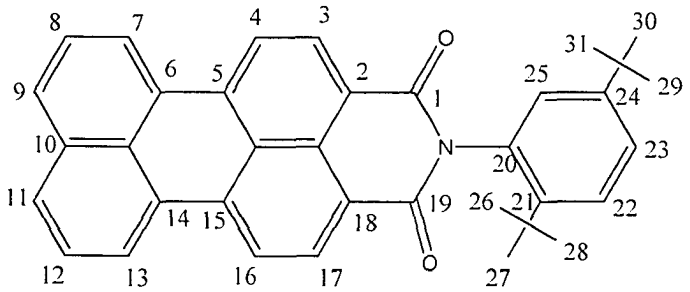

Figure 5.1 Atomic position of N-(2,5-di-*tert*-butylphenyl) perylene-3,4-dicarboximide.

5.2.3 Synthesis of perylene-3,4-dicarboxylic anhydride (4, Scheme 5.1)[15]

1.02 g of **(2)** and 2.8 g of KOH (85%) are dispersed in *tert*-butyl alcohol (94ml), and the mixture is refluxed for 2 hrs. After reflux for 1 hr, a brown colored solution and a yellow precipitate are formed. The hot reaction mixture was poured into 150ml of acetic acid and the mixture was vigorously stirred for 5 mins. And then, to the mixture, 200ml of H_2O was added. The precipitate was collected by filtration. The precipitate was washed with H_2O and fried in oven at 130°C overnight. The crude solid (0.7g) was boiled in the 400ml of 10% K_2CO_3 for 2hrs. As hot, the dark green solution was filtered and washed with hot water. The filtrate was neutralized by acetic acid with stirring, the resulting mixture was filtered by vacuum. After drying in oven, the 0.5g (77.6%) of (4) was collected. –IR (KBr): 1750.4 cm^{-1} (s, C=O), 1724 cm^{-1} (s, C=O), 1592 cm^{-1} (s), 1569.5 cm^{-1} (s), 1499.6 cm^{-1} (m), 1372 cm^{-1} (m), 1341.1 cm^{-1} (s), 1283.5 cm^{-1} (s),1232.7 cm^{-1} (m), 1131.5 cm^{-1} (s), 1019.8 cm^{-1} (s), 996.9 cm^{-1} (m), 810.2 cm^{-1} (s), 741.3 cm^{-1} (s). –MS (EI), m/z(%): 324 (3.4), 323 (23.4), 322 [$M^{+\bullet}$] (100), 279 (3.6), 278 [$M^{+\bullet}$-CO_2] (14.3), 251 (10.0), 250[$M^{+\bullet}$ -CO_2 -CO] (47.5), 249 (11), 248 (17.3), 125 (35.3), 124 (30.1), 123 (9.5).

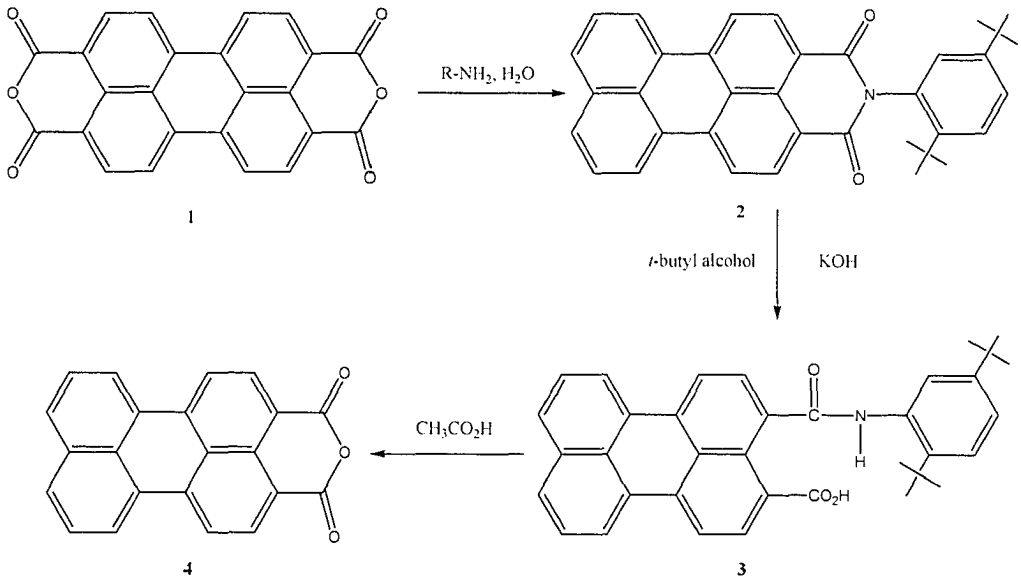

Scheme 5.1 Synthesis of perylene 3,4-dicarboxylic anhydride.

5.2.4 Synthesis of PDMS-end-perylene M900 (6) (Scheme 5.2)

Three different molecular weights of ~900, 1500, and 3000 of PDMS were used for the synthesis of (**6**), (**7**) and (**8**), (Scheme 5.2) respectively. In a round bottom flask, 0.32g (0.1mmol) of perylene-3,4-dicarboxylic anhydride **(4)**, 3.6g (0.4mmol) of amine terminated polydimethylsiloxane (DMS-A11, **5**) and 0.2g of isoquinoline were dispersed in 15ml of *m*-cresol and the solution was slowly heated to 200°C. The reaction mixture was stirred at 200°C for 4h, cooled to room temperature, and poured into 300ml of methanol. The precipitated solid was filtered, repeatedly washed with aqueous sodium hydroxide (1N) solution, followed by water and methanol, and dried to get the crude solid. It was dissolved in chloroform and then chromatographed with chloroform over silica gel. After evaporating the solvent, and drying in the vacuum at 60°C, the yield was

1.05g (86.1%) of M900 **(6)**. –^{1}H NMR ($CDCl_3$): 0.17, 0.25, 0.31(CH_3), 0.80 (2H) and 0.93 (2H), 1.60 (2H), 1.82 (2H), 3.95 (2H) and 4.05 (2H), 7.49(t, 9, 11-H), 7.76 and 7.78(d, 8,12-H), 8.04 and 8.06(d, 7,13-H), 8.13 and 8.15(d, 4,16-H), 8.29 and 8.31(d, 3,17-H). –IR (KBr): 1692.5, 1649.8, 1594.8, 1379.7, 1354.9, 1250, 1094, 839.5, 809.1, 751.6.

M1500 (**7**) (with DMS-A12) –^{1}H NMR ($CDCl_3$): 0.09, 0.13, 0.19, 0.24(CH_3), 0.75 (4H), 1.78 (4H), 3.93 (2H), 4.02 (2H), 7.40 (2H), 7.60 (2H), 7.70 (2H), 7.79 (2H), 8.0 (2H). –IR (KBr): 1692.3, 1650.9, 1593.5, 1379.8, 1355, 1259, 1094.9, 1060.4, 839.2, 809.2, 752.5

M3000 (**8**) (with DMS-A15): –^{1}H NMR ($CDCl_3$): 0.2(CH_3), 0.75 (4H), 1.78 (4H), 3.95 (2H), 4.17 (2H), 7.44 (2H), 7.65 (2H), 7.75 (2H), 7.85 (2H), 8.06 (2H). –IR (KBr): 1694.7, 1650, 1597, 1382, 1356.9, 1261.1, 798.5, 752.

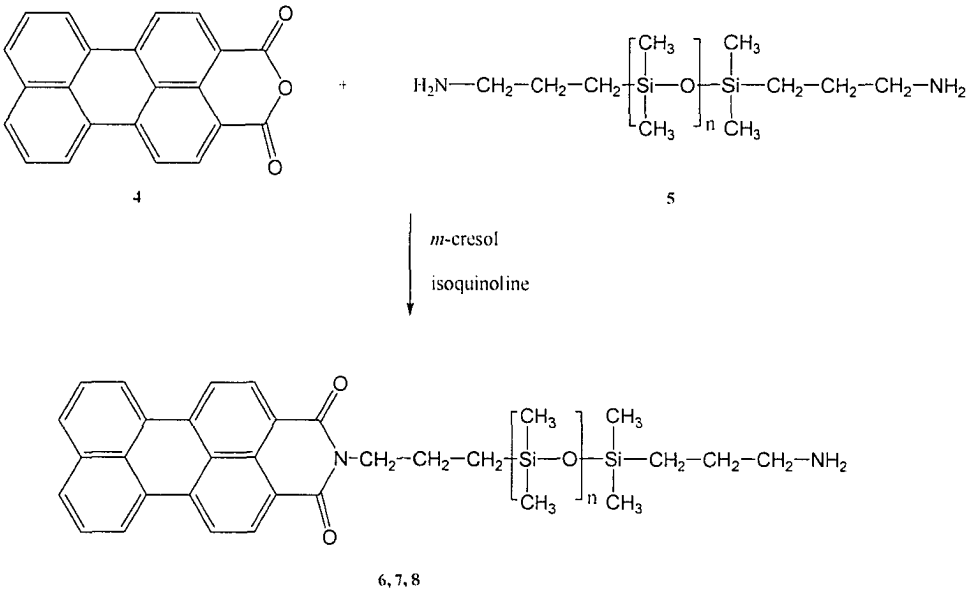

Scheme 5.2 Synthesis of PDMS-end-perylene: (6) n ≈ 10; (7) n ≈ 20; (8) n ≈ 40.

5.3 Results and Discussion

5.3.1 Synthesis

Imides can be prepared in a single step by heating an anhydride and an amine together in a polar solvent such as NMP, DMAc or *m*-cresol at high temperature. Imide-siloxane copolymers are prepared in a similar manner by copolymerization of a dianhydride, a diamine and a siloxane containing diamine.[16] In this chapter we describe the synthesis and characterization of perylene end-capped poly(dimethyl siloxane) (perylene end PDMS) which has been made by reaction of perylene-3,4-dicarboxylic anhydride with an amino terminated polysiloxane in *m*-cresol at elevated temperatures (compounds **6**, **7** and **8**, Scheme 5.2). We used a 4-fold excess of the amino terminated polysiloxane so as to preferentially synthesize polysiloxane that are endcapped at only one end with perylene

moieties. The crude materials were washed by 1N aqueous sodium hydroxide, in order to change any unreacted perylene 3,4-dicarboxylic anhydride to disodium perylene dicarboxylate and remove it. The column chromatography can remove trace amino-terminated PDMS and other unpurified materials. The reaction was monitored using FT-IR, by observing the wave number of carbonyl group shift from a broad peak between 1730 and 1780 cm^{-1} for the anhydride to peaks at 1690 to 1650cm^{-1} upon imide formation. ^1H NMR ($CDCl_3$ solution) further confirmed the formation of perylene end-cap PDMS as chemical shifts between 8.0-8.6 ppm correspond to perylene hydrogens, 0.7-4.2 ppm, due to the hydrogens of the alkyl groups (α-, β- and γ- to the nitrogen atom) and chemical shifts lower than 0.5 due to hydrogens of the methyl groups attached directly to the silicon atoms were observed (Figure 5.2).

The question arises as to the possibility of both ends of the PDMS chain being substituted with perylene. As noted above, a 4-fold excess of amino terminated polysiloxane was used. During the chromatographic separation process, the free amino-terminated main product would have higher interaction with the silica gel and it will be the slower eluent, compared to the product that reacted on both sides. ^1H NMR showed only the expected spectrum. The TLC plate also showed one eluent. The final product was easily soluble in most common solvents. This would not be the case, if the perylene substitution occurred on the both ends of the polymer. Since amino-terminated PDMS is soluble in common solvents such as methanol and acetone, repeated wash with methanol would remove any unreacted amino-terminated PDMS. As an aside, repeated washing with 1N aqueous sodium hydroxide is not expected to cause any scission of the Si—O bonds. This

procedure has been used during the preparation of perylene containing polymers with alkyl chains,[11,17] and it is known that the bond energy of the Si—O bond is ~5 Kcal.mol^{-1} higher that of the C—C bond.[18]

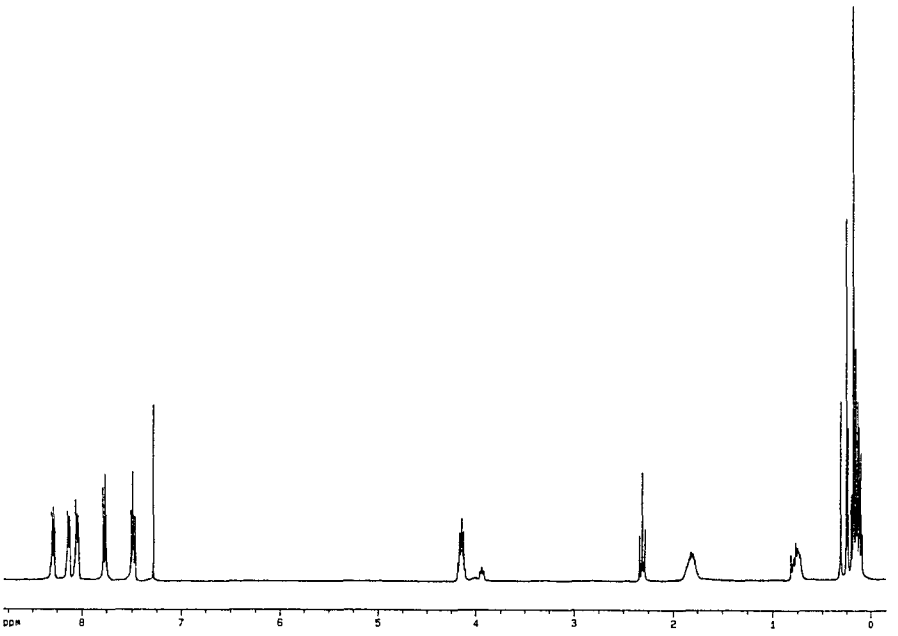

Figure 5.2. ^{1}H NMR of M900 using 400MHz NMR instrument.

5.3.2 Crystallization and Melting Behavior

The as-prepared perylene end-cap PDMS was found to be semicrystalline. Figure 5.3 shows the DSC results on M900 and M3000. All three polymers **(6-8)** showed reversible melting and crystallization. M900 initially shows two melting transitions at 175 and 210°C in the first scan (Figure 5.3a), and crystallization transitions upon cooling (Figure 5.3b). Similar occurrence of multiple melting peaks has been reported for other

polymers.[19] It has been suggested[19b] that the low temperature endotherm is due to the melting of crystals that exist prior to the heating scan and that the higher temperature endotherm is the result of melting of crystals formed by simultaneous melting and recrystallization (reorganization) during the DSC scan. The two melting endotherms become closer for the second scan (Figure 5.3c), with the peak position at 195°C. M1500 and M3000 are also semicrystalline, with a T_m of 225°C for M3000. The DSC trace for M3000 is shown in Figure 5.3d. These results suggest the presence of molecular aggregation of the perylene units in the solid state and the resulting crystallinity. Note that the T_m of perylene by itself from its crystalline state is 278-280°C.[20] The lower melting temperatures observed here is due to the less perfect ordering of the perylene units relative to its single crystal.

We observe that the T_m of the perylene in M900 is lower than in the case of M3000. It would seem that the longer, flexible PDMS segments facilitate aggregation of the perylene chain ends. This is corroborated by the heat of fusion as well. The value of ΔH, normalized for the weight fraction of perylene, is 80J/g for M900, and it increases to 130 J/g for M1500 and M3000. It is known that perylene derivatives form liquid crystalline phases.[21] However, we do not observe consistent multiple transitions in this case on heating and cooling that would indicate such liquid crystalline transitions. In addition, Figure 5.3d shows a small melting endotherm at –50°C, which is attributed to melting of the PDMS segment. This endotherm was not seen with the lower molecular weight samples (e.g., M900).

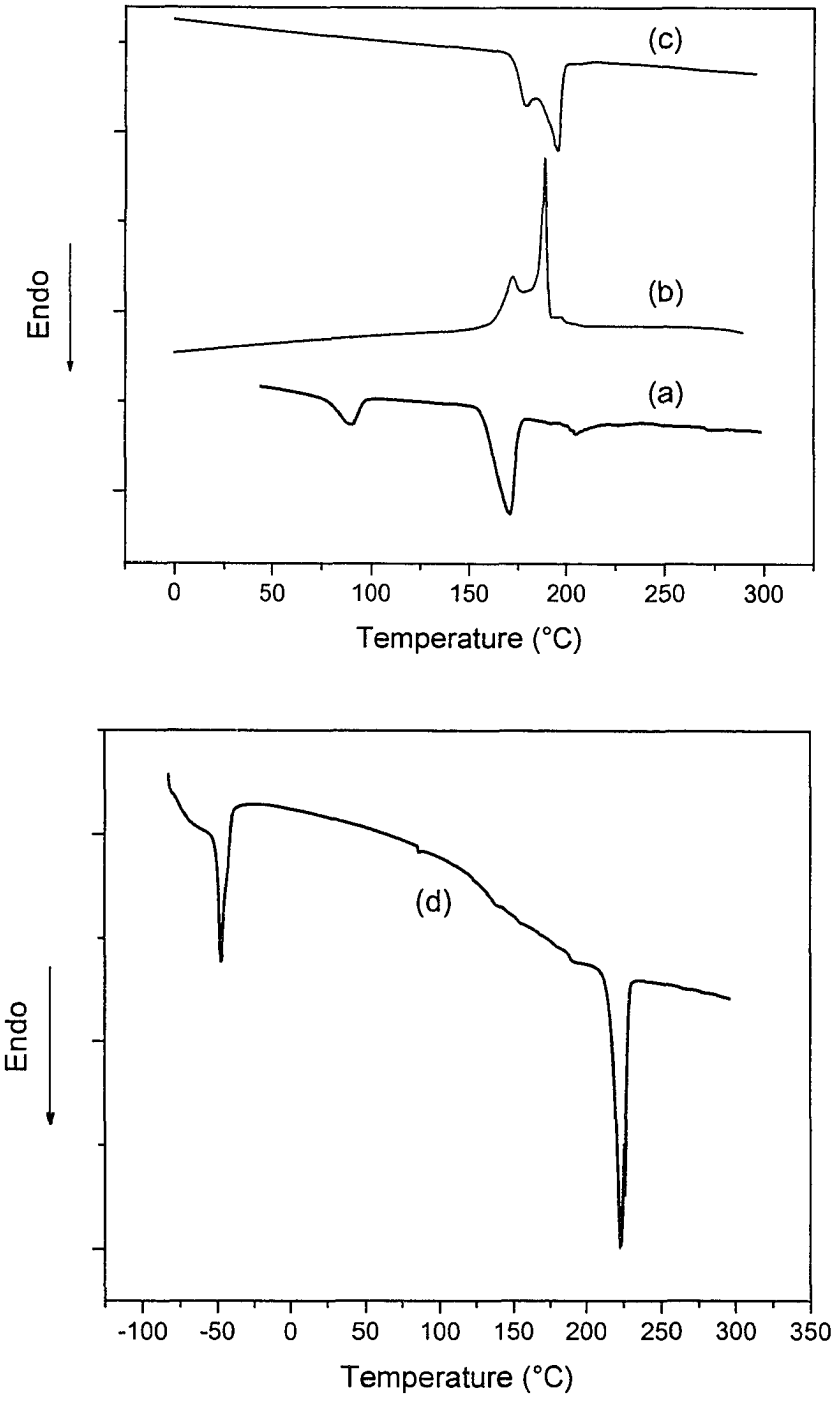

Figure 5.3 DSC thermograms of M900, (a) first heating, (b) cooling, and (c) second heating; (d) DSC thermogram of M3000 at the second run.

5.3.3 X-ray Diffraction

The X-ray diffraction trace from M1500 is shown in Figure 5.4. Four strong, well resolved reflections are seen, with *d*-spacings of 24.66, 7.70, 3.61, and 3.35Å. The diffraction patterns from M900 and M3000 were similar. The 3.61 Å reflection corresponds to the π-stacking of the perylene, and 7.70 Å, to the side-to-side packing distance. The length of the perylene unit including the three CH_2 groups is about 12.3 Å, which is half the spacing at 24.66 Å. Thus, the three principal packing directions of the perylene unit are seen in the X-ray diffraction. Note that PDMS itself crystallizes only below -50°C. The crystalline peaks seen in Figure 5.4 are due to perylene aggregation.

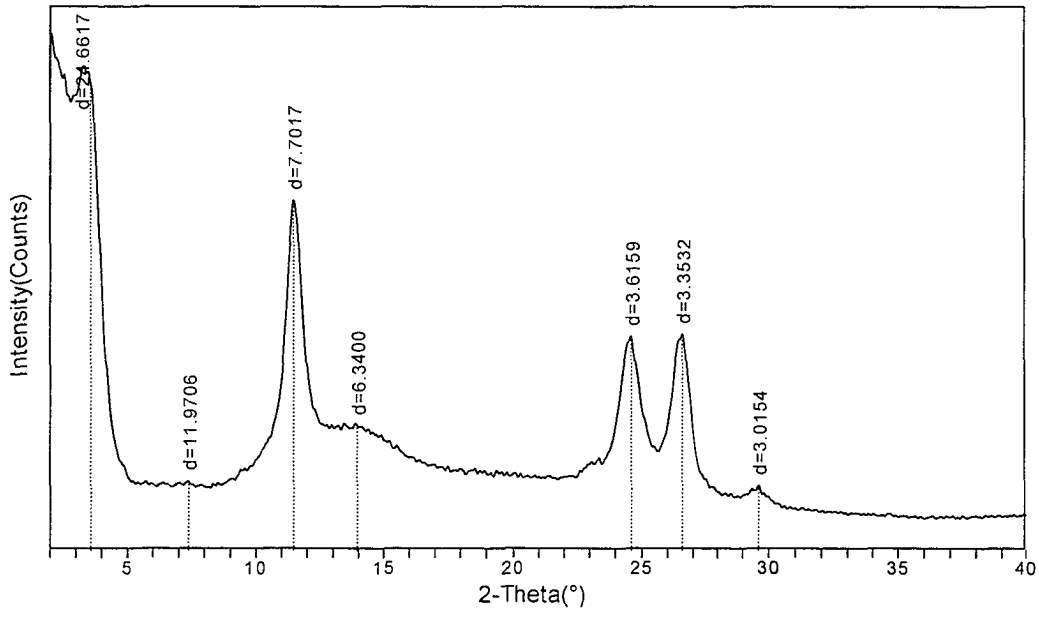

Figure 5.4 Powder X-ray diffractogram of M1500.

5.3.4 UV-visible and Fluorescence Spectra

The UV-visible and fluorescence spectra were recorded in dichloromethane, chloroform, dichlorobenzene, carbon tetrachloride and hexane, as well mixtures of hexane with either of the chlorinated solvents. The concentrations are $2.0x10^{-5}$ –$2.0x10^{-6}$ M, depending on the molecular weight. The solubility of M900, M1500 and M3000 in hexane is low.

Figure 5.5 shows the UV-visible spectra from these solvents and their mixtures for M900, and M3000. There are two significant changes that occur with increasing ratio of hexane. First, the absorption peaks become sharper and the doublets become well resolved. This difference is pronounced when the spectra from dichloromethane are compared with those from hexane. Secondly, the absorption maxima blue shift by 7 to 9 nm. With M900 in dichloromethane, peaks occur at 503 and 481 nm, and the ratio of the intensities of these peaks is 1.092. With hexane, these peaks shift to 495 and 467 nm, respectively, with a ratio of 1.042. In addition, a third peak appears at 443nm. The spectra for M1500 and M3000 in hexane also show the presence of the third peak at 443nm and 438nm, respectively. With chloroform, the peaks occur at 505 and 482 nm. These shift to lower wavelengths with increasing ratio of hexane. In the case of M1500 and M3000, the ratio of the intensities of these peaks increases to the range of 1.2 to 1.4. It was noted by Neuteboom et al[14] that in the case alternating copolymers of perylene bisimide and poly (THF) in *o*-dichlorobenzene, the blue shift of the absorption maximum is consistent with the formation of H aggregates.

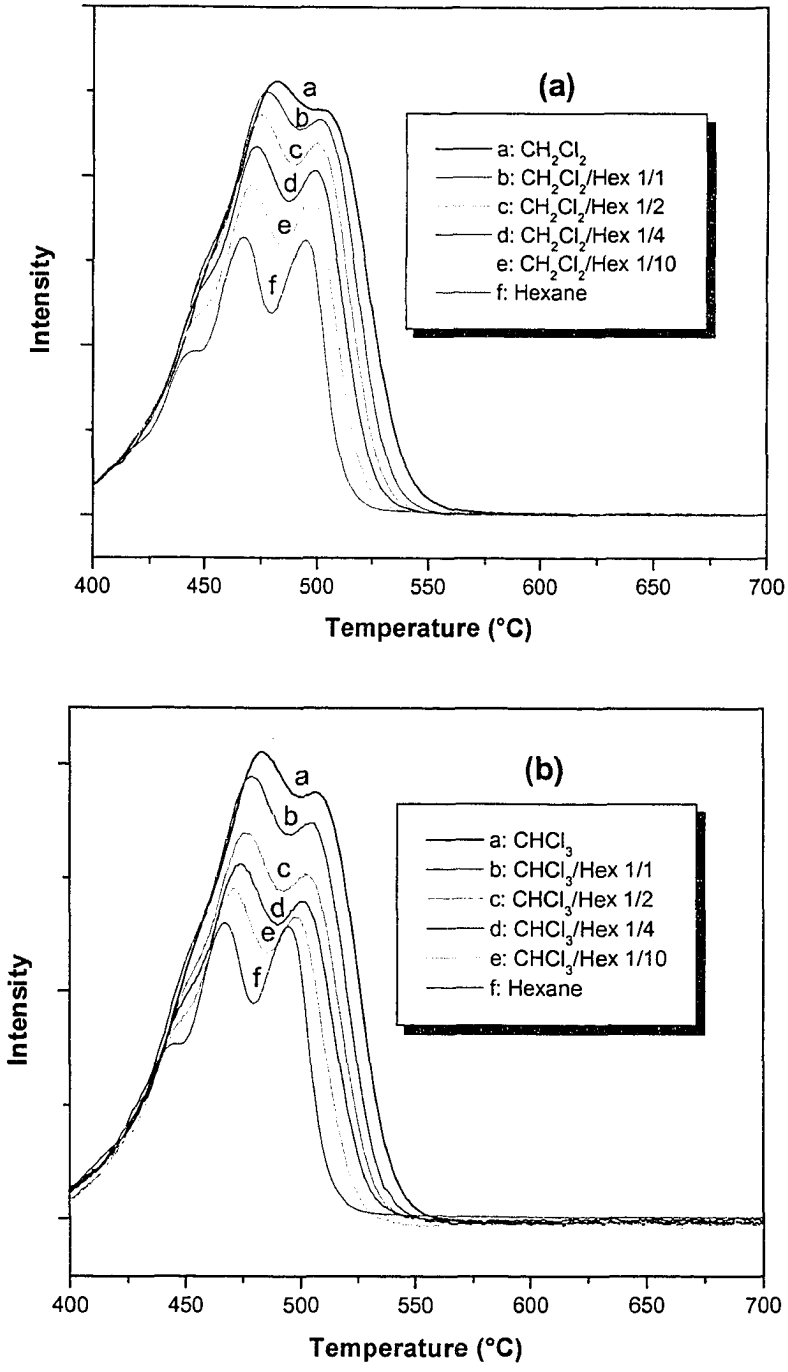

Figure 5.5 UV-visible spectra for M900 in (a) mixtures of dichloromethane and hexane, (b) mixture of chloroform and hexane.

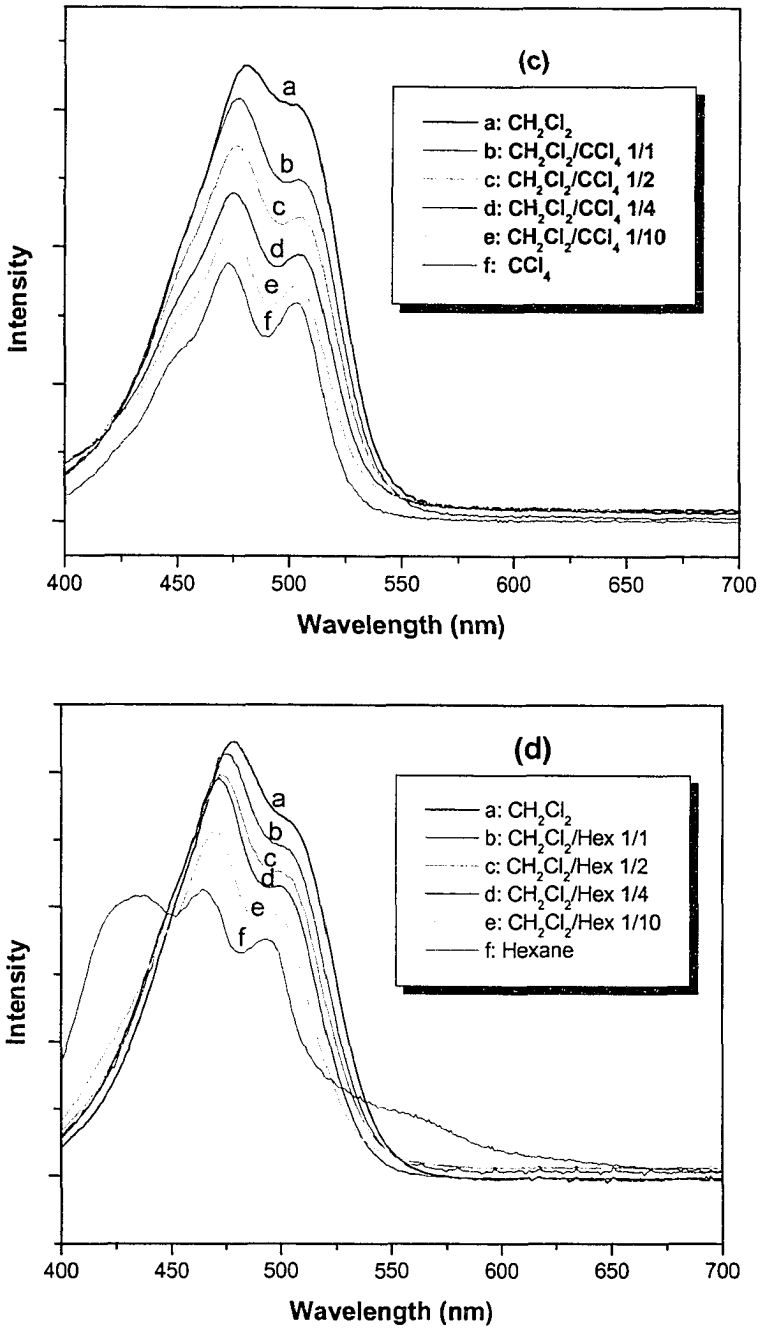

Figure 5.5 UV-visible spectra for M900 in (c) mixture of dichlorobenzene and carbon tetrachloride; (d) M3000 in mixtures of dichloromethane and hexane.

Figure 5.5c shows the spectra from carbon tetrachloride, dichloromethane, and their mixtures. It is seen that although both are chlorinated solvents, the doublets in the spectra from CCl_4 are well resolved compared to that in CH_2Cl_2. The nature of the solvent thus plays a role. The solubility parameter (δ) for PDMS is 14.9 $MPa^{1/2}$. Those for hexane, CCl_4, $CHCl_3$ and CH_2Cl_2 are 14.9, 17.6, 19 and 20.3 $MPa^{1/2}$ respectively, with increasing polarity.[22] Thus the difference in δ between PDMS and hexane is close to zero, while it is large between PDMS and $CHCl_3$ or CH_2Cl_2. The interaction parameter χ between PDMS and hexane is 0.3-0.4, while it is 0.36, 0.6 and 0.69 with CCl_4, $CHCl_3$ and CH_2Cl_2 respectively.[22] The aggregation of the perylene segment would thus depend on the interaction between the solvent and PDMS. This is reflected in the vesicular morphology as seen from TEM.

Fluorescence spectra were recorded in the mixtures of dichloromethane and hexane. Figure 5.6 shows the fluorescence spectra for M900 and M1500. M3000 showed a similar spectrum. Excitation wavelength of 500nm was used since all three compounds have strong absorption at that wavelength. Fluorescence spectra have the very similar pattern to UV absorption. With increasing the ratio of mixture of hexane and dichloromethane, the peaks shift to lower wavelength and the ratios of the lower and the higher wavelength peaks become larger.

5.3.5 Transmission Electron Microscopy (TEM) Analysis

The intent in this chapter is to show that the perylene end-capped PDMS forms micellar and vesicular morphology. It is realized that the method of sample preparation would

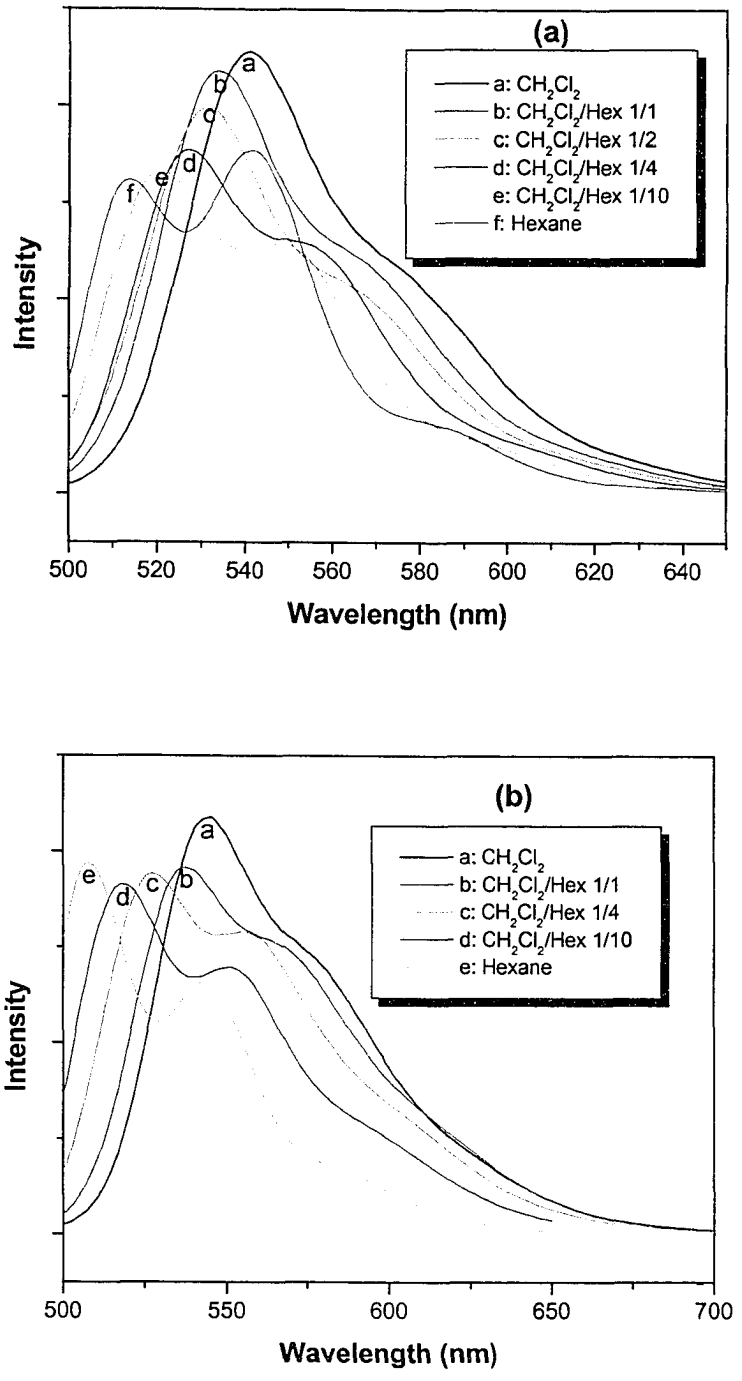

Figure 5.6. Comparison of fluorescent spectra in mixtures of dichloromethane and hexane for (a) M900, and (b) M1500.

have a significant influence on the observed morphology. The samples for TEM analysis were prepared in a manner similar to that used for studying the morphology of block copolymer vesicles in aqueous media.[1-6] The TEM micrographs are shown in Figure 5.7, including the cryo-TEM images of M900, vesicles are seen (marked by arrows) with the dark region corresponding to PDMS surrounded by the shell formed by perylene. The interaction of the chlorinated solvent with perylene can be expected to be stronger than with M900. (The dark region is identified with PDMS, due to the presence of the silicon atom. Note that the large "bubble-like" features are due to the lacey grid used for the TEM analysis, and not to be confused with the vesicles). These are similar the morphologies observed in the case of equilibrium vesicular structures formed with PS_{300}-b-PAA_{44} in THF/water mixtures.[23] In that case, the size of the vesicles can be changed reversibly by changing the water content. In this initial study, only one concentration was used in each case. With M900 in chloroform, the size of the vesicle is about 30 nm, with a perylene layer thickness of around 2-3 nm. The structure of the vesicles from dichloromethane was similar.

With the cryo image of M900 in chloroform (Figure 5.7c), the structure is similar to that shown in Figure 5.7a. The features are somewhat irregular, perhaps due to non-uniform solvent content. Although the same solvent was used, the size of the vesicles (100-300nm) in Figure 5.7c is much larger than that of Figure 5.7a (~30nm). This demonstrates the diverse morphologies that the system could adopt, depending on the sample preparation and history. Such mixed morphologies, depending on solvation and other conditions have been observed in the cryo-TEM studies of surfactants[24,25] and PEO-

based block copolymers.[26] These can also be compared with mixed morphologies obtained in the case of block copolymers.[1-6] With the same sample, some parts of the image appear micellar, as shown in Figure 5.7b. Note that PDMS crystallizes at the low temperatures used here (see DSC trace in Figure 5.3d). With M1500 and M3000 from chloroform, more aggregated compound vesicles were observed, perhaps due to association that develops in the solution. In the case of PS410-b-PAA13, these compound vesicle formation was attributed to non-equilibrium trapped morphologies.

The vesicles observed in the TEM image of M900 from the mixtures of chloroform/ hexane (figure not shown here) and dichloromethane/hexane (Figure 5.7d) as well as from hexane (Figure 5.7e) are larger than that from chloroform or dichloromethane. The vesicle diameters of M900 are 240 nm in chloroform/hexane, 290 nm in dichloromethane /hexane, and 180 nm in hexane. In fact, these seem to form a trilayer vesicle, with the perylene layer surrounded on either side by PDMS. A slightly enlarged view of a vesicle is shown in Figure 5.7f, to show the dark/light/dark layers corresponding to PDMS/perylene/PDMS. This is different from the morphology observed with the chlorinated solvents. We attribute this to the favourable interactions between the PDMS and hexane. A schematic of the trilayer structure is shown as an insert in Figure 5.7e. The PDMS layers are about 1.2 nm thick, and the perylene layer is 2.8 nm wide. A model based on a simple molecular mechanics simulation of this structure is shown in Figure 5.8. The length of the perylene segment is about 1.1 nm, and an edge-to-edge packing of the perylene would give rise to a spacing of about 2.6 nm. The perylene layer appears wider in some of images, due perhaps to the sample preparation. As mentioned before,

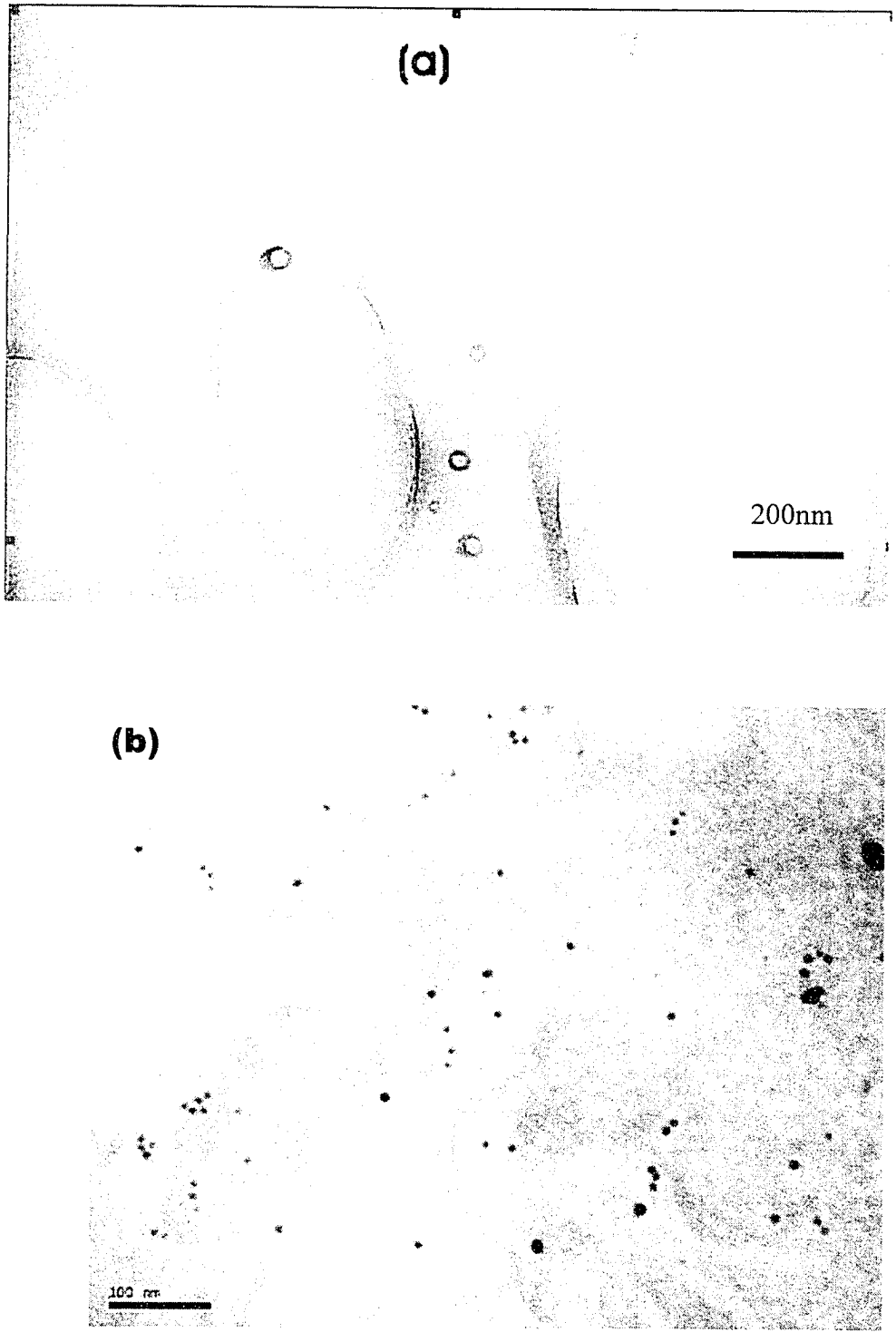

Figure 5.7 TEM images of (a) M900 in $CHCl_3$; (b) cryo-TEM image of M900 in $CHCl_3$.

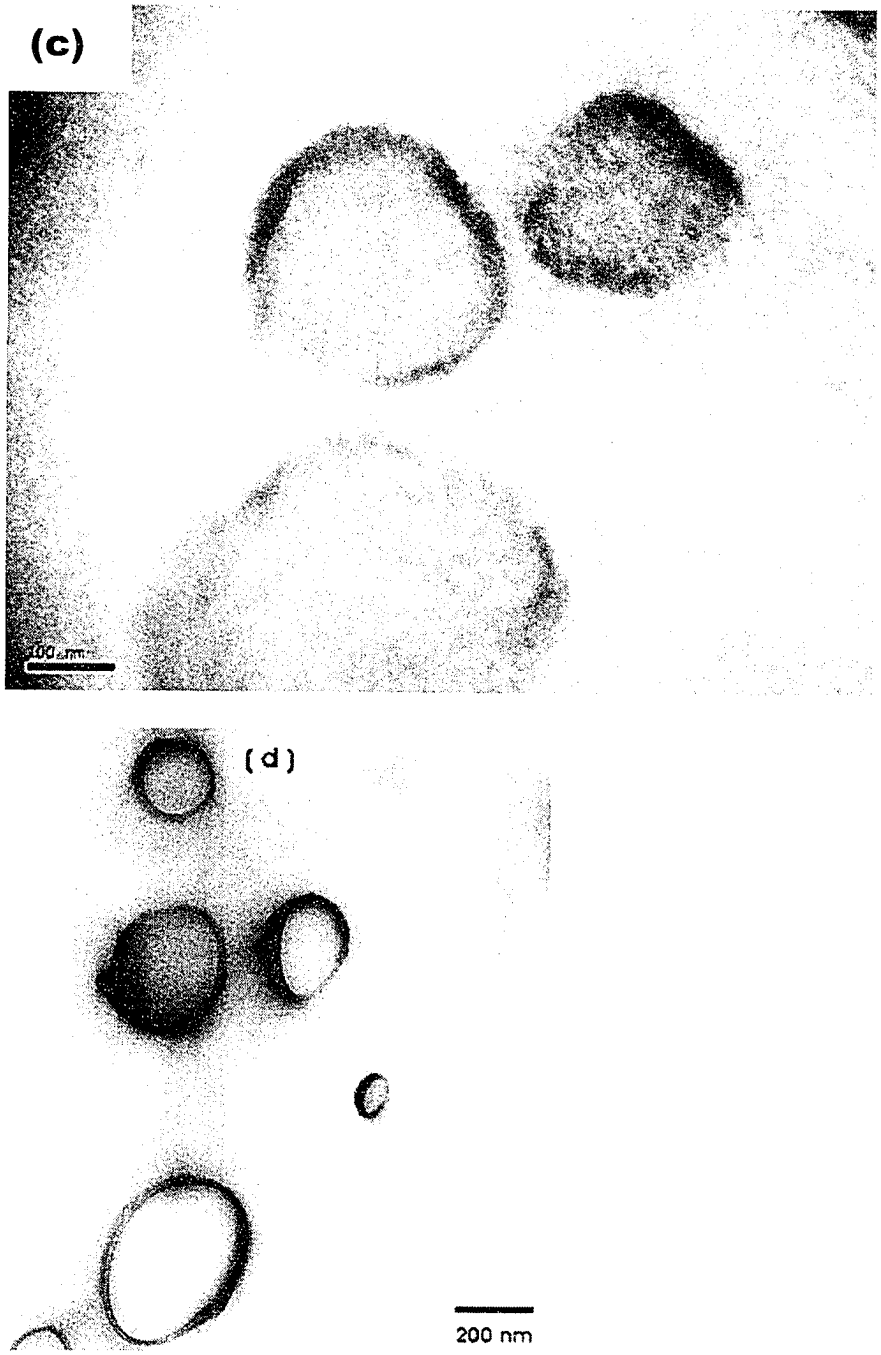

Figure 5.7 TEM images of (c) cryo-TEM image of M900 in $CHCl_3$; (d) M900 in CH_2Cl_2/ hexane (50:50).

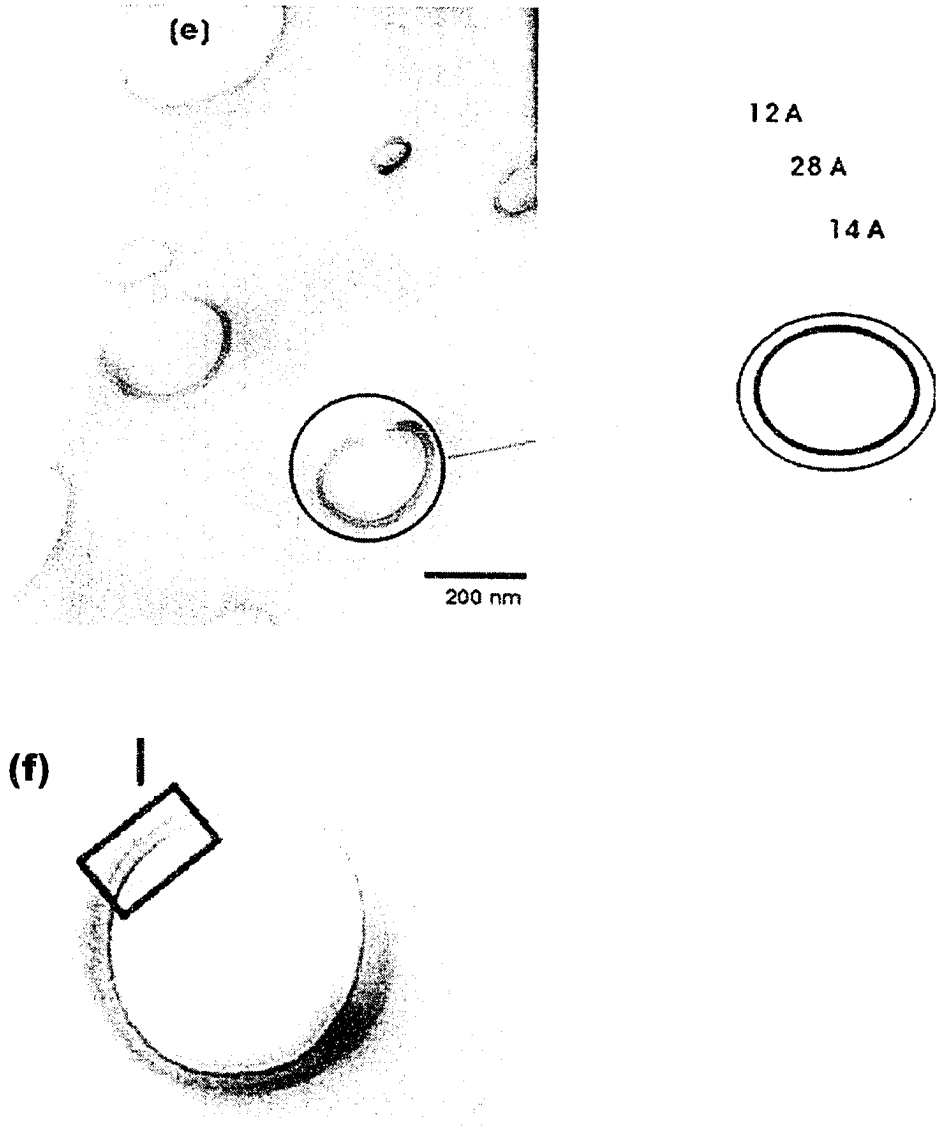

Figure 5.7. TEM images of M900 (e) in hexane; (f) an enlarged view of a vesicle of M900 in hexane.

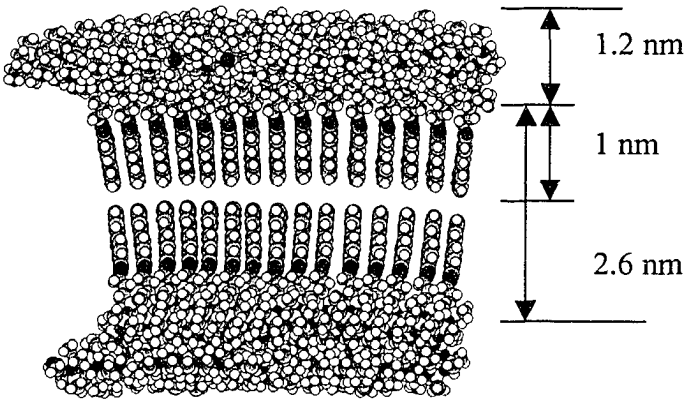

Figure 5.8. Trilayer packing model of perylene end-cap PDMS (from molecular mechanics modeling using Hyperchem).

we followed the procedure similar to that of other authors for TEM analysis. Since a drop of the solution was cascaded on to the TEM grid, any dilation due to surface tension during drying could cause the layer to enlarge. Irrespectively, the vesicle formation is clearly evident in the micrographs.

Figure 5.7 shows that the vesicles that formed with $CHCl_3$ or $CHCl_2$ are much smaller compared to those formed with hexane or hexane mixtures. The former are also bi-layered, with (the dark region corresponding to) PDMS surrounded by the shell formed by perylene. It was discussed above that the difference in solubility parameters (and interaction parameters χ) is large between PDMS and $CHCl_3$ or $CHCl_2$. This leads to the perylene forming the outer shell in this case. With hexane or hexane mixtures, the

polarity decreases, and the difference in solubility parameters with PDMS is also very small. This causes the trilayer structure, with PDMS forming the outer and inner layers, and the perylene segment sandwiched in between.

5.3.6 Conclusions

We have shown that the copolymer perylene end-cap PDMS, which is like a surfactant, forms vesicles in non-aqueous media. The perylene segment forms crystalline aggregate, with well defined melting temperature, and reversible melting and crystallization. The absorption spectra depend on the solvent used. Significant shifts in the absorption frequencies and changes in the relative intensities of the doublets are seen with the concentration of hexane in dichloromethane or chlorofrom. Thus, the packing of perylene can be changed by the choice of the solvent system. TEM images of the vesicles show a tri-layer structure, depending on the solvent. These observations were rationalized on the basis of the solubility parameters of PDMS and those of the solvents, as well as the interaction parameter χ between PDMS and the solvents used. This initial attempt to prepare vesicles in non-aqueous media has been successful, and may be applicable to similar systems, e.g., with a non-crystallizable polymer such as polymethylphenylsiloxane and other types of photoactive / electroactive molecules. Part of the model for the tri-layer structure shown in Figure 5.8 resembles the mushroom morphology described by Stupp et al[27] for a rod-coil triblock molecule. Our study indicates that by varying the nature of the solvent, different types of supramolecular nanostructures can be obtained, as envisioned by Stupp et al.[27]

II. Poly(dimethyl siloxane) Perylene Bisimides (PDMS Perylene Bisimide)

5.4 Synthesis of PDMS Perylene Bisimides D900 (9) (Scheme 5.3)

Three different molecular weights of ~900, 1500, and 3000 of PDMS were used for the synthesis of (**9**), (**10**) and (**11**), (Scheme 5.3) respectively. In a round bottom flask, 7.2g (8 mmol) of amine terminated polydimethylsiloxane (DMS-A11) and 0.2g of isoquinoline were dissolved in 15ml of *m*-cresol and the solution was slowly heated to 180°C. In 2 h, 0.78g (2 mmol) of perylene 3,4,9,10-tetracarboxylic dianhydride was slowly added into the solution The reaction mixture was stirred at 200°C for another 4 h, cooled to room temperature, and poured into 300ml of methanol. The precipitated solid was filtered, washed with methanol to remove unreacted polydimethylsiloxane, and dried in the vacuum at 60°C to yield 3.77g (86.0%) of **D900**. -^{1}H NMR: 0.10 (Si-CH_3), 0.75 (1,1'-CH_2, 4H), 1.78 (2,2'-CH_2, 4H), 3.95 and 4.17 (3,3'-CH_2, 4H), 8.53 (4H), and 8.62 (6H) (Aromatic). –IR (KBr): 1698.2, 1654.1, 1596.0, 1441.9, 1403.3, 1346.6, 1260.9, 1098.0, 1022.9, 800.9, 745.2 cm^{-1}. -UV-visible (CH_2Cl_2): 527, 490, 461 nm.

D1500: 0.10 (Si-CH_3), 0.73(1,1'-CH_2, 4H), 1.80 (2,2'-CH_2, 4H), 4.22 (3,3'-CH_2, 4H), 8.45 (4H), and 8.57 (6H) (Aromatic). –IR (KBr): 1698.4, 1652.9, 1596.6, 1442.5, 1403.2, 1381.1, 1262.0, 1097.8, 1022.7, 798.5, 744.8 cm^{-1}. –UV-visible (CH_2Cl_2): 526, 489, 459 nm.

D3000: 0.10 (Si-CH_3), 0.73 (1,1'-CH_2, 4H), 1.80 (2,2'-CH_2, 4H), 4.21(3,3'-CH_2, 4H), 8.59 (4H), and 8.67 (6H) (Aromatic). –IR (KBr): 1698.2, 1655.3, 1595.9, 1262.0, 1100.0, 1020.1, 807.4, 745.2 cm^{-1}. –UV-visible (CH_2Cl_2): 524, 489, 459 nm.

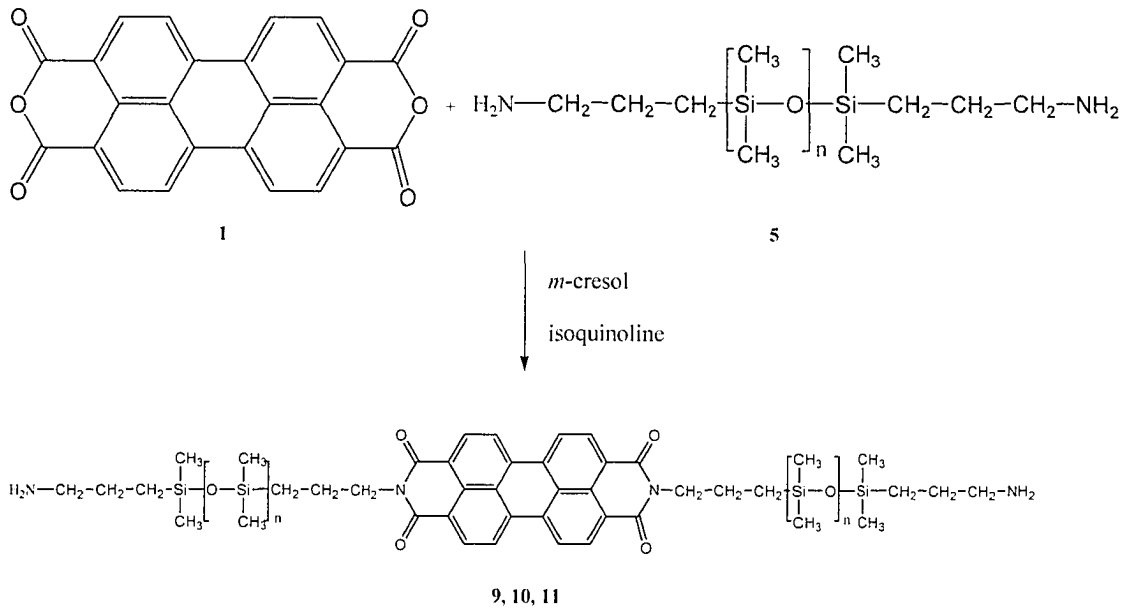

Scheme 5.3. Synthesis of PDMS perylene bisimides: (9) n ≈ 10; (10) n ≈ 20; (11) n ≈ 40.

5.5 Results and Discussion

5.5.1 Synthesis

For comparison with PDMS-end-perylene, we also synthesized poly(dimethyl siloxane) perylene bisimide (PDMS perylene bisimide) by reaction of perylene 3,4,9,10-tetracarboxylic dianhydride with amino terminated polysiloxane in *m*-cresol at elevated temperatures. The reaction condition is same as (PDMS-end-perylene), except that perylene 3,4,9,10-tetracarboxylic dianhydride should be slowly added into the solution of amino terminated polysiloxane, isoquinoline, and *m*-cresol, so that only 2 moles of amino terminated poly(dimethyl siloxane) react with 1 mole of perylene 3,4,9,10-tetracarboxylic dianhydride. The appearances of PDMS perylene bisimides are similar to

PDMS-end-perylene. All of them are dark red. However, the solubility is lower than PDMS-end-perylene. PDMS-end-perylene can dissolve in most common chlorinated solvents, such as, dichloromethane, chloroform, dichlorobenzene. However, PDMS perylene bisimides only dissolve in chloroform lower than 10^{-3}M, and even lower in dichloromethane.

^{1}H NMR ($CDCl_3$ solution) shows that 0.7-4.2 ppm, due to the hydrogens of the alkyl groups (α-, β- and γ- to the nitrogen atom), between 8.4-8.6 ppm correspond to perylene hydrogens, and chemical shifts lower than 0.5 due to hydrogens of the methyl groups attached directly to the silicon atoms were observed (Figure 5.9)

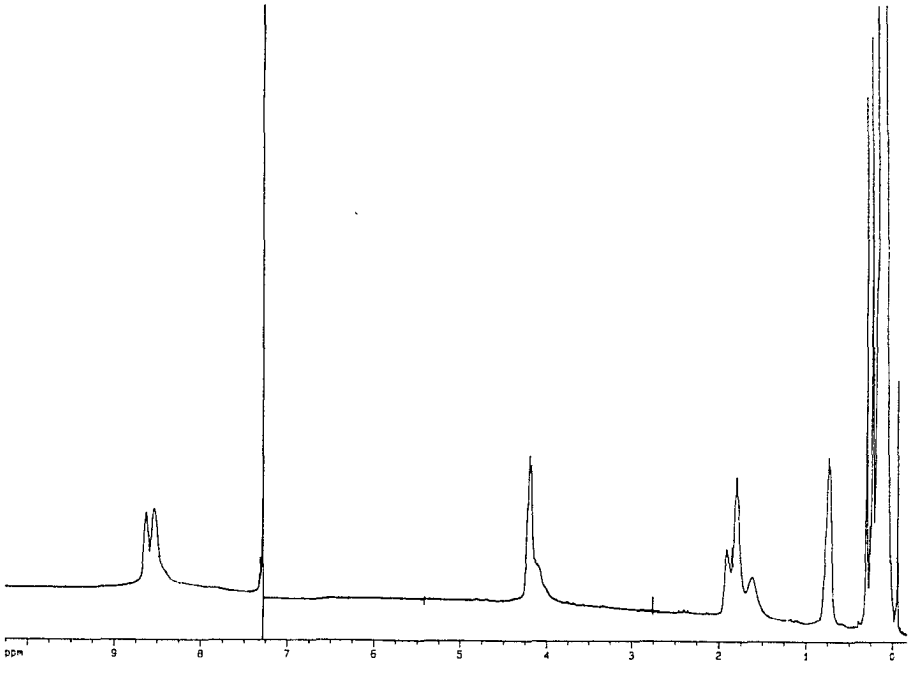

Figure 5.9. ^{1}H NMR of D900

5.5.2 Thermal Properties

Unlike PDMS-end-perylene, PDMS perylene bisimides have no melting point or transition temperature (Figure 5.10). This property is more like normal perylene bisimides. For most of perylene bisimides, melting points are over 300°C or even above the decoposition temperature, which cause that melting cannot be observed from DSC. Similar to M3000, D3000 also has a melting point at -50°C, which indicates the melting of PDMS segment.

The stability of these compounds are very good, 387°C for D900, 423°C for D1500, and 406°C for D3000 at 5% decomposed samples (Figure 5.11). It is surprising that D900 has the lowest decomposition temperature.

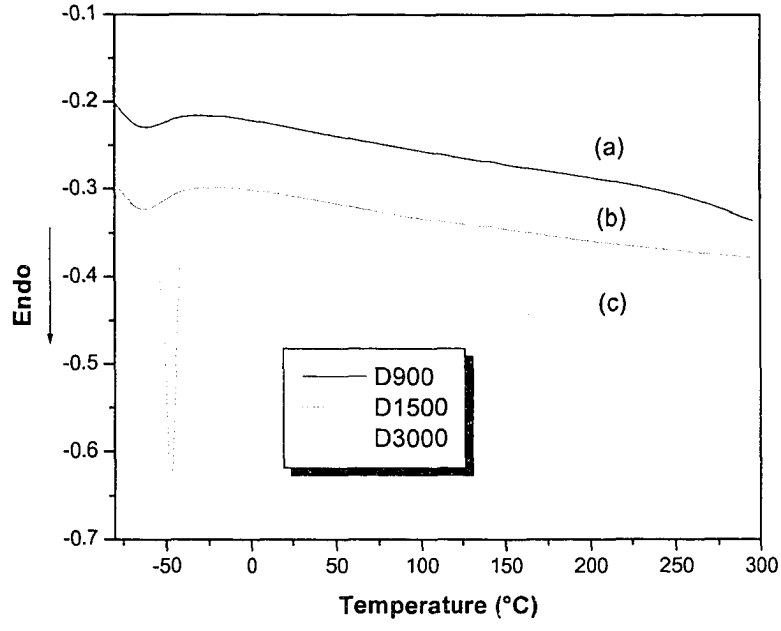

Figure 5.10. DSC thermograms of (a) D900, (b) D1500, (c) D3000 at the second run.

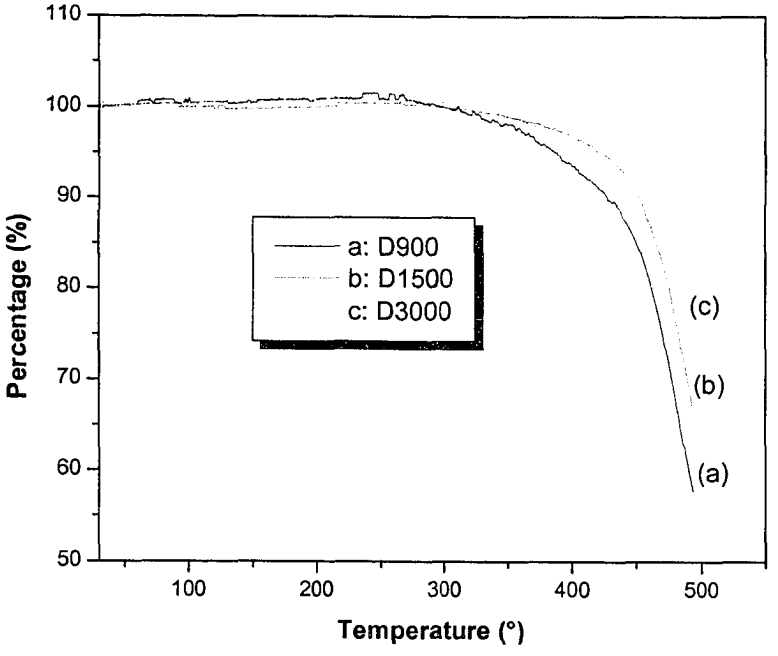

Figure 5.11 TGA thermograms of (a) D900, (b) D1500, (c) D3000.

5.5.3 X-ray Diffraction

It was surprising that all PDMS perylene bisimides are amorphous (Figure 5.12). Only there are broad peaks at 7.52 and 3.51 Å of d-spacing. This is probably due to the long chain of PDMS causing perylene to loose the π-π stacking system. It seems the first time non-substituent perylene bisimides are observed in the amorphous state.

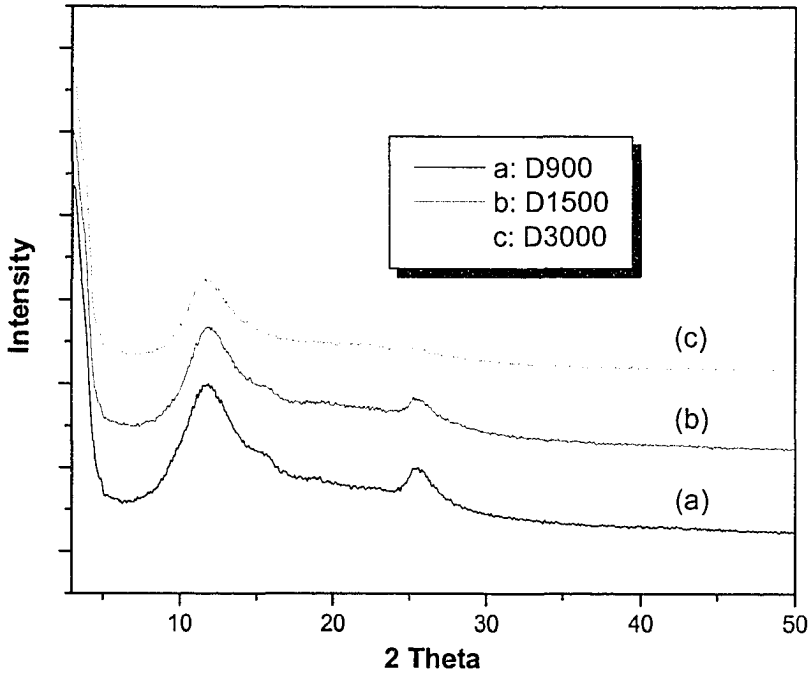

Figure 5.12. X-ray diffraction of (a) D900, (b) D1500, and (c) D 3000.

5.5.4 UV-visible Spectra

The concentrations for UV-visible spectra were 2.0×10^{-5} M. Figure 5.13 shows the absorptions of D900 have small blue shift. Also the ratios of two main peaks are increased when the content of hexane is increased. These phenomena are similar to M900.

5.5.5 TEM Analysis

Unlike M-series compounds, all D-series samples cannot form vesicles. This is the reason that D-series have both side N-substituents, which have equal properties. Vesicles or micelles usually form due to the different polarity, hydrophilicity or hydrophobisity of two sides of the molecules.

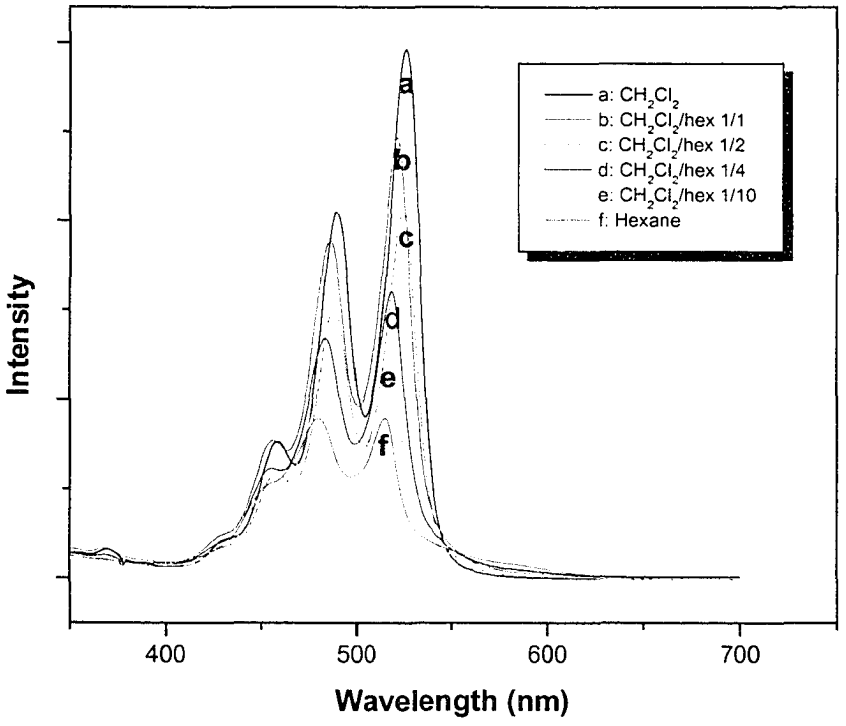

Figure 5.13 UV-visible absorption spectrum of D900 in different solvents.

5.5.6 Conclusions

PDMS perylene bisimides have similar properties to PDMS-end-perylene, in appearances, thermal stability, and UV-visible absorption. However, PDMS perylene bisimides are amorphous materials, no melting point before melting. Especially, they cannot form vesicles due to equality of molecular dipole moment.

References

1. Burke, S.; Shen, H.; Eisenberg, A. *Macromol. Symp.* **2001**, *175*, 273-283.

2. Discher, D.; Eisenberg, A. *Science* **2002**, *297*, 967-973.

3. Yu, K.; Eisenberg, A. *Macromolecules* **1996**, *29*, 6359-6361.

4. Zhang, L.; Eisenberg, A. *Macromolecules* **1996**, *29*, 8805-8815.

5. Zhang, L.; Eisenberg, A. *J. Am. Chem. Soc.* **1996**, *118*, 3168-3181.

6. Yu, K.; Eisenberg, A. *Macromolecules* **1998**, *31*, 3509-3518.

7. Massey, J.; Power, K. N.; Manners, I.; Winnik, M. A.*J. Am. Chem. Soc.* **1998**, *120*, 9533-9540.

8. (a) Law, K.-Y. *Chem. Rev.* **1993**, *93*, 449-486. (b) Kazmaier, P. M.; Hoffmann, R. *J. Am. Chem. Soc.* **1994**, *116*, 9684-9691. (c) Graser, F.; Hädicke, E. *Justus Liebigs Ann. Chem.* **1980**, 1994. (d) Hädicke, E.; Graser, F. *Acta Crystallogr.* **1986**, *C42*, 189. (e) Bender, T. P.; Duff, J. M.; Vong, C.; Hamer, G. K. US Patent 6,656,651B1 (**2003**). (f) Hsiao, C-K.; Hor, A-M.; Duff, J. M.; Baranyi, G.; Allen, C. G. US Patent 6,051,351 (**2000**).

9. Liu, S.-G.; Sui, G.; Cormier, R. A.; LeBlanc, R. M.; Gregg, B. A. *J. Phys. Chem. B* **2002**, *106*, 1307-1315.

10. Arnaud, A.; Belleney, J.; Boue, F.; Bouteriller, L.; Carrot, G.; Wintgens, V. *Angew. Chem. Int. Ed.* **2004**, *43*, 1718-1721.

11. Wang, Z. Y.; Qi, Y.; Gao, J. P.; Sacripante, G. G.; Sundararajan, P. R.; Duff, J. D. *Macromolecules* **1998**, *31*, 2075-2079.

12. Ghassemi, H.; Zhu, J. H. *J. Polym. Sci. Polym. Phys.* **1995**, *33*, 1633-1639.

13. Thelakkat, M.; Posch, P.; Schmidt, H-W. *Macromolecules* **2001**, *34*, 7441-7447.

14. Neuteboom, E. E.; Meskers, S. C. J.; Meijer, E. W.; Janssen, R. A. *Macromol. Chem. Phys*. **2004**, *205*, 217-222.

15. Feiler, L.; Langhals, H.; Polborn, K. *Liebigs Ann*. **1995**, 1229-1244.

16. Arnold, C. A.; Summers, J. D.; McGrath, J. E. *Polym. Eng. and Sci*. **1989**, *29*, 1413-1418.

17. Yao, D.; Wang, Z. Y.; Sundararajan, P. R. *Polymer* **2005**, *46*, 4390-4396.

18. Pauling, L. *The Nature of the Chemical Bond*, **1960**, Cornell University Press,Ithaca, N. Y. p. 85.

19. (a) Liu, S. L.; Chung, T. S.; Oikawa, H.; Yamaguchi, A. *J. Polym. Sci., Polym. Phys.* **2000**, *38*, 3018-3031. (b) Lee, Y.; Porter, R. S. *Macromolecules* **1987**, *20*, 1336-1341.

20. O'Neil Maryadele, Ed., *Merk Index 13th Ed.*; Merck &Co. **2001**, 7261.

21. (a) Cormier, R. A.; Gregg, B. A. *Chem. Mater*. **1998**, *10*, 1309. (b) Struijk, C. W.; Sieval, A. B.; Dakhorst, J. E. J.; van Dijk, M.; Kimkes, P.; Koehorst, R. B. M.; Donker, H.; Schaafsma, T. J.; Picken, S. J.; van de Craats, A. M.; Warman, J. M.; Zuilhof, H.; Sudholter, E. J. R. *J. Am. Chem. Soc*. **2000**, *122*, 11057-11066.

22. Du, Y.; Xue, Y.; Frisch, H. L. in *Physical Properties of Polymers Handbook*, Mark, J. E. (Ed.); American Institute of Physics Press, N. Y. **1996**, Chapter 16; Orwoll, R. A.; Arnold, P. A. *ibid*, Chapter 14.

23. Luo, L.; Eisenberg, A. *Langmuir*, **2001**, *17*, 6804-6811.

24. Hammarström, L.; Velikian, I.; Karlsson, G.; Edwards, K. *Langmuir*, **1995**, *11*, 408-410.

25. Zheng, Y.; Lin, Z.; Zakin, J. L.; Talmon, Y.; Davis, H. T.; Scriven, L. E. *J. Phys. Chem. Part B* **2000**, *104*, 5263-5271.

26. Won, Y-Y.; Brannan, A. K.; Davis, H. T.; Bates, F. S. *J. Phys. Chem. Part B* **2002**, *106*, 3354.

27. Stupp, S. I.; LeBonheur, V.; Walker, K.; Li, L. S.; Huggins, K. E.; Keser, M.; Amstutz, A. *Science* **1997**, *276*, 384-389.

Chapter 6

Conclusions and Recommendations for Future Work

Conclusions

The purpose of this thesis was to study the structure and morphology of perylene-containing polyimides. Due to the diverse applications of these perylene-containing polyimides, we were interested in investigating their structure and properties.

It was found that perylene-containing polyimides with alkyl chain spacers of different lengths have extended conformations, regardless of odd or even number of CH_2 groups. Due to the poor solubility of these polyimides in common solvents, the oriented X-ray diffraction could not be obtained. So the detailed chain conformation in the crystalline state could not be derived. The crystallinity of these polyimides increases with the alkyl chain length. Annealing improves the crystallinity of polyimides with spacers longer than five number of CH_2 groups. Also, annealing causes time dependent structural transformations, indicated by changes in UV-visible spectra, and X-ray diffraction. The UV-visible absorption shows 3-10 nm red-shift maximum. Extended annealing results in a smectic-like transition as indicated by X-ray diffraction and the time for such transition depends on the temperature of annealing and the length of the spacer, i.e., the less time will be needed to reach the smectic-like transitions at the high temperature, vice versa.

To improve the solubility and other properties, the perylene-containing copolyimides with 6FDA were synthesized. This copolymerization of perylenetetracarboxylic dianhydride and 6FDA with 1,12-diaminododecane leads to "*conformational* isomorphism". The 6FDA segment does not change the chain contour of PPI-12 significantly, and as a result, the d-spacings in the X-ray diffraction pattern remain the

same. The X-ray reflection at 3.3Å corresponds to the distance of perylene π-π stacking. The crystallinity decreases linearly with increasing the content of 6FDA, due mainly to the decreasing ratio of the perylene units with respect to the degree of polymerization and finally becomes amorphous when the percentage of 6FDA is more than 80%. In contrast, the T_g decreases significantly between 40 and 50% of 6FDA. Because the perylene conjugation is not extended by 6FDA, the positions of the absorption maxima in the UV-visible spectra do not change. As designed, the solubility increases with increasing 6FDA ratio, and Cop80 can dissolve in most conventional solvents, such as, chloroform, dichloromethane, THF, etc. Thus, the desired solubility and processibility can be achieved with 6FDA-based copolymers of perylene polyimides.

The possibility of self-assembly causes the design of perylene end-cap PDMS compounds. These perylene end-cap PDMS copolymers, like a surfactant in water, form vesicles in non-aqueous media. The perylene segment forms crystalline aggregate, with well defined melting temperature, and reversible melting and crystallization. The absorption spectra depend on the solvent used, which indicate J-type or H-type aggregates were formed. Therefore, the packing of perylene can be controlled by the choice of the solvent system. TEM images of the vesicles show a bilayer or a trilayer structure, depending on the solvent. These observations were rationalized on the basis of the solubility parameters of PDMS and those of the solvents, as well as the interaction parameter χ between PDMS and the solvents used.

Recommendations for Future Work

Perylene end-cap PDMS copolymers have very unique properties, which form vesicles in organic solvents. In this thesis, only PDMS was used as one segment. In the future, water soluble segments can be used. The resulting copolymers may be dissolved or dispersed in the water and form the similar vesicles. The good candidates for this purpose must be flexible and have different solubility from perylene, such as, amines with mono or bi poly(ethylene oxide) chains with molecular weight between 1000 to 10,000, or amine with mixture of poly(ethylene oxide) and poly(propylene oxide). The latter amines are called Jeffamine, which have different molecular weights and ratios of polyethylene oxide and polypropylene oxide.

Most polyimides have poor solubility in common solvents. However, if substituents, such as, chloro, bromo, or phenoxy, are used in the bay area (related information in Chapter 1), the solubility will significantly be increased. So, these works can be done by the future students.